Departamento de Física y Ciencias de la Tierra

UNIVERSIDADE DA CORUÑA

Luis Fernando Barral Losada y Rebeca Bouza Padín, como directores de la Tesis Doctoral de Sara Malmir, con NIE n° Y3877449P, autorizamos su presentación para depósito.

Luis Fernando Barral Losada Rebeca Bouza Padín

Development of new materials based on polymeric reinforced and self-reinforced biocomposites from natural resources

Author: Sara Malmir

Doctoral Thesis UDC / 2017

Directors: Prof. Luis Fernando Barral Losada

Dr. Rebeca Bouza Padín

Doctoral program of Applied Physics

UNIVERSIDADE DA CORUÑA

To whom that without his support I never be what I am,

To my husband

Aknowledgments

I want to deeply thank my dear supervisors, Prof. Luis Barral and Dr. Rebeca Bouza, whom provide me the great opportunity of doing my PhD in the polymer group of University of A Coruña in a wonderful country, Spain. Luis and Rebeca, you made me grow up academically and personally. This is what will be with me forever and this is why I owe you forever. Luis, thank you for being patient with me specially in the beginning of my work. Rebeca, thank you for your positive energy. You always let me to express my opinions without any fear even if they were wrong. You always heard me with passion, corrected my mistakes and these helped me a lot to proceed in the project.

Also, I want to thank my lovely familiy; my parents, my sisters, Tahereh and Tayebeh, and specially my husband, Shahrouz. It seems that I was far from you during my PhD study but in reallity, you were beside me in all moments. You gave me the power to move forward. Dear Shahrouz, thank you so much for your support. I really appreciate you.

Last but not least, I want to appreciate all members of the polymer group of University of A Coruña who helped me a lot from the beginig to the end. Thank you for your kindness. I enjoyed a lot being with you and will keep in mind my beatiful memories from you. ¡Cordial Saludo a todos!

Abstract

The present thesis has focused on the development and study of biodegradable polymeric biocomposites obtained from natural resources for food packaging industry. Two types of biopolymer matrix i.e. poly (3-hydroxybutyrate-co-3-hydroxyvalerate) (PHBV) and potato starch and two types of filler i.e. cellulose nanocrystals (CNC) and PHBV microparticles were used. Fillers were introduced into the matrices with different methods including solvent cast film, melt mixing and extrusion. In this regard, two approaches of reinforcing and self-reinforcing were followed. As a result, three different compositions were developed namely PHBV/CNC and starch/PHBV microparticles in the reinforcing approach and PHBV/PHBV microparticles in the self-reinforcing approach.

The main aim was to produce biocomposites with modified thermal, mechanical and morphological properties and also with higher crystallinity and barrier properties. Results showed that in all cases, the filler acted as nucleating agent inside the matrix. Consequently, biocomposites with improved properties were obtained which made these ecological materials to be good candidates for packaging applications.

Resumen

La presente tesis se ha centrado en el desarrollo y estudio de biocompuestos poliméricos biodegradables obtenidos a partir de recursos naturales para la industria de envase y embalaje de alimentos. Se usaron dos tipos de matrices de biopolímero, poli (3-hidroxibutirato-co-3-hidroxivalerato) (PHBV) y almidón de patata y dos tipos de relleno, nanocristales de celulosa (CNC) y micropartículas de PHBV. Los rellenos se introdujeron en las matrices con diferentes métodos, incluyendo el cast film, mezcla en estado fundido y extrusión. En este sentido, se aplicaron dos enfoques de refuerzo y auto-refuerzo. Se desarrollaron tres composiciones diferentes: PHBV/CNC y almidón/micropartículas de PHBV en el enfoque de refuerzo y PHBV/micropartículas de PHBV en el enfoque de auto-refuerzo.

El objetivo principal fue producir biocompuestos con propiedades térmicas, mecánicas y morfológicas modificadas y también con mayor cristalinidad y propiedades barrera. En todos los casos, el relleno actuó como agente nucleante dentro de la matriz. En consecuencia, se obtuvieron biocompuestos con propiedades mejoradas que hacen a estos materiales ecológicos ser buenos candidatos para aplicaciones de envase y embalaje.

Resumo

A presente tese centrouse no desenvolvemento e estudo de biocomposites poliméricos biodegradables obtidos de recursos naturais para a industria do envase e embalaxe de alimentos. Foron utilizados dous tipos de matrices de biopolímeros, poli (3-hidroxibutirato-co-3-hidroxivalerato) (PHBV) e almidón de pataca e dous tipos de recheo, nanocristais de celulosa (CNC) e micropartículas de PHBV. Os recheos foron introducidos nas matrices con diferentes métodos, incluido cast film, mestura en fundido e extrusión. A este respeto, aplicáronse dous enfoques de reforzo e auto-reforzo. Desenvolvéronse tres composicións diferentes: PHBV/CNC e almidón/micropartículas de PHBV no enfoque de reforzo e PHBV/micropartículas de PHBV no enfoque de auto-reforzo.

O obxectivo principal foi producir biocomposites con propiedades térmicas, mecánicas e morfolóxicas modificadas e tamén con maior cristalinidade e propiedades barreira. En todos os casos, o recheo actuou como axente nucleante dentro da matriz. Consecuentemente, obtivéronse biocomposites con propiedades melloradas que fan que estes materiais ecolóxicos sexan bos candidatos para aplicacións de envase e embalaxe.

List of contents

List of figures

List of tables

List of abbreviations

AFM	Atomic force microscopy
ANOVA	Analysis of variance
ASTM	American Society for Testing and Materials
CDTR	Carbon dioxide transmission rate
CNC	Cellulose nanocrystals
CNF	Cellulose nanofibers
CNW	Cellulose nanowhiskers
DMA	Dynamic mechanical analysis
DSC	Differential scanning calorimetry
HA	Humidity absorption
HB	Hydroxybutyrate
HDPE	High density polyethylene
HV	Hydroxyvalerate
ISO	International Organization for Standardization
LDPE	Low density polyethylene
OTR	Oxygen transmission rate
PBAT	Poly (butylene adipate-co-terephthalate)
PET	Polyethylene terephthalate
PHA	Polyhydroxyalcanoates
PHB	Polyhydroxybutyrate
PHBV	Poly (3-hydroxybutyrate-co-3-hydroxyvalerate)
PLA	Polylactic acid
POM	Polarized optical microscopy

PP	Polypropylene
PS	Polystyrene
PVC	Polyvinylchloride
SAXS	Small angle X-ray scattering
SDS	Sodium dodecyl sulfate
SEM	Scanning electron microscopy
TEM	Transmission electron microcopy
TGA	Thermogravimetric analysis
WAXS	Wide angle X-ray scattering
WVTR	Water vapor transmission rate

CHAPTER 1: Introduction

1.1. Biopolymers

1.1.1. Why biopolymers?

Nowadays, it is well accepted that oil-based synthetic plastic wastes are considered as serious threats with remarkable detrimental effects on environment. As of 2015, nearly 6300 Mt of oil-based plastic waste has been generated. Only 9% was recycled while around 12% was burned and around 79% was accumulated in landfills or in the nature. It is anticipated that if the current trend continue, the amount of accumulated plastic wastes in natural environments or landfills will reach roughly to 12000 Mt by 2050 that is a serious growing concern that should be managed and dealt with. Figs. 1.1 and 1.2 show global primary plastic production and waste generation according to industrial use sector from 1950 to 2015, respectively [1]. It is obvious that packaging industry has a significant accelerated contribution in both production and waste generation aspects. Some conventional polymers which are consumed in packaging industry are high density polyethylene (HDPE), low density polyethylene (LDPE), polypropylene (PP), polystyrene (PS), polyvinylchloride (PVC) and polyethylene terephthalate (PET). Polyethylene and polypropylene are the most used fossil hydrocarbons in packaging application. These polymers are accumulated in the nature instead of decompose and cause serious environmental negative consequences.

Further, oil-based plastics have toxic side products and residues and high costs of combustion or separating and recycling. They come from oil resources which are limited and considered as non-renewable resources. All these reasons are giving rise to the importance of developing biodegradable and compostable materials. Accordingly, in last decades, polymers derived from renewable sources were being investigated deeply as high global demanded

alternatives for conventional oil-based products. In this regard, a notable effort had been carried out to introduce eco-friendly products to the different industries and markets such as drug delivery, medicine, coatings, cosmetic or food packaging, which are currently dominated by oil-based materials [2, 3]. This is for satisfying environmental concerns such as considerable amount of oily waste production, their contamination effects on the eco-system and also reduction the dependency on fossil sources. Biopolymers applied in these industries are derived from biomass which is come from crops such as wheat, potato or sugar beet.

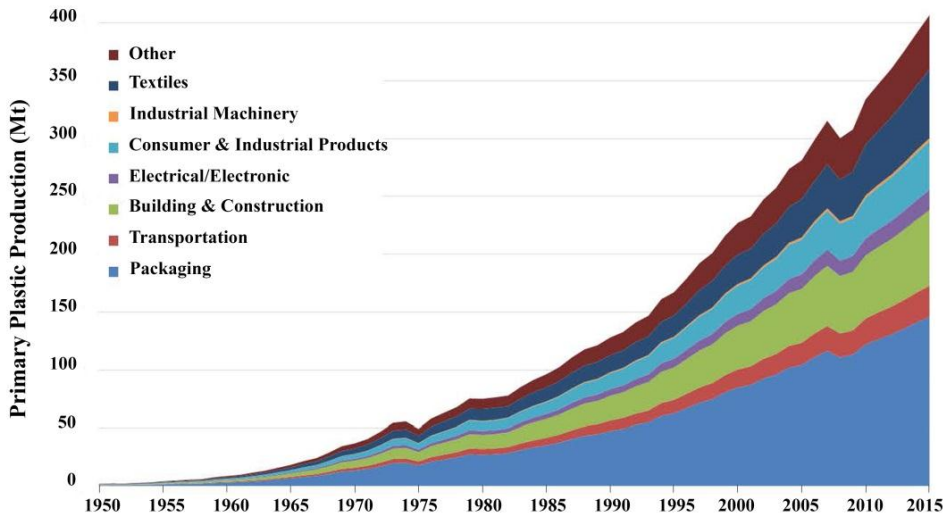

Figure 1.1: Global primary plastic production according to industrial use sector from 1950 to 2015.

Proteins, different types of starch, glycogen, polyhydroxyalcanoates (PHA), polyhydroxybutyrate (PHB) and polylactic acid (PLA) are some well-known examples of biodegradable polymers which are currently used and studied widely [4-8]. Many biopolyesters are naturally made by bacteria and in

commercial scale; they can be produced by fermentation process. PHB and PHBV are two examples of biopolyesters that can be used instead of plastics such as polystyrene or polyethylene.

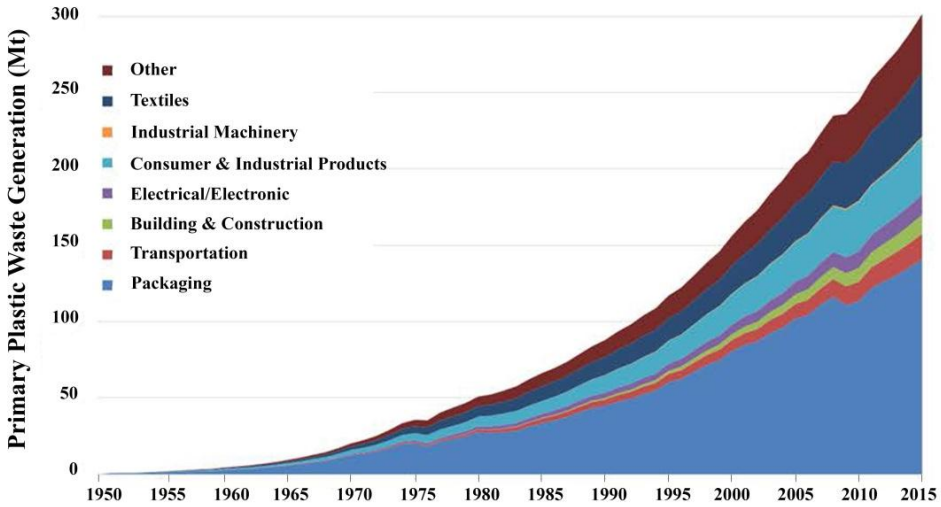

Figure 1.2: Global primary plastic waste generation according to industrial use sector from 1950 to 2015.

1.1.2. Advantages, drawbacks and strategies

Biopolymer materials exhibit several benefits such as sustainability, carbon neutrality, renewability, non toxicity, biocompatibility and biodegradability. Meanwhile degradation process by microorganisms, they are converted to carbon dioxide (CO_2) and water. For this, they called biodegradable. Also, they are potential to cut carbon emission and decrease CO_2 content in the atmosphere. This is due to this fact the CO_2 gas that is released during their degradation can be absorbed by crops. Consequently the quantity of released CO_2 in the atmosphere would reduce. This is the reason why biopolymers are

called carbon neutral. Also some biopolymers can be degraded up to 90% in the period of six months. These biopolymers are called compostable. They will receive a special compostable symbol from European Standard EN 13432 (2000).

Although environmental concerns are satisfied by using bio-based polymeric materials but their application might be limited due to some disadvantages such as high price and less mechanical, thermal and barrier properties once compared with traditionally oil-based polymers. In order to overcome mentioned drawbacks and obtain more efficient products, copolymerization, compounding or using different kinds of fillers and additives are common strategies [9, 10]. Hietala et al. [11] reported modified mechanical properties of starch by reinforcing with cellulose nanofiber. Sridhar et al. [10] declared that graphene particles acted as nucleating agents for crystallization of poly (3-hydroxybutyrate-co-3-hydroxyvalerate) (PHBV) and as a consequence, mechanical properties of final product were improved. Wang et al. [12] concluded that modified acetylated chitin nanocrystals caused promotion in thermo-mechanical properties of PHBV/chitin nanocomposites. Ten et al. [13] discussed about dual effect of cellulose nanowhiskers (i.e., nucleation and confinement) on PHBV nucleating process. Several similar research works were carried out for biodegradable polymers e.g. poly (butylene adipate-co-terephthalate) (PBAT) [14], PHB [15-17], PHBV [18-20] and PLA [21, 22]. Other approach for improvement the properties of biopolymers is introducing antioxidants that can prevent some feature meanwhile melt processing such as chain scission, oxidation and undesired recombination. It worth to note that in industrial aspects, incorporation of antioxidants is of great importance due to the fact that melt processing is the most desirable process in industrial scale production [23].

1.2. Poly (3-hydroxybutyrate-co-3-hydroxyvalerate) (PHBV)

Numerous different types and groups of biopolymers exist in the planet. Group of biopolyesters is one of the most important groups of biopolymers. Polyhydroxyalcanoate (PHA) biopolyesters is a family of renewable and biodegradable thermoplastics. Poly (3-hydroxybutyrate-co-3-hydroxyvalerate) (PHBV), the most common PHA copolyester, is a natural organic polyester, biosynthesized by microorganisms, i.e. by many types of bacteria and some types of plants [18]. There are two main steps in its production process namely fermentation and extraction. In the fermentative stage, the microorganisms are added to the reactors which contain butyric acid or fructose. Then microorganisms start to metabolize the available sugar and store the produced PHBV inside the inner part of the cell. In the extraction stage, PHBV which was accumulated in the microorganism inner cell is extracted and purified with adequate solvents to be ready for next usages [23].

PHBV can be used for industrial applications, tissue engineering, controlled release of drugs, medical implants and orthopedic devices. Thanks to its combined properties such as excellent biocompatibility, renewability and harmless degradation residues, it has attracted considerable interest as an eco-friendly biodegradable material for use in packaging industry [24-26]. In its bacterial degradation process, PHBV is converted to CO_2 and water and it acts as energy source for microorganisms.

Fig. 1.3 shows the chemical structure of PHBV. Depending on the percent of hydroxybutyrate (HB) and hydroxyvalerate (HV) units, a wide range of properties and processability can be obtained. It was reported that increase in the HB blocks (first block in the Fig. 1.3) results in higher melting point and glass transition temperature, water permeability and tensile strength. Increasing the amount of HV blocks (second block in the Fig. 1.3) lead to more

ductility and less crystallinity [27]. Table 1.1 lists thermal and mechanical properties of PHB and different types of PHBV depending on the concentration of HV block in its chemical structure [28].

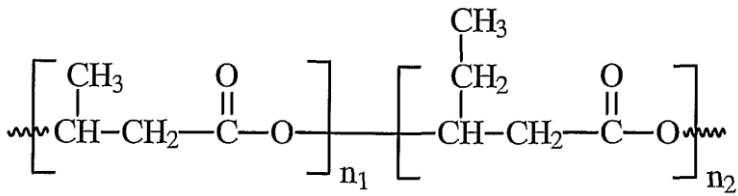

Figure 1.3: Chemical structure of PHBV.

Table 1.1: Thermal and mechanical properties of PHB and different types of PHBV at 25 °C.

Composition Mol %HV	Melting temperature (°C)	Glass transition temperature (°C)	Tensile strength (MPa)	Elongation (%)	Elastic modulus (GPa)
0	175	9	45	4	3.8
11	157	2	38	5	3.7
20	114	-5	26	27	1.9
28	102	-8	21	700	1.5
34	97	-9	18	970	1.2

Although some properties of PHBV can be adjusted by controlling mentioned HB and HV units, application of this polymer is restricted due to some drawbacks such as narrow range of processing due to lack of thermal stability, high brittleness, low rate of crystallization, barrier and mechanical properties and high price [23, 29]. Wang et al. reported that mentioned drawbacks could be attributed to low nucleating density and crystallization rate of PHBV [12].

As stated before, strategies like compounding with other polymers or introducing suitable fillers could be applied in order to overcome these negative characteristics efficiently. Several publications had been devoted to blending, reactive blending, reinforcing and modifying PHBV with different biopolymers and fillers such as PHBV/zinc oxide [30], PHBV/monoterpene derivative [31], PHBV/graphene [10], PHBV/ethylene vinyl acetate [32], PHBV/ poly (l-lactide) [33], PHBV/cellulose nanowhisker [34], PHBV/carbon nanotubes [35] and PHBV/poly (3-hydroxybutyrate) [36].

1.3. Cellulose nanocrystals (CNC)

There are many types of fillers and nanofillers for production of biopolymeric composites. As well-known filler, cellulose nanocrystals are used in biodegradable matrices due to their desirable properties. It is one of the green fillers derived from natural sources like cotton and wood. Cellulose is the most abundant biopolymer on the earth. About 33% of all plant matter is cellulose. For example, 90% of cotton and 50% of wood is composed of cellulose. CNC can act as nucleating agent; it has good mechanical properties, low density and high surface activity. Figure 1.4 shows the chemical structure of cellulose nanocrystals.

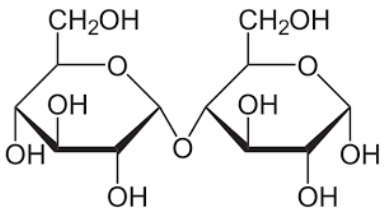

Figure 1.4: Chemical structure of cellulose.

CNC is capable of forming hydrogen bonds through hydroxyl groups (OH) on its surface [37]. It means that hydrogen atoms in the hydroxyl groups in CNC surface are capable of interact electrostatically with functional groups which contain more electronegative atoms such as nitrogen or oxygen atoms in other molecules. In a well dispersed CNC nanocomposite, higher thermal, mechanical and barrier properties can be obtained in comparison with unfilled matrix. Yu et al. [38–40] stated that presence of cellulose nanocrystals in PHBV matrix resulted in improved thermal, mechanical, crystallization and biodegradation properties. Also, it was showed that PHBV/CNC nanocomposites exhibited less migration rate to both polar and nonpolar food simulants and had better mechanical, thermal and barrier properties compared to PHBV [41]. Elsewhere, it was proved that well-dispersed CNC could dramatically increase tensile strength, Young modulus and thermal stability of PHBV [40]. Yu et al. [38] observed modified morphological, thermal and mechanical properties of PHBV via addition of cellulose nanocrystals. However, it was reported that mechanical and thermal properties of PHBV/CNC nanocomposites were dependent on the type of the residual functional groups of CNC surface [39]. It is accepted that the main reason for these efficient effects of CNC in PHBV matrix is that CNC could be served as a nucleating agent to increase crystallization rate of PHBV.

1.4. Starch

Another important group of biodegradable polymeric materials is different kinds of starch. It can be found in plants such as wheat, potato, corn and tapioca. Starch as a promising potential candidate has been tried widely in production of edible films, agricultural foils, compostable bags, garbage and food packaging [7, 42-44]. A developing approach has been done in order to

incorporate modified starch in food packaging industry which possesses a considerable contribution of oil-based plastic wastes in all over the world. This is in the light of its unique combination of beneficial properties such as inherent biocompatible and biodegradable properties, renewability, abundance, non toxicity, low cost, versatility, purity and processability [45-47]. By the way, starch is not a thermoplastic material in its pristine state since its granule internal section are mostly based on lipids while amino acids, enzymes and proteins are found to be the main constituents of the external parts [48]. Thereby, it undergoes some structural changes and modifications by addition of different types of plasticizers, normally water or water soluble plasticizers and polyols, in order to the destruction of its crystalline structure and its conversion from native semicrystalline starch to thermoplastic modified starch. Thermoplastic starch then could be simply processed through different techniques which are applied for conventional synthetic polymers such as extrusion, molding, thermoforming and blowing [42, 49]. Type and amount of used plasticizer as well as other gelatinization process conditions including time, temperature and shear are deeply determinative to the final performance of plasticized starch. Hence, it should be tended to adjust optimum condition which might lead to a flexible product with balanced properties regarding the particular specified application. Glycerol, sorbitol, ethylene glycol, xylitol, urea and maltitol have been proposed in previously reported investigations as plasticizers for various types of starch [47]. In a combined act of plasticizer, shear, heat and/or pressure, starch molecular interactions would be destroyed and plasticized partially crystalline binary mixture of amylose and amylopectin macromolecules would be resulted. Linear amylose, consisting of α-(1-4)-linked D-glucose and branched amylopectin, consisting of both α-(1-4)-linked and α-(1-6)-linked D-glucose

units are known as glycosidic polymers which starch is composed from. Figure 1.5 shows the chemical structure of amylose and amylopectin.

Also, it is believed that crystalline zones are made up of double helix formed from arrangement of same or different amylopectin branches [50, 51]. Globally, in a wide range of starch types, approximate average weight percent of amylose and amylopectin chains are believed to be 80% and 20%, respectively, but some types are available which their formulations differ from this. In reality, the botanical resource is strongly a key factor in the determination of the composition of starch granule and is complex to judge about it when the origin is not clear. Starch presents a group of favorable properties. But it should be underlined that humidity sensitivity, low mechanical efficiency and poor dimensional stability are identified as some of the most important undesired properties of it which are commonly related to its hydrophilic nature. Further, crystallization and retrogradation phenomena during aging would lead to loss of properties of starch. Some solutions to eliminate or improve these critical drawbacks and make starch to furnish more functionability, stability and efficiency might be modifications in the composition, compounding, grafting or introducing fillers and reinforcing agents [45, 46, 48].

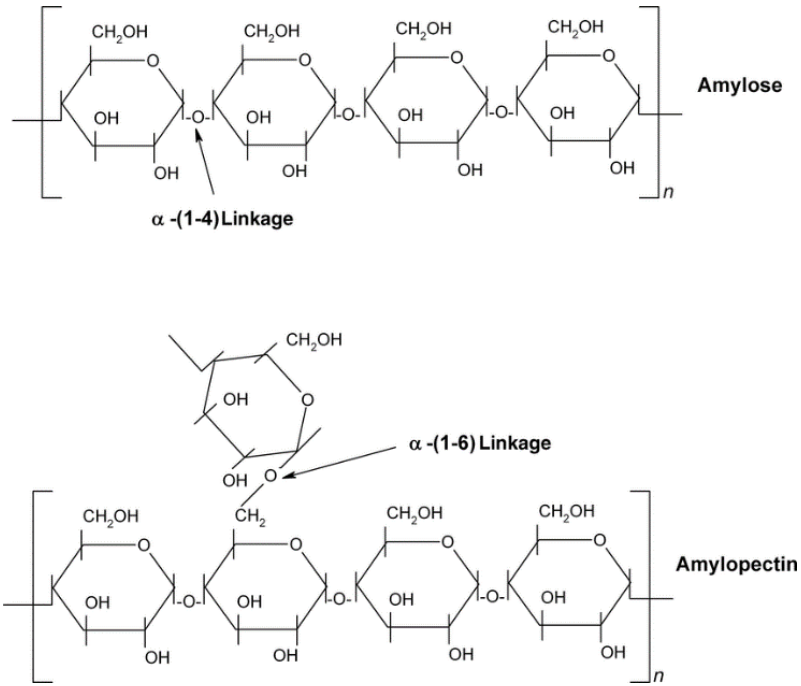

Figure 1.5: Chemical structure of amylose and amylopectin.

Fillers such as chitin, kaolin, layer silicates, carbon nanotubes and cellulose fibers are reported as effective fillers in different starch matrices [52-56]. Obviously, both the matrix/filler interphase interactions and the dispersion state of filler inside the matrix play an essential role in achieving the expected modified properties.

1.5. Main goals and structure of the thesis

1.5.1. Goals of the thesis

The present thesis has focused on reinforced and self-reinforced biocomposites for food packaging applications. In this regard, two types of

polymeric matrix, i.e. poly (3-hydroxybutyrate-co-3-hydroxyvalerate) and potato starch were selected.

Application of mentioned polymeric matrices is restricted due to some undesirable characteristics such as low crystallinity and barrier properties, poor mechanical and thermal properties. Thus, this doctoral thesis has focused on the modification of these drawbacks and the development of efficient packaging materials. Since based on literature, one of the well-known strategies is introducing a filler, two types of filler namely cellulose nanocrystals and PHBV microparticles were selected and incorporated to the matrices. Solvent cast film, melt mixing and extrusion methods were applied for sample preparation. Also, two different approaches were considered namely reinforcing and self-reinforcing. As a result, three different groups of packaging materials were developed and studied including PHBV/CNC nanocomposites and starch/PHBV microparticles as reinforced biocomposites and PHBV/PHBV microparticles as self-reinforced biocomposites. Biocomposites were evaluated and characterized in different aspects such as crystallinity, thermal, mechanical and morphological properties as well as humidity absorption and barrier properties.

1.5.2. Structure of the thesis

The present work was divided in four parts: introduction, experimental, results and conclusion. In the first part that includes chapter one, an introduction about biopolymers and their properties is presented. In the second part that includes chapter two, used materials, tests and equipments are explained. The third part is dedicated to results and discussion that includes the chapters three to seven. Structure and properties of reinforced bionanocomposites of PHBV/CNC prepared with different methods i.e. solvent cast film, internal

mixing and extrusion were studied in chapters three to five. In the chapter six, structure and properties of the reinforced biocomposites of starch/PHBV microparticles were investigated. In the chapter seven, self-reinforced biocomposites of PHBV/PHBV microparticles prepared via solvent cast film method were analyzed. In the fourth part which includes the chapter eight, the conclusion of the total work is presented.

1.6. References

[1] R. Geyer, J. R. Jambeck, K. L. Law, Supplementary materials for production, use, and fate of all plastics ever made, Science Advances, 3: e1700782 (2017)

[2] V. K. Thakur, Green Composites from Natural Resources, CRC Press, Florida (2013)

[3] S. Kalia, Biodegradable Green Composites, John Wiley & Sons, New Jersey (2016)

[4] L. Averous, E. Pollet, Biodegradable Polymers, Springer, New York (2012)

[5] L. Han, H. Xu, X. Sui, L. Zhang, Y. Zhong, Z. Mao, Preparation and properties of poly (ε-caprolactone) self-reinforced composites based on fibers/matrix structure, Journal of Applied Polymer Science, 134: DOI: 10.1002/APP.44673 (2017)

[6] L. T. Sin, A. R. Rahmat, W. A. W. A. Rahman, Polylactic Acid. PLA Biopolymer Technology and Applications, Elsevier, Oxford (2013)

[7] R. L. Whistler, J. N. BeMiller, Starch Chemistry and Technology, Elsevier, Oxford (2009)

[8] R. Ipsita, P. M. Visakh, Polyhydroxyalkanoate (PHA) based Blends, Composites and Nanocomposites, Royal Society of Chemistry, Cambridge (2014)

[9] P. A. Pawar, A. H. Purwar, Biodegradable polymers in food packaging, American Journal of Engineering Research, 2: 151 (2013)

[10] V. Sridhar, I. Lee, H. H. Chun, H. Park, Graphene reinforced biodegradable poly (3-hydroxybutyrate-co-3-hydroxyvalerate) nanocomposites, Polymer Letters, 7: 320 (2013)

[11] M. Hietala, A. P. Mathew, K. Oksman, Bionanocomposites of thermoplastic starch and cellulose nanofibers manufactured using twin-screw extrusion, European Polymer Journal, 49: 950 (2013)

[12] B. Wang, J. Li, J. Zhang, H. Li, P. Chen, Q. Gu, Z. Wang, Thermo-mechanical properties of the composite made of poly (3-hydroxybutyrate-co-3-hydroxyvalerate) and acetylated chitin nanocrystals, Carbohydrate Polymers, 95: 100 (2013)

[13] E. Ten, L. Jiang, M. P. Wolcott, Crystallization kinetics of poly (3-hydroxybutyrate-co-3-hydroxyvalerate)/cellulose nanowhiskers composites, Carbohydrate Polymers, 90: 541 (2012)

[14] L. Bastarrachea, S. Dhawan, S. S. Sablani, Engineering properties of polymeric-based antimicrobial films for food packaging: a review, Food Engineering Review, 3: 79 (2011)

[15] S. Angelini, P. Cerruti, B. Immirzi, G. Santagata, From biowaste to bioresource: Effect of a lignocellulosic filler on the properties of poly (3-hydroxybutyrate), International Journal of Biological Macromolecules, 71: 163 (2014)

[16] S. Ansari, T. Fatma, Polyhydroxybutyrate - a Biodegradable Plastic and its Various Formulations, International Journal of Innovative Research in Science, Engineering and Technology, 3: 9598 (2014)

[17] K. K. Darani, D. Z. Bucci, Application of Poly (hydroxyalkanoate) In Food Packaging: Improvements by Nanotechnology, Chemical and Biochemical Engineering Quarterly, 29: 275 (2015)

[18] A. Buzarovska, A. Grozdanov, M. Avella, G. Gentile, M. Errico, Poly (3-hydroxybutyrate-co-3-hydroxyvalerate)/titanium dioxide nanocomposites: a degradation study, Journal of Applied Polymer Science, 114: 3118 (2009)

[19] B. Bittmann, R. Bouza, L. Barral, J. Diez, C. Ramirez, Poly (3-hydroxybutyrate-co-3-hydroxyvalerate)/clay nanocomposites for replacement of mineral oil based materials, Polymer Composites, 34: 1033 (2013)

[20] X. Wang, Z. Chen, X. Chen, J. Pan, K. Xu, Crystallization kinetics and mechanical properties of Poly (3-hydroxybutyrate-co-3-hydroxyvalerate)(PHBV)/Poly (3-hydroxybutyrate-co-4-hydroxybutyrate)(P3/4HB) blends, Journal of Applied Polymer Science, 117: 838 (2010)

[21] M. D. Sanchez-Garcia, J. M. Lagaron, Novel clay-based nanobiocomposites of biopolyesters with synergistic barrier to UV light, gas and vapor, Journal of Applied Polymer Science, 118: 188 (2010)

[22] J. Ahmed, S. K. Varshney, R. Auras, Rheological and thermal properties of polylactide/silicate nanocomposite films, Journal of Food Science, 75: 17 (2010)

[23] D. G. Brunel, W. M. Pachekoski, C. Dalmolin, J. A. M. Agnelli, Natural additives for poly (hydroxybutyrate - co - hydroxyvalerate) - PHBV: effect on mechanical properties and biodegradation, Materials Research, 17(5): 1145 (2014)

[24] L. Martino, M. A. Berthet, H. Angellier-Coussy, N. Gontard, Understanding external plasticization of melt-extruded PHBV-wheat straw fibers biodegradable composites for food packaging, Journal of Applied Polymer Science, 132: DOI: 10.1002/APP.41611 (2015)

[25] V. Chea, H. Angellier-Coussy, S. Peyron, D. Kemmer, N. Gontard, Poly (3-hydroxybutyrate-co-3-hydroxyvalerate) films for food packaging: physical-chemical and structural stability under food contact conditions, Journal of Applied Polymer Science, 133: DOI: 10.1002/APP.41850 (2016)

[26] M. A. Berthet, H. Angellier-Coussy, V. Chea, V. Guillard, E. Gastaldi, N. Gontard, Sustainable food packaging: valorising wheat straw fibres for tuning PHBV based composites properties, Composites: Part A, 72: 139 (2015)

[27] I. Chodak, Polyhydroxyalkanoates: Origin, Properties and Applications. In: M. Belgacem, A. Gandini, editors. Monomers, polymers and composites from renewable resources, Oxford, Elsevier (2008)

[28] M. Avella, E. Martuscelli, M. Raimo, Review properties of blends and composites based on poly (3-hydroxy)butyrate (PHB) and poly (3-hydroxybutyrate-hydroxyvalerate) (PHBV) copolymers, Journal of Materials Science, 35: 523 (2000)

[29] H. Y. Yu, Z. Y. Qin, Surface grafting of cellulose nanocrystals with poly (3-hydroxybutyrate-co-3-hydroxyvalerate), Carbohydrate Polymers, 101: 471 (2014)

[30] A. M. Diez-Pascual, A. L. Diez-Vicente, ZnO-reinforced poly (3-hydroxybutyrate-co-3-hydroxyvalerate) bionanocomposites with antimicrobial function for food packaging, Applied Materials and Interfaces, 6: 9822 (2014)

[31] L. Pilon, C. Kelly, Modification of poly (3-hydroxybutyrate-co-3-hydroxyvalerate) properties by reactive blending with a monoterpene derivative, Journal of Applied Polymer Science, 133: DOI: 10.1002/APP.42588 (2016)

[32] S. H. El-Taweel, M. Khater, Mechanical and Thermal Behavior of Blends of Poly (hydroxybutyrate-co-hydroxyvalerate) with Ethylene Vinyl Acetate Copolymer, Journal of Macromolar Science Part B: Physics, 54: 1225 (2015)

[33] N. Jiang, H. Abe, Miscibility and morphology study on crystalline/crystalline partially miscible polymer blends of 6-arm poly (l-lactide) and poly (3-hydroxybutyrate-co-3-hydroxyvalerate), Polymer, 60: 260 (2015)

[34] L. Jiang, E. Moreluis, J. Zhang, M. Wolcott, J. Holbery, Study of the poly (3-hydroxybutyrate-co-3-hydroxyvalerate)/cellulose nanowhisker composites prepared by solution casting and melt processing, Journal of Composite Materials, 42: 2629 (2008)

[35] H. Y. Yu, Z. Y. Qin, B. Sun, X. G. Yang, J. M. Yao, Reinforcement of transparent poly (3-hydroxybutyrate-co-3-hydroxyvalerate) by incorporation of functionalized carbon nanotubes as a novel bionanocomposite for food packaging, Composite Science and Technology, 94: 96 (2014)

[36] M. Scandola, M. L. Focarete, G. Adamus, W. Sikroska, I. Baranowska, S. Swierczek, M. Gnatowski, M. Kowalczuk, Z. Jedlinski, Polymer blends of natural poly (3-hydroxybutyrate-co-3-hydroxyvalerate) and a synthetic atactic poly (3-hydroxybutyrate). Characterization and biodegradation studies, Macromolecules, 30: 2568 (1997)

[37] R. C. Goy, D. Britto, O. B. G. Assis, A review of the antimicrobial activity of chitosan, Polimeros: Ciencia e Technologia, 19: 241 (2009)

[38] H. Y. Yu, Z. Y. Qin, Z. Zhou, Cellulose nanocrystals as green fillers to improve crystallization and hydrophilic property of poly (3-hydroxybutyrate-co-3-hydroxyvalerate), Progress in Natural Science: Materials International, 21: 478 (2011)

[39] H. Y. Yu, Z. Y. Qin, L. Liu, X. G. Yang, Y. Zhou, J. M. Yao, Comparison of the reinforcing effects for cellulose nanocrystals obtained by sulfuric and hydrochloric acid hydrolysis on the mechanical and thermal properties of bacterial polyester, Composite Science and Technology, 87: 22 (2013)

[40] H. Y. Yu, Z. Y. Qin, Y. N. Liu, L. Chen, N. Liu, Z. Zhou, Simultaneous improvement of mechanical properties and thermal stability of bacterial polyester by cellulose nanocrystals, Carbohydrate Polymers, 89: 971 (2012)

[41] H. Yu, B. Sun, D. Zhang, G. Chen, X. Yang, J. Yao, Reinforcement of biodegradable poly (3-hydroxybutyrate-co-3-hydroxyvalerate) with cellulose nanocrystal/silver nanohybrids as bifunctional nanofillers, Journal of Material Chemistry B, 2 (48): 8479 (2014)

[42] F. Xie, E. J. Pollet, P. Halley, L. Avérous, Starch-based nano-biocomposites, Progress in Polymer Science, 38: 1590 (2013)

[43] A. M. Shi, L. J. Wang, D. Li, B. Adhikari, Characterization of starch films containing starch nanoparticles: part 1: physical and mechanical properties, Carbohydrate Polymers, 96: 593 (2013)

[44] T. H. Yun, S. D. Yoon, Effect of amylose contents of starches on physical properties and biodegradability of starch/PVA-blended films, Polymer Bulletin, 64: 553 (2010)

[45] M. J. Fabra, A. Lopez-Rubio, J. Ambrosio-Martin, J. M. Lagaron, Improving the barrier properties of thermoplastic corn starch-based films containing bacterial cellulose nanowhiskers by means of PHA electrospun coatings of interest in food packaging, Food Hydrocolloids, 61: 261 (2016)

[46] H. Angellier, S. Molina-Boisseau, P. Dole, A. Dufresne, Thermoplastic starch-waxy maize starch nanocrystals nanocomposites, Biomacromolecules, 7: 531 (2006)

[47] K. Gonzalez, A. Retegi, A. Gonzales, A. Eceiza, N. Gabilondo, Starch and cellulose nanocrystals together into thermoplastic starch bionanocomposites, Carbohydrate Polymers, 117: 83 (2015)

[48] D. Le Corre, J. Bras, A. Dufresne, Starch Nanoparticles: A Review, Biomacromolecules, 11: 1139 (2010)

[49] M. J. Fabra, R. Perez-Masia, P. Talens, A. Chiralt, Influence of the homogenization conditions and lipid self-association on properties of sodium caseinate based films containing oleic and stearic acids, Food Hydrocolloids, 25: 1112 (2011)

[50] C. G. Oates, Towards an understanding of starch granule structure and hydrolysis, Trends in Food Science & Technology, 8: 375 (1997)

[51] D. J. Gallant, B. Bouchet, P. M. Baldwin, Microscopy of starch: evidence of a new level of granule organization, Carbohydrate Polymers, 32: 177 (1997)

[52] P. R. Chang, R. Jian, J. Yu, X. Ma, Starch-based composites reinforced with novel chitin nanoparticles, Carbohydrate Polymers, 80: 420 (2010)

[53] A. J. F. Carvalho, A. A. S. Curvelo, J. A. M. Agnelli, A first insight on composites of thermoplastic starch and kaolin, Carbohydrate Polymers, 45: 189 (2001)

[54] L. Lendvai, A. Apostolov, J. Karger-Kocsis, Characterization of layered silicate-reinforced blends of thermoplastic starch (TPS) and poly (butylene adipate-co-terephthalate), Carbohydrate Polymers, 173: 566 (2017)

[55] J. Cheng, P. Zheng, F. Zhao, X. Ma, The composites based on plasticized starch and carbon nanotubes, International Journal of Biological Macromolecules, 59: 13 (2013)

[56] A. A. S. Curvelo, A. J. F. Carvalho, J. A. M. Agnelli, Thermoplastic starch‐cellulosic fibers composites: preliminary results, Carbohydrate Polymers, 45: 183 (2001)

CHAPTER 2: Materials and tests

2.1. Materials

In the present thesis, two types of polymeric matrix were used, namely PHBV and potato starch. PHBV biopolymer with 12 wt.% hydroxyvalerate (HV) content with granule size of 5 mm and with 10 wt.% of citric acid plasticized pellets was purchased from Goodfellow, U.K. Potato starch with 20 % amylose was purchased from Roquette Feres S. A. Lestrem, France.

Also, two types of filler were used, namely cellulose nanocrystals and PHBV microparticles. CNC with 1.05 wt.% sulfur content were supplied by the University of Maine, USA. PHBV microparticles were produced in our laboratory with emulsification/solvent evaporation method. In this regard, PHBV was dissolved in dichloromethane in a concentration of 1% w/v using sonication. The aqueous phase was prepared by dissolving sodium dodecyl sulfate (SDS) in water in concentration of 15% w/v. PHBV solution was poured on the aqueous solution. The ratio between both phases was 1:2 organic to aqueous phase. The emulsion was formed by stirring for 1h using mechanical stirrer followed by sonication in an ice bath for 3 min using conventional sonication bath. The organic solvent was evaporated by stirring overnight at 40 °C. The particles were collected in the aqueous solution, washed with deionized water for several times and then lyophilized.

SDS and dichloromethane solvent with 99.9% of purity were purchased from Scharlau, Spain. Chloroform solvent with 99.9% of purity was supplied from Cienytech Company, Spain. Glycerol (purity of 99.5%, molar mass 92.09 g mol^{-1}) was supplied from Sigma-Aldrich, Spain. All solvents were used as received without further purification.

In order to perform the humidity absorption tests (chapters 5 and 6), three types of salts with analytical grade were used to provide test mediums with different relative humidity of 95% (potassium nitrate, KNO_3), 75% (sodium

chloride, NaCl) and 54% (magnesium nitrate hexahydrate, $Mg(NO_3).6H_2O$). The salts were supplied from Scharlab S. L., Spain.

In order to perform the antimicrobial test (chapter 5), chitosan powder (from shrimp shells, >75% deacetylated) and zinc oxide (particle size < 100 nm, density 1.6-1.8 g/ml, pH 6-8) were supplied from Sigma-Aldrich, Spain. Silver particles were silver phosphate glass BC A 21-41 from Sanitized AG, Switzerland. These additives were used as antimicrobial agents in PHBV matrix.

2.2. Tests and equipments

2.2.1. Thermal analysis

Differential scanning calorimetry (DSC): A differential scanning calorimeter measures the difference between the heat flux supplied to a sample under study and a reference, both exposed to the same temperature program. The samples have to be measured precisely (few mg) and the pans have to be identical of well-known heat capacity. Software must control the temperature of both pans to be almost identical through the experiment which is done normally under inert atmosphere. During the experiment, both sample and reference pans are heated up (or cooled down) at the same rate. The amount of heat required for each of the sample and reference pans to reach the same temperature is recorded. As the sample pan contains the sample material while the reference is empty, more heat is required to heat the sample pan. The energy difference supplied to the sample or the reference is equal to the change in heat capacity (C_p) [1]. The thermal transition may be endothermic or exothermic depending on the change in heat capacity. Thus, DSC can be used

to observe transitions such as melting, crystallization, glass transition and gelatinization temperature. Figure 2.1 shows a DSC scheme.

In the present thesis, differential scanning calorimetry was performed by a Perkin Elmer Diamond (Perkin Elmer España SL, Spain) under nitrogen atmosphere. Samples were heated from 30 °C to 200 °C at 20 °C min^{-1} and kept 5 min at 200 °C to remove thermal history. Subsequently, specimens were cooled to 30 °C at 10 °C min^{-1}, kept 1 min at 30 °C and heated again to 200 °C at 10 °C min^{-1} (chapters 3, 5 and 7)

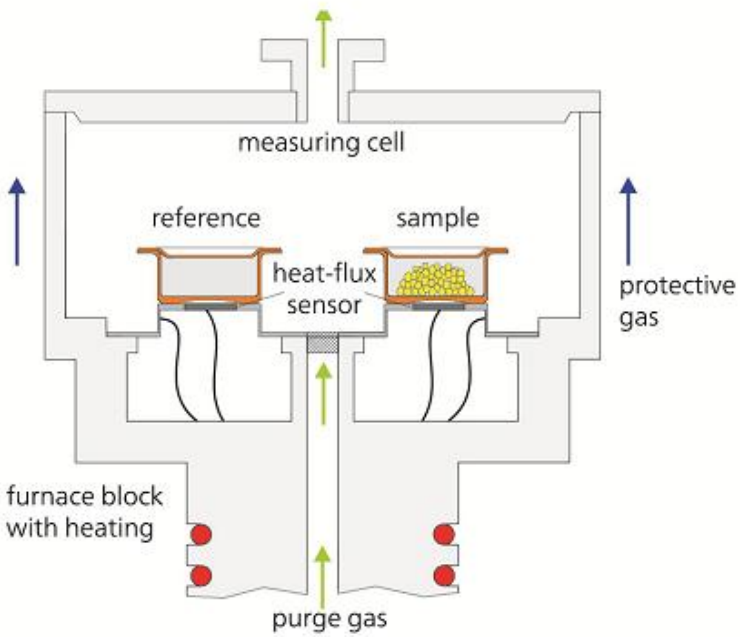

Figure 2.1: DSC scheme.

In the case of dynamic DSC, samples were subjected to a thermal cycle consistent of holding the samples at 200 °C for 5 min and subsequently cooling to 30 °C at four different cooling rates of 2, 5, 10 and 20 °C min^{-1}. After each cooling process, the samples were reheated to 200 °C at a rate of 10 °C min^{-1} (chapter 4).

Developed crystallinity (X_c) was calculated taking into account the weight fraction of the PHBV (ϕ), the enthalpy of crystallization of the composites (ΔH_c) and the melting enthalpy of a 100% crystalline PHBV (ΔH_{100} (109 J g^{-1})) [2], Eq. (1):

$$X_c = \frac{\Delta H_c}{\Delta H_{100} \cdot \phi} \cdot 100 \qquad (1)$$

Thermogravimetric analysis (TGA): The thermogravimetric analysis allows the study of the thermal degradation of the material as well as the calculation of the residual mass obtained at a certain temperature. The sample used for TGA is normally of few milligrams. The furnace must be controlled through software to insure the required rate for increasing the temperature. The thermal analysis can be done in an environment of different gases like nitrogen, oxygen, air and argon. During the test, the thermobalance records how the weight of the sample varies depending on the temperature or the time. The first derivation of the TGA curves is used for more depth understanding and analysis. The TGA is useful for the determination of decomposition temperature and the weight changes during the decomposition. Also it provides some information about composition of the sample or the percentage of water in some hydrophilic polymers.

In the present thesis, thermogravimetric analysis tests were conducted by a PerkinElmer TGA-7 instrument, USA (chapter 6). Degradation process was

monitored while samples were heated from 50 to 600 °C and were subjected to an inert atmosphere (argon) with flow rate of 20 mL min^{-1}.

2.2.2. Crystallinity analysis

X-ray scattering: This technique includes scattering of X-rays by a crystal which is the bases of X-ray crystallography which is used to determine the structure of crystals or molecules. The technique involves directing a beam of X-rays at a crystalline sample and recording the scattered X-rays on a photographic plate. The scattering pattern consists of a pattern of spots on the plate, and the crystal structure can be worked out from the positions and intensities of the diffraction spots. X-rays are scattered by the electrons in the sample. Based on the scattering pattern from the sample surface, crystalline structure, size, type and composition can be determined. In wide angle X-ray scattering (WAXS) measurements, the distance between sample and detector is short. So, diffraction peaks at larger angles are observed. Small angle X-ray scattering (SAXS) technique is the same as WAXS and the only difference is in the distance between the sample and the detector which is longer in the SAXS technique.

In the present thesis, WAXS patterns were performed using a Siemens D5000 (Siemens AG, Germany) diffractometer (chapters 3 and 6) with wavelength of the copper anode λ (K_α) = 1.5418 Å. The device was operating at a voltage of 40 kV and a current of 30 mA. Scanning was performed in the range of 2θ between 5° and 40° at a rate of 0.02° min^{-1}.

Time - resolved synchrotron for small and wide angle X-ray scattering: Another type of radiation which can be directed to the samples is synchrotron radiation which is occurred when charged particles like electrons are accelerated with very high speed even up to light speed in curved path with

specific magnetic fields. In this case, charged particles will emit synchrotron radiation or synchrotron light which is channeled down beamlines to experimental workstations where it is used for different researches such as analyzing the crystalline structure of the material.

In the present thesis, time - resolved synchrotron for small and wide angle X-ray scattering were done simultaneously at the BL-11 non-crystalline diffraction beamline of the ALBA synchrotron installation, Spain (chapters 4, 5 and 7). The scattering was detected using an ADSC (Quantum 210r CCD) and Rayonix (LX255-HS) as detectors. The parameters used in the experiments were incident wavelength λ = 1.2398 Å with a collection rate of 1 frame/1.5 s for WAXS and SAXS data. The calibration of spacing was obtained by means of silver behenate and chromium(III) oxide (Cr_2O_3) standards. Samples were packed in aluminum sheet and placed in a Linkam hot stage connected to liquid nitrogen flow. An empty aluminum sheet sample holder was used as background and subtracted from SAXS/WAXS profiles. Samples were quite thin to assure that temperature fluctuations in different depth of the samples were prevented. SAXS/WAXS experiments were performed meanwhile cooling and heating scans as defined in the DSC section. The simultaneous time evolution of the SAXS patterns was estimated from the Lorentz – corrected intensity.

2.2.3. Morphological aspects

Transmission electron microcopy (TEM): Transmission electron microscopy is a microscopy technique in which a beam of electrons is transmitted through a specimen to form an image. The specimen is most often an ultrathin section less than 100 nm thick or a suspension on a grid. An image is formed from the interaction of the electrons with the sample as the beam is transmitted through the specimen. The image is then magnified and focused onto an

imaging device, such as a fluorescent screen, a layer of photographic film, or a sensor such as a charge-coupled device. Transmission electron microscopes are capable of imaging at a significantly higher resolution than light microscopes. This enables the instrument to capture fine detail even as small as a single column of atoms, which is thousands of times smaller than a resolvable object seen in a light microscope. Transmission electron microscopy is a major analytical method in the physical, chemical and biological sciences. TEM is used in materials science as well as nanotechnology and semiconductors research. At lower magnifications, TEM image contrast is due to differential absorption of electrons by the material due to differences in composition or thickness of the material. At higher magnifications, complex wave interactions modulate the intensity of the image, requiring expert analysis of observed images.

In the present thesis, transmission electron microcopy images (chapters 3, 4 and 7) were taken with a JEOL JEM 2010 (JEOL Inc., USA) operating at an accelerated voltage of 100 keV.

Scanning electron microscopy (SEM): The scanning electron microscope allows high resolution images to be obtained in stony, metallic and organic materials. The light is replaced by a beam of electrons, the lenses by electromagnets and the non-conducting samples become conductive by metallizing their surface with specific metals such as gold (Au), silver (Ag), platinum (Pt) and iridium (Ir). The object to be observed is covered with conducting atoms. This layer of conducting atoms does not form a negative charge when the beam of high-energy electrons explores it. It interacts with the electron cloud of the sample and gives off low-energy electrons. A charged secondary electron detector immediately draws all low-energy electrons into

the interior of the tube. Each capture corresponds to a pixel in the image of the surface of the object.

The computer transforms the signal, variable from pixel to pixel, from the sweep of a surface into the corresponding visible image on a cathode ray tube. The raised points of the sample appear white on the screen; the low points appear dark. The points inclined towards the detector look a little brighter and those inclined in the opposite direction, somewhat more muted. Fig. 2.2 shows a scheme of a scanning electron microscope.

In the present thesis, scanning electron microscopy (SEM) images (chapters 3 to 7) were taken by a FESEM Ultra Plus microscope from ZEISS (ZEISS, Germany) in very high vacuum condition. A thin layer of iridium (Ir) coated surfaces of the films prior to observation with the microscope.

Polarized optical microscopy (POM): Polarized optical microscopy is a technique that employs polarized light to study the microstructure of materials. With the aid of POM, it is possible to observe the crystalline and the amorphous area of the polymers. This device uses polarized light, which is different from the light used by conventional optical microscopes. Normal light is not polarized, but it can be polarized. The polarization types can be categorized as linear, circular, and elliptical. In the case of the appearance of light as an in-plane wave, the polarization type is linear. When two waves with different amplitudes and 90° difference in phase go through space, then the polarization type is circular. Finally, when the phase difference value is not 90°, the polarization is elliptical.

In the present thesis, polarized optical microscopy (chapters 3 and 7) was performed with a Leica DM 2500 M microscope (Leica Microsystems GmbH, Germany). Samples were heated from room temperature to 200 °C with the

rate of 20 °C min^{-1} and equilibrated for 2 min to eliminate any crystals. Then cooled with rate of 20 °C min^{-1} until 120 °C and then with rate of 5 °C min^{-1} until 90 °C. Images were recorded during cooling step every 10 s.

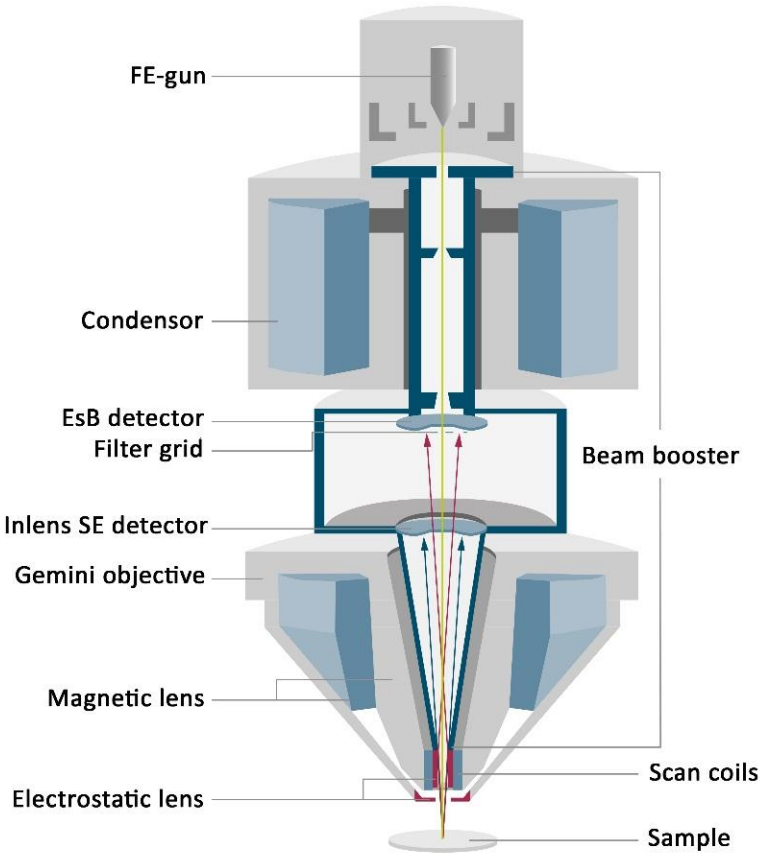

Figure 2.2: Scheme of a scanning electron microscope (SEM).

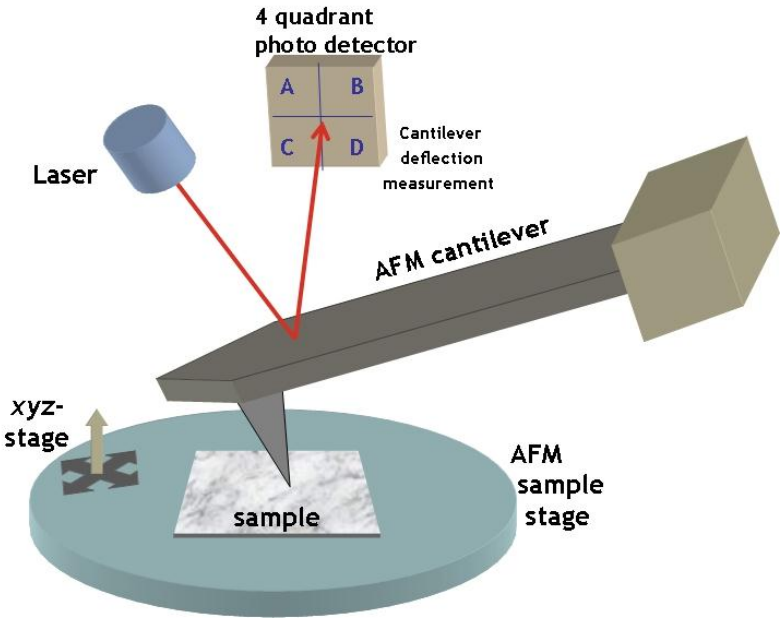

Figure 2.3: Scheme of an atomic force microscope (AFM).

Atomic force microscopy (AFM): Atomic force microscopy is a very high-resolution type of scanning probe microscopy with resolution in the order of nanometers. The information is gathered by feeling or touching the surface with a mechanical probe which is attached to a cantilever beam. The tip of the probe runs over the ridges and valleys in the material being imaged. By this way, it feels the surface. As the probe moves up and down due to the surface, the cantilever deflects. In one basic configuration, a laser shines on the cantilever at an oblique angle and allows for the direct measurement of the deflection in the cantilever by simply changing the angle of incidence of the laser beam. In this way, an image will be created revealing the configuration of the molecules being imaged by the machine. Fig. 2.3 shows a scheme of an AFM.

In the present thesis, atomic force microscopy measurements (chapters 3 and 7) were performed with a Micro-Thermal Analyzer, μTA 2990 microscope (TA Instruments, USA) to investigate the micro scale surface topography of the films. The samples were scanned in tapping mode in the air via Si cantilevers and the scan rate was 100 μm s^{-1}.

2.2.4. Mechanical properties

Tensile test: In a tensile test, a specimen is normally deformed until breaking, at constant strain rate. The tensile force is applied uniaxially along the axis of the specimen. The test machine is designed to measure the instantaneous force applied and the resulting elongation continuously and simultaneously. In a typical tensile test, the strength (σ) and strain (ε) data are obtained while testing at a constant temperature and strain rate. The obtained curves $\sigma = \sigma(\varepsilon)$ varying with the nature of the polymer and with the test conditions.

In the present thesis, tensile tests were performed (chapter 4) by an Instron 5566 universal mechanical testing machine (Instron, Canton, USA) at room temperature. Crosshead speed of the machine was 2 mm min^{-1}. The load cell was 1kN. Orthorhombic shape samples were used with dimensions of 70 mm x 4 mm x 1.5 mm. Young modulus (E) and strength and strain at yield point (σ_y and ε_y) were calculated from the resulting curves as the average of eight measurements for each sample.

Dynamic mechanical analysis (DMA): Dynamic mechanical analysis studies how the viscoelastic behavior of materials subjected to tension, extension or periodic deformation varies according to the temperature of the sample. During the test, a sinusoidal stress is applied on the sample and the resulted

strain is measured, allowing to determine the storage complex modulus. The temperatures of the sample or the frequency are often varied, leading to variations in the storage complex modulus. This approach is used to determine the glass transition temperature and other molecular motions of the material.

In the present thesis, dynamic mechanical properties were studied (chapter 6) with a dinamomechanical analyzer, DMA 7, from Perkin Elmer (USA) in the film extension mode. Storage modulus E', loss modulus E'' and damping factor tan $\delta = E''/E'$ were determined and recorded versus temperature during the test. Samples were cut in rectangular shape with dimensions of 20 mm x 4 mm. Thickness of the samples was measured in three points and averaged. To avoid thermal degradation, helium atmosphere was employed during tests. Temperature range was -70 °C to 60 °C with the heating rate of 2 °C min^{-1}. A static force of 300 mN and a dynamic force of 75 mN at the constant frequency of 1 Hz were applied to the film samples.

2.2.5. Barrier properties

Water vapor transmission rate (WVTR): water vapor transmission rate is considered as a vital factor for films in packaging industry. In this test, the amount of passed water vapor through the sample film which is in contact with two different relative humidity mediums is measured. Test is done under stable and specific temperature and pressure condition same as defined in related standards.

In the present thesis, water vapor transmission rate (chapters 3 to 7) was measured with a Permatran-W, model 1/50 G, Mocon equipment, (Mocon Inc., USA) complying ASTM E-398 standard. Smooth and uniform parts of film samples were selected. Masks with 5 cm^2 test area were used for putting samples in the cell of the equipment at 37.8 °C. Water vapor transmission rate

was calculated by counting passed molecules through the film every 30 min. Passed molecules were carried to counting part of the equipment by nitrogen carrying gas, which was purged continuously during the test. Tests were done until obtain steady line for transmission rate under a continuous mode (WVTR, in g $(m^2\ day)^{-1}$).

Oxygen transmission rate (OTR): In this test, the amount of passed oxygen gas through the sample film which is in contact with two different gas mediums (oxygen and another gas as carrying gas) is measured. Test is done under stable and specific temperature and pressure condition same as defined in related standards.

In the present thesis, oxygen transmission rate (chapter 3, 4 and 7) was investigated with an OX-TRAN, model 1/50 G, Mocon equipment (Mocon Inc., USA) complying ASTM D-3985 standard. Smooth and uniform parts of film samples were selected. Masks with 5 cm^2 test area were used for putting samples in the cell of equipment. Temperature of cell was 23 °C. One side of the film was exposed to dry oxygen flow with relative humidity of 0% and pressure of 27.7 psi. Then diffusion process of oxygen molecules to the film started. Oxygen transmission rate was calculated by counting passed molecules through the film every 30 min. Passed molecules were carried to counting part of the equipment by dry nitrogen carrying gas, which was purged continuously with the pressure of 28.1 psi during the test. Tests were done until obtain steady line for transmission rate under continuous mode (OTR, in $cm^3\ (m^2\ day)^{-1}$).

Carbon dioxide transmission rate (CDTR): In this test, the amount of passed carbon dioxide gas through the sample film which is in contact with two

different gas mediums (carbon dioxide and another gas as carrying gas) is measured. Test is done under stable and specific temperature and pressure condition same as defined in related standards.

In the present thesis, carbon dioxide transmission rate (chapters 4 and 7) was investigated with a Permatran-C, model 4/41, Mocon equipment (Mocon Inc., USA) complying ASTM F-2476 standard. Masks with 5 cm^2 test area were used for putting samples in the cells of the equipment. Temperatures of cells were 23 °C. One side of the films was exposed to dry carbon dioxide flow, relative humidity of 0%, with flow rate of 20 SCCM (standard cubic centimeters per minute). Then diffusion process of carbon dioxide molecules to the film started. Carbon dioxide transmission rate was calculated by counting passed molecules through the film every 30 min. Passed molecules were carried to counting part of the equipment by dry nitrogen carrying gas which was purged continuously with the flow rate of 20 SCCM during the test (CDTR, in cm^3 $(m^2$ $day)^{-1}$).

2.2.6. Humidity absorption

Gravimetric method was used for investigating the humidity absorption of the samples (chapters 5 and 6). Before starting the test, all samples were dried in oven at 70 °C. Then they were cooled by keeping in the sealed glass bottle containing relative humidity of 8% at 20 ± 2 °C. After that, sample species were placed in three different sealed glass bottles containing saturated salt solutions with specific different relative humidity of 54%, 75% and 95% as it is described in the UNE-EN ISO 483:1988. Further, in order to study the humidity absorption of the samples with PHBV matrix, they were merged in distilled water too. Consequently, they were permitted to absorb water until reaching a constant weight. They were taken out of the bottles in specific intervals and

their weights were recorded by time. All tests were done at room temperature (20 ± 2 ºC). The humidity absorption of the samples was calculated from equation (2):

$$HA\ (\%) = \frac{W_t - W_0}{W_0} \times 100 \qquad (2)$$

Where W_0 is the weight of the sample in dry state and W_t is the weight in the t time.

Samples with PHBV matrix were in bulk form while samples with starch matrix were in film form.

2.2.7. Accelerating artificial weathering

To simulate the environmental conditions to which the sample can be subjected in outdoor applications (UV radiation, temperature and humidity), an accelerated artificial weathering chamber was used.

In the present thesis, in order to study the effect of artificial weathering (chapter 5), a Xenotest arc-type equipment (Alpha LM-W instrument, Atlas, USA) was used. The samples were exposed to alternating cycles of UV light, rain, and dryness according to method A of testing standard ISO 4892-2:2013.

2.2.8. Antimicrobial studies

The antimicrobial activity of the samples was tested against food-borne pathogens (chapter 5). Assayed strains *Listeria monocytogenes* CECT 7467, *Escherichia coli* CECT434, *Salmonella enterica* CECT 4300, and *Staphylococcus aureus* CECT240 were obtained from the Spanish Type Culture Collection (CECT, Spain). Previous to each antimicrobial assay, a loopful of bacteria was transferred to 5 ml of BHI broth in the case of *L. monocytogenes* or TSB medium for the remaining strains and incubated at 37 °C overnight. Bacterial

suspension was inoculated onto the total surface petri plates prepared with the corresponding culture medium, now supplemented with 1.7% of agar, using a sterile swap. After 2 min, 100 mg of the samples with approximate dimensions of 30 mm x 5 mm x 3 mm, previously sterilized by microwave, were placed on the inoculated surface. Bacterial growth on the agar plates under the samples were examined after incubation at 37 °C for 24 h. Antimicrobial tests were performed in triplicate with individually prepared samples.

2.2.9. Biocompatibility studies

The biocompatibility studies of the samples were tested (chapter 5).

Cell culture

The mouse BALB/c macrophage cell line J774A.1 was a gift from Dr. Oreste Gualillo (Neuroendocrine Interactions in Rheumatology and Inflammatory Diseases, Institute of Biomedical Research of Santiago de Compostela, Spain). J774A.1 macrophages were cultured in Dulbecco's Modified Eagle Medium (DMEM) (Lonza Group Ltd, Switzerland) supplemented with 10% heat-inactivated fetal bovine serum (FBS) (Merck KGaA, Germany), 1% penicillin/streptomycin antibiotics and 1% L-glutamine (Sigma-Aldrich, USA) at 37 °C and 5% CO_2.

Preparation of PHBV and its nanocomposites for cell treatment

Chloroform diluted samples were centrifuged at 10.000 xg/5 min at room temperature. The samples were washed twice with ethanol 70° by centrifugation and re-suspended in 60 µL chloroform and 960 µL phosphate buffered saline (PBS, pH 7.4) sterile to reduce the amount of chloroform. For cell treatment, different concentrations of samples (1, 10, 100, 1000 µg/mL)

were added to the culture medium as previously described for 24 h [3]. As control of the chloroform effect on cells, the same amount of chloroform for each concentration of samples was added to the culture medium. To eliminate the effect of possible lipopolysaccharide (LPS) contamination in the samples, polymyxin B (10 µg/mL) (Sigma-Aldrich, USA) was added to the treatments to inhibit LPS signalling [4, 5].

MTT viability assay

Toxicity of the samples was determined using the 3-(4,5-dimethylthiazol-2-yl)-2,5-diphenyltetrazolium bromide (MTT) cell viability assay. MTT is a yellow compound that when reduced by functioning mitochondria, produces purple formazan crystals that can be measured spectrophotometrically. The quantity of formazan is presumably directly proportional to the number of viable cells and their metabolic activity [6]. For this purpose, J774A.1 macrophages were treated for 24 h with 1-1000 µg/mL samples and 4 h before the expiry of this period with 0.5 mg/mL MTT (Sigma-Aldrich, USA). After overnight incubation at 37°C, absorbance at 550 nm was measured in a microplate reader (MultiscanEX, Thermo Fisher Scientific, USA).

Nitrite assay

Nitrite accumulation was measured in the culture medium by Griess reaction. Briefly, after 24 h of J774A.1 macrophages incubation with 1-1000 µg/mL samples, 50 µL of cell culture medium was mixed with 50 µL of Griess reagent (equal volumes of 1% sulfanilamide in 5% phosphoric acid and 0.1% naphtylethylenediamine HCl) incubated at room temperature for 10 min and then the absorbance at 550 nm was measured in a microplate reader. Fresh culture medium was used as blank. The amount of nitrite production was

calculated from a sodium nitrite standard curve freshly prepared in culture medium. Lipopolysaccharide (LPS) 250 ng/mL (*E. coli serotype* O55:B5, Sigma-Aldrich, USA) was used as positive control and culture medium from untreated cells as negative control.

Statistical analysis

All experimental data were obtained from 6 independent experiments. Data are expressed as mean ± SEM. Statistical analysis was performed using the Wilcoxon signed-rank test as implemented in Prism 5 (GraphPad Software Inc., USA).

2.3. References

[1] R. P. Chartoff, A. K. Sircar, Thermal analysis of polymers: Encyclopedia of Polymer Science and Technology, Hoboken, NJ, USA: John Wiley & Sons, Inc. (2004)

[2] M. Scandola, M. L. Focarete, G. Adamus, W. Sikroska, I. Baranowska, S. Swierczek, M. Gnatowski, M. Kowalczuk, Z. Jedlinski, Polymer blends of natural poly (3-hydroxybutyrate-co-3-hydroxyvalerate) and a synthetic atactic poly (3-hydroxybutyrate). Characterization and biodegradation studies, Macromolecules, 30: 2568 (1997)

[3] J. P. Peñaloza, V. Marquez-Miranda, M. Cabaña-Brunod, R. Reyes-Ramirez, F. M. Llancalahuen, C. Vilos, F. Maldonado-Biermann, L. A. Velasquez, J. A. Fuentes, F. D. Gonzalez-Nilo, M. Rodriguez-Diaz, C. Otero, Intracellular trafficking and cellular uptake mechanism of PHBV nanoparticles for targeted delivery in epithelial cell lines, Journal of Nanobiotechnology, 15, 1, DOI:10.1186/s12951-016-0241-6 (2017)

[4] W. Harvey, M. Wilson, S. Meghji, In vitro inhibition of lipopolysaccharide-induced bone resorption by polymyxin B, The British Journal of Experimental Pathology, 67(5): 699-705 (1986)

[5] S. Kimakhe, D. Heymann, J. Guicheux, P. Pilet, B. Guimelli, G. Daculsi, Polymyxin B inhibits biphasic calcium phosphate degradation induced by lipopolysaccharide-activated human monocytes/macrophages, Journal of Biomedical Materials Research, 40(2): 336-340 (1998)

[6] T. L. Riss, R. A. Moravec, A. L. Niles, S. Duellman, H. A. Benink, T. J. Worzella, L. Minor, Cell Viability Assays, Assay Guid Man, 740: 33-43 (2004)

CHAPTER 3: Nanocomposites of PHBV/CNC: solvent cast film method

3.1. Introduction

As it was explained in the introduction chapter, biopolymers exhibit combined behavior. On the one hand they show expected eco-friendly properties as mentioned before and on the other hand they have some disadvantages like high price and less mechanical, thermal and barrier properties than petroleum based polymers. Also it was mentioned that these negative properties can be solved or promoted by taking some strategies. For example: copolymerization [1-3], blending with other polymers [4, 5] or introducing suitable fillers and nanofillers [6-10].

In this chapter, PHBV was selected as a biodegradable matrix due to its excellent biodegradability and biocompatibility properties and also because PHBV has capability for applications in the industry of food packaging. Also, as one of the most effective solutions to overcome undesired properties of biopolymers, the introduction of a nanofiller was selected. Cellulose nanocrystals were introduced to the PHBV matrix as green filler with approved effectiveness in biodegradable polymeric systems. It was believed that CNC might act as nucleating agent. Hydroxyl groups of CNC would interact via hydrogen bonds with carbonyl groups of PHBV and this would result in the modification of the matrix properties. Nanocomposite samples were prepared by solvent cast film method. The influence of cellulose nanocrystals concentration on crystallization and thermal, morphological and barrier properties (against oxygen and water vapor) is analyzed in detail.

3.2. Experimental

3.2.1. Materials and processing

Used materials were PHBV, CNC and chloroform.

Nanocomposites of PHBV/CNC with different concentration of CNC (2 wt.%, 4 wt.% and 6 wt.%) were prepared via solvent cast film method. PHBV was dried in an oven at 70 °C for 24 h before using and then dissolved in chloroform at 50 °C for 1 h. CNC suspension in chloroform was added to PHBV solution and was ultra-sonicated in an ice bath for 1 h. Subsequently, the mixture was placed in a petri dish and was left overnight for evaporation the solvent at room temperature. All films were kept in desiccator with silica gel for one week prior to do any experiments.

3.2.2. Characterization techniques

Used characterization techniques were DSC, WAXS, TEM, SEM, POM, AFM, WVTR (sample thickness 40 μm, relative humidity of 10% and 100% in both sides) and OTR (sample thickness 80 μm).

3.3. Results and discussions

3.3.1. Thermal properties and crystallization

In order to study the effect of the CNC particles in thermal properties and crystallization behavior of the nanocomposites, DSC test was done. Fig. 3.1a gives DSC crystallization exotherms of neat PHBV and its nanocomposites with different concentrations of CNC obtained during cooling from 200 °C to 30 °C at 10 °C min^{-1}. Table 3.1 summarizes the thermal parameters. The presence of CNC on the crystallization behavior of PHBV implies a shift of the crystallization peak temperature to higher temperatures. T_c increases by 5 °C for the nanocomposite with 2 wt.% of CNC. The addition of CNC had a heterogeneous nucleation capacity to accelerate the crystallization process of PHBV. However, for the 4 wt.% of CNC, the shift in T_c is lower than that

observed for 2 wt.% of CNC composites. This may attribute to more restricted molecular movement of PHBV chains due to the formation of hydrogen bonds. Hydrogen bonds made CNC particles and PHBV chains to connect to each other via electrostatically interactions between hydrogen in OH groups of CNC and nitrogen in carbonyl groups of PHBV. This would reduce free mobility of polymeric chains. In fact, the presence of particles of CNC involves a high number of hydrogen bonds acting as a barrier to the free movement and folding of polymer chains, which induces a limitation on the growth of polymer crystals [11-13]. In the sample with 6 wt.% of CNC due to poor dispersion of CNC, agglomerates are formed. The presence of these agglomerates produced an impediment to the formation of hydrogen bonds between hydrogen in OH groups of CNC and nitrogen in carbonyl groups of PHBV. Subsequently, poor dispersion of CNC nanoparticles happened in this sample.

The values of crystallinity of these composites increase with the increase of filler content, although the differences are small (between 49.9 % and 57.5 %) [14, 15].

As DSC heating curves demonstrate, bimodal endothermic melting peaks could be seen for all the samples. The first and second melting peaks of nanocomposites shift to higher temperatures than those of the neat PHBV, Fig. 3.1b. The lower one was referred to melting of the crystals with low perfection and thinner lamella and the higher one was related to melting of more perfect recrystallized crystals [16].

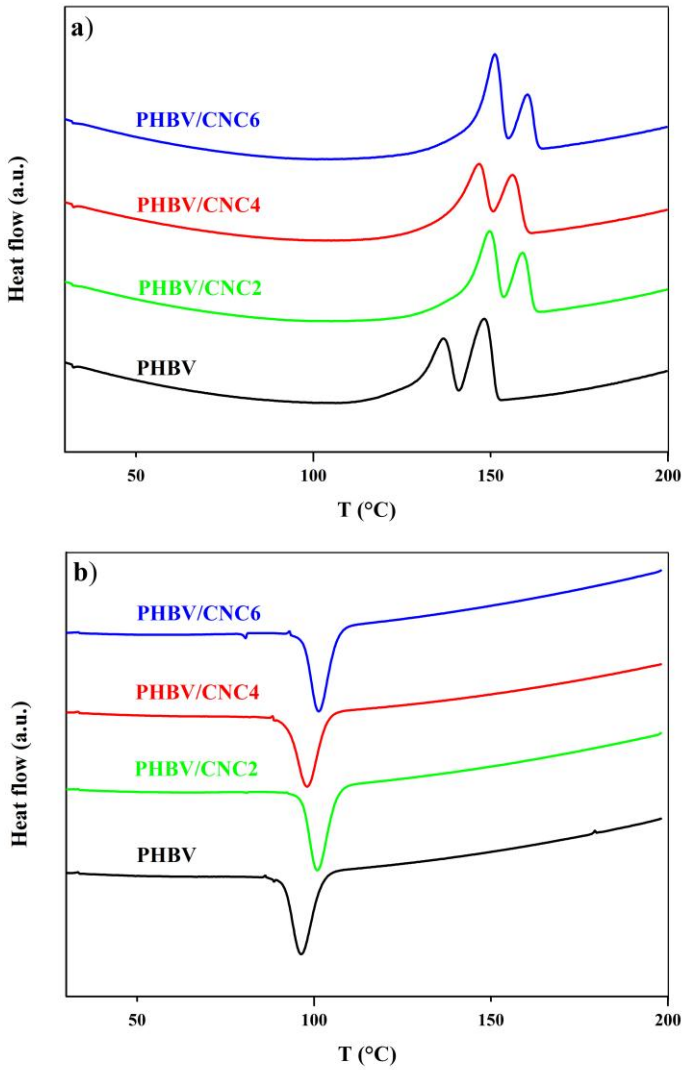

Figure 3.1: DSC thermograms during cooling from the melt (a) and posterior heating (b) of neat PHBV and PHBV/CNC nanocomposites.

In the case of PHBV, the formed crystals are more perfect. The lower melting peak can be attributed to the melting of the original crystals and the higher

melting peak can be attributed to the new generated crystals. With the addition of CNC, there is a change in the ratio of the intensities of the melting peaks. The CNC acts as a heterogeneous nucleation agent of PHBV, inducing greater rate of crystallization. Therefore, smaller crystals are formed which leads to an increase in the area of the low temperature melting peak. The new perfect crystals are more difficult to subject to melting-crystallization-melting, decreasing the peak area at high temperature with the amount of CNC, Fig. 3.1b.

Table 3.1: Thermal parameters of non-isothermal crystallization and melting process of neat PHBV and its nanocomposites.

Sample	**T_c (°C)**	**T_{m1} (°C)**	**T_{m2} (°C)**	**ΔH_c (J g^{-1})**	**X_c (%)**
PHBV	96.5	136.8	148.3	54.3	49.9
PHBV/CNC2	101.0	149.6	159.1	56.4	51.7
PHBV/CNC4	98.0	146.8	156.3	58.3	53.5
PHBV/CNC6	101.2	151.1	160.4	62.7	57.5

3.3.2. Crystal structure

Wide-angle X-ray scattering (WAXS) diffractograms of neat PHBV, CNC and PHBV/CNC nanocomposites are performed to determine whether incorporation of CNC affects the crystal structure. The main characteristic diffraction peaks of PHBV and its composites can be observed in Fig. 3.2. The diffraction peaks at 2θ = 13.4° and 17° correspond to planes (020) and (110) characteristic of orthorhombic PHBV α – type structure [17]. Comparison

between diffractograms of neat polymer and its nanocomposites shows that WAXS patterns were similar, new peaks do not appear and they do not shift to higher or lower angles in the nanocomposites. PHBV exhibits the unusual phenomenon of bijective morphism, since can crystallize in any PHB unit cell or PHV unit cell [18]. It has been reported that 2θ = 17° is associated with the (110) diffraction of PHB type lattice and 2θ =18° corresponding to the (020) diffraction of PHV type lattice [19]. No diffraction peak appears at 2θ = 18° in any of the samples, so there is only PHB type lattice for both PHBV and its composites.

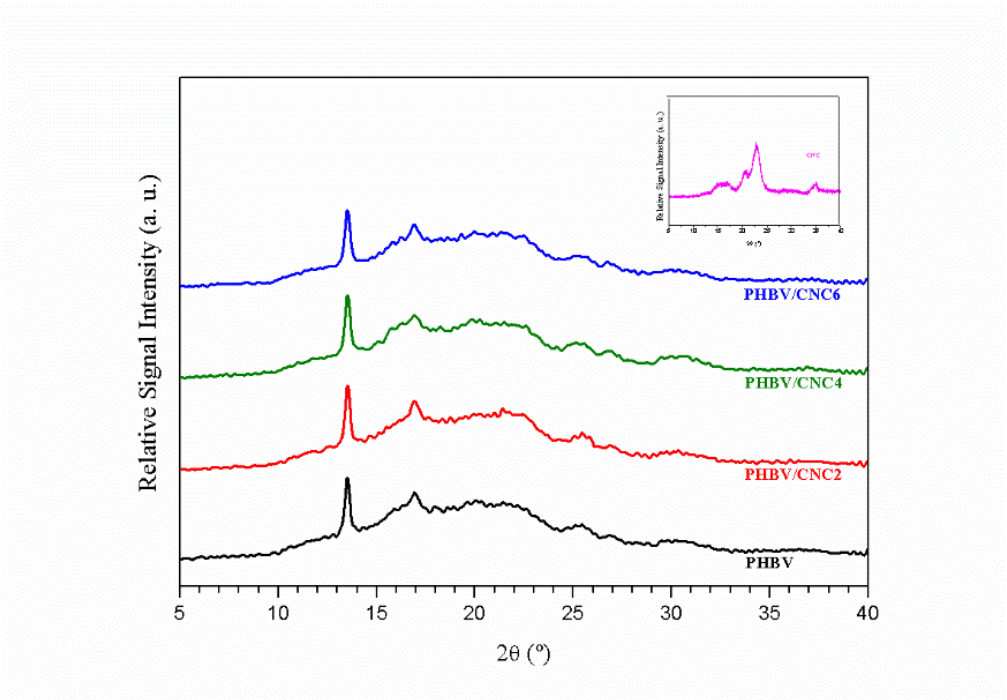

Figure 3.2: WAXS patterns of neat PHBV, CNC and PHBV/CNC nanocomposites.

3.3.3. Morphology of the nanocomposites

As it is well known, the state of dispersion of the filler has a significant role on the final properties of the composites. This depends on several parameters like interactions between filler and matrix, method of preparation of the samples and filler concentration. Besides, it is well accepted that a poor dispersion can result in a weaker performance of the polymer composites than unfilled polymer. In this regard, for study the morphology and the dispersion state of CNC in the PHBV matrix, TEM was done and related images are shown in Fig. 3.3. PHBV and CNC images are shown in Fig. 3.3a and Fig. 3.b. As Fig 3.3c shows, individual well dispersed nanoparticles can be observed in the nanocomposite with 2 wt.% of CNC. Considering TEM images of nanocomposites with 4 wt.% and 6 wt.% of CNC, it can be seen that whereas relatively slight jammed particles were appeared in nanocomposite with 4 wt.% of CNC (Fig. 3.3d), more percentage of denser agglomerations with bigger size were identified in sample with 6 wt.% of CNC (Fig. 3.3e). The nanocomposite with 4 wt.% of CNC had homogeneous and uniform dispersion of the embedded particles.

In order to study the surface morphology of the films, SEM was carried out. SEM image of unfilled PHBV matrix shows a porous morphology with many visible open volumes in the entire sample (Fig. 3.4a). The incorporation of 2 wt.% of CNC in PHBV matrix led to reduce pore size (Fig. 3.4b). This change was intensified significantly with increasing CNC concentration up to 4 wt.%. In the sample with 4 wt.% of CNC nearly compact morphology with no pores can be seen (Fig. 3.4c). It can be explained by hydrogen bonds between OH groups in the filler and carbonyl groups in the biopolymer. These bonds extended in all directions in the sample due to the good dispersion of nanoparticles in the PHBV matrix. So, it could be said that CNC nanoparticles and PHBV chains

connected to each other through hydrogen bonds in all parts of the sample. In this case, hydrogen bonds could have effect of compatibilizer. They enhanced compatibility between filler and matrix and acted as bridges for connecting PHBV chains, increasing the length of the PHBV chains, reducing the free volume in the matrix and covering the pores. By contrast, when concentration is 6 wt.% of CNC, there are agglomerations and the pores can be seen again (Fig. 3.4d).

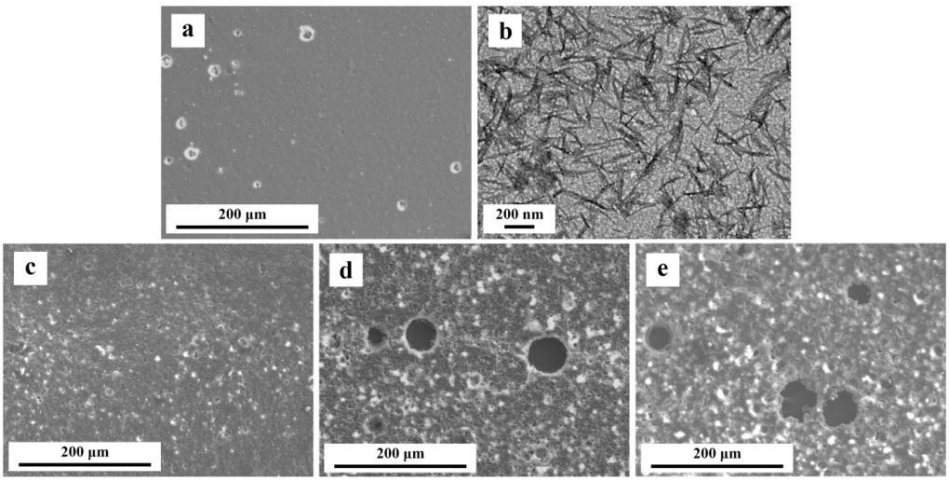

Figure 3.3: TEM images of neat PHBV (a), CNC (b), PHBV/CNC2 (c), PHBV/CNC4 (d) and PHBV/CNC6 (e).

Image J software was used to measure mean pore diameters in all samples. Mean pores diameter for neat polymer and nanocomposites with 2 wt.% and 6 wt.% of CNC were 2.2 µm, 1.3 µm and 1.7 µm, respectively. Obviously, there is no pore in the sample with 4 wt.%. So, the software could not measure the pores diameter for mentioned sample correctly. Similar results were reported elsewhere for PHBV/graphene [20] and PLA/graphene nanocomposites [21].

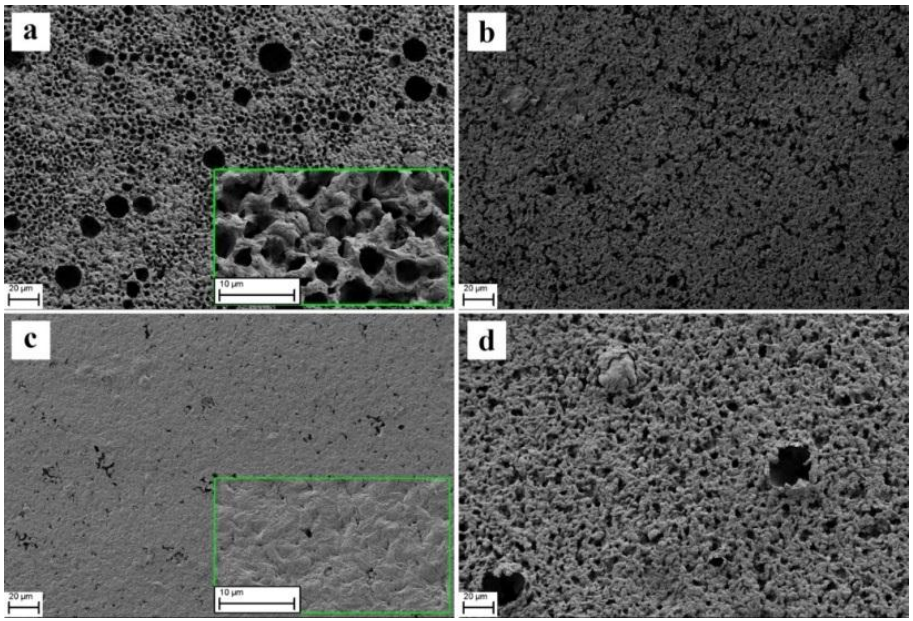

Figure 3.4: SEM images of neat PHBV (a), PHBV/CNC2 (b), PHBV/CNC4 (c) and PHBV/CNC6 (d).

Direct POM monitoring was applied in order to investigate the spherulitic morphology of the samples and the nucleating impact of CNC particles in the PHBV matrix. During cooling step, photos were taken and some of them are given in Fig. 3.5. It can be easily observed that neat PHBV contains less quantity of spherulites with bigger size and more perfect appearance whereas more spherulites with smaller size and more imperfections were formed in the nanocomposites samples. In neat PHBV, more space was available for spherulites for radial growing uniformly before they contact each other. By other hand, in the samples with CNC particles, this space was restricted due to increment of the spherulites quantities, which acted as barrier for neighbor growing spherulites. Results showed this restriction was amplified with

enhancement of the concentration of the particles significantly and small disordered spherulites were formed consequently. Fig. 3.5a-d shows morphology of spherulites at 105 °C (a few seconds before the end of crystallization process). Higher density and accelerated growing rate of the spherulites in all the samples with 2 wt.%, 4 wt.% and 6 wt.% of CNC in comparison with neat polymer, confirmed the role of CNC as nucleating agent (Fig. 3.5b and 3.5d). Although, there is a mobility restriction of polymer chains, which were connected to each other by hydrogen bonds in the sample with 4 wt.% of CNC, acting as an obstacle for forming crystalline zones (Fig. 3.5c). In other words, hydrogen bonds limited the mobility of the polymeric chains dramatically through enhancement in the length of the PHBV chains by connecting them to each other and as a result more entanglements in the matrix and because of this, slower nucleating and growing of the spherulites happened in this sample than for the sample with 2 wt.% of CNC. Fig. 3.5e-h shows morphology of spherulites at 100 °C. From these images, it can be concluded that while decreasing temperature to 100 °C, growing procedure of the spherulites finished completely for neat PHBV and nanocomposites with 2 wt.% and 6 wt.% of CNC (Fig. 3.5e, 3.5f and 3.5h). Sample with 4 wt.% of CNC (Fig. 3.5g) required more time for finalization of crystallization process. Fig. 3.5k presents completed growing process of this sample, which occurred at 97.6 °C. It is notable that POM results are in great agreement with DSC findings.

To complete the morphological study aspects, AFM was performed and images of surface topography of all samples are displayed in Fig. 3.6. This figure suggests that surface of neat polymer was nearly plain and smooth. After incorporation of the CNC particles in the matrix and with increasing the amount of CNC, smoothness of the surface of the films was affected.

Therefore, more roughness can be observed in the images of the nanocomposites. This was intensified with increasing the concentration up to 4 wt.% of CNC. It is worth to mention that obtained information from TEM, SEM, POM and AFM agreed reasonably well.

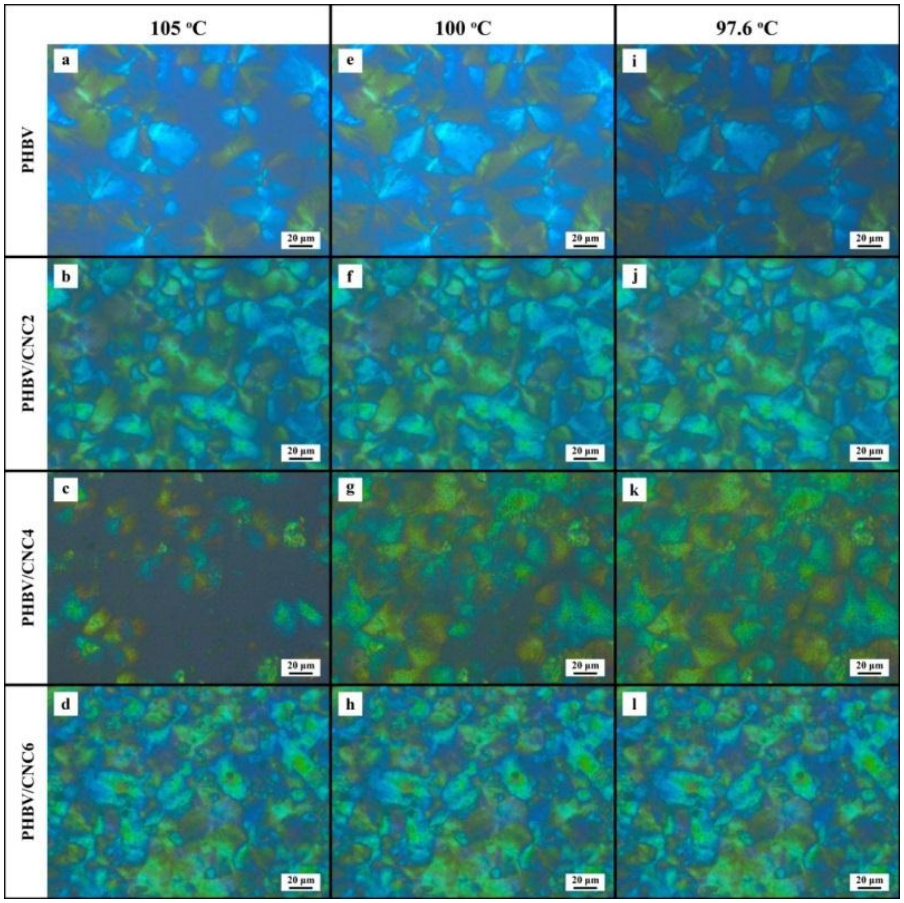

Figure 3.5: POM images of neat PHBV, PHBV/CNC2, PHBV/CNC4 and PHBV/CNC6 at 105 °C (a-d), 100 °C (e-h) and 97.6 °C (i-l).

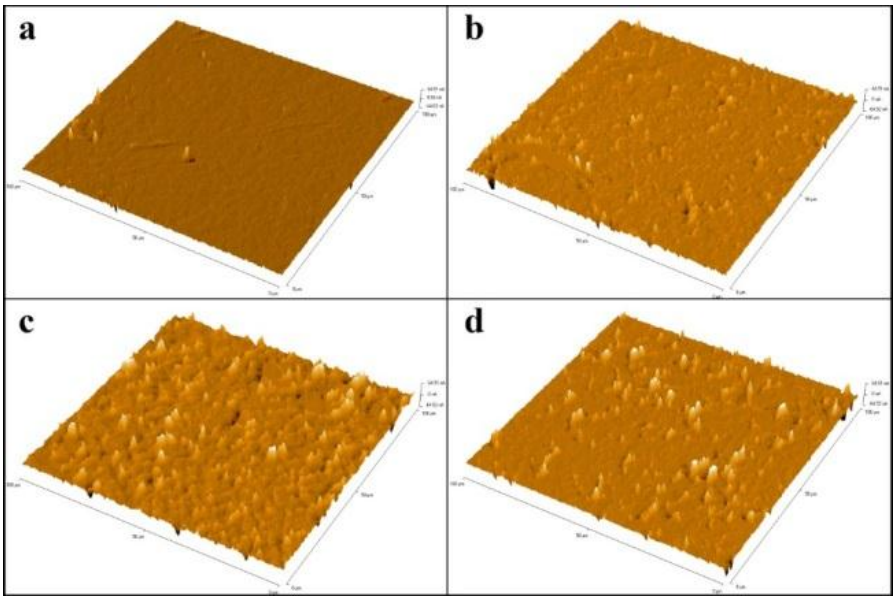

Figure 3.6: AFM images of neat PHBV (a), PHBV/CNC2 (b), PHBV/CNC4 (c) and PHBV/CNC6 (d).

3.3.4. Water vapor and oxygen transmission rate

Shelf life, safety and health of the packaged food are strongly affected by the humidity content inside packaging, because humidity is one of the necessary factors, which provide suitable environment for undesired microorganisms to grow. Therefore, one of the followed aims of incorporating nanoparticles in polymeric matrices is reducing water vapor and oxygen transmission rate of final product. In this regard, water vapor and oxygen transmission rate of neat PHBV and PHBV/CNC nanocomposites were studied and results are presented in Fig. 3.7. As Fig. 3.7 presents, water vapor and oxygen transmission rate of PHBV were reduced dramatically upon incorporation of CNC nanoparticles. This can be explained by modified crystallization of PHBV and existence of

more crystalline zones and consequently, more tortuosity. These zones increased tortuosity in the matrix and can act as barriers for running water vapor and oxygen molecules and limit their pathways. Therefore, transmission rate of nanocomposites dropped dramatically. As mentioned above, this means eliminating or reducing one of the required parameters for growing undesired bacteria and microbial organisms inside food packaging. This is significantly helpful for extending storing time of packaged foods. In reference to the results of SEM, it can be stated that water vapor and oxygen transmission rate results were expected due to notable changes occurred in the morphology of nanocomposites in comparison with neat polymer. As it was shown there, large number of pores and cavities in neat PHBV were approximately disappeared in nanocomposites with 4 wt.% of CNC. It is clear that low permeation of the nanocomposite with 4 wt.% of CNC was result of its compatibilized morphology through hydrogen bonds which led to formation of a more compact morphology with less free volumes, less pores and longer PHBV chains with more entanglements and also, increased crystallinity. While CNC content is higher than 4 wt.%, water vapor and oxygen transmission rate parameters increased slightly, which can be due to weak dispersion and formation of agglomerations of CNC nanoparticles. Although these transmission rate values were still well below the unfilled polymer. In total, it can be stated that all morphology results agree well with water vapor and oxygen transmission rate values.

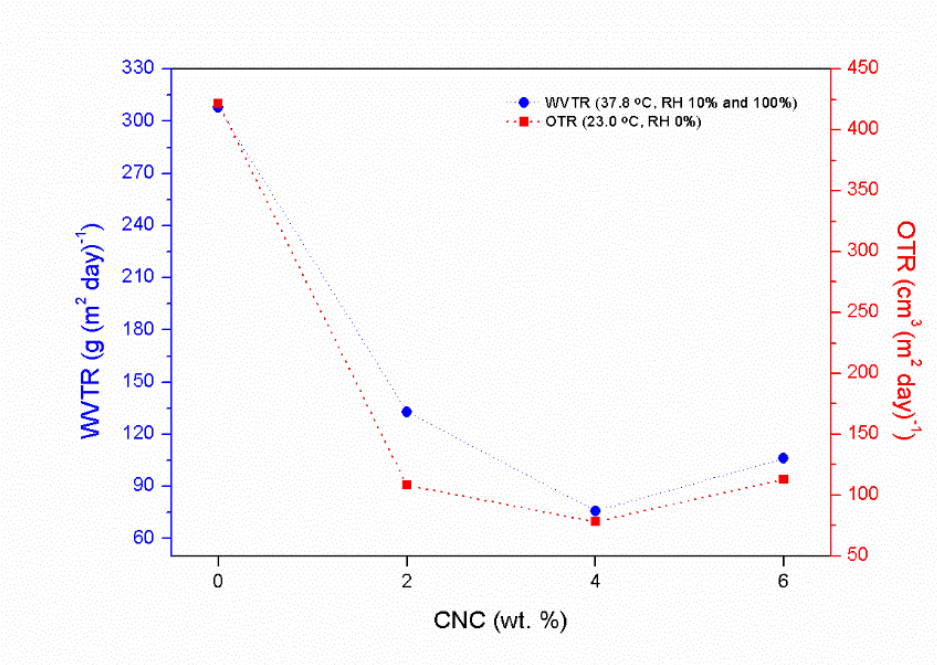

Figure 3.7: Water vapor and oxygen transmission rate against CNC content for neat PHBV and PHBV/CNC nanocomposites.

3.4. Conclusions

Thermal properties and crystallization behavior of PHBV/CNC nanocomposites prepared by solvent cast film method were studied. DSC results showed that during cooling scan step, crystallization process started earlier and continued with higher rate in nanocomposites in comparison with neat polymer. This confirmed the nucleating agent effect of CNC in PHBV matrix. Moreover, the CNC did not modify the crystalline structure of PHBV as was shown by WAXS. TEM images clearly showed the homogeneous distribution of the CNC particles in the matrix in concentrations of the 2 wt.% and 4 wt.% of CNC, although in the latter case slight jammed particles appeared. Whereas with increasing

concentration up to 6 wt.% of CNC, presence of agglomerations was clear. SEM results revealed a considerable change in the morphology of all samples, from porous morphology for neat PHBV to very compact morphology for the nanocomposite with 4 wt.% of CNC. It was assigned to compatibilizing effect of CNC nanoparticles by forming hydrogen bonds that acted as bridges for connecting PHBV chains and cover pores. Good dispersion of CNC nanoparticles in the PHBV matrix in this nanocomposite caused bridging effect of CNC to occur in all parts and directions in the sample. Obtaining porous morphology happened once again in the highest concentration. POM results demonstrated reduction in size and increment in the quantity of the spherulites in the nanocomposites in comparison with neat PHBV. Consequently, it confirmed nucleating agent role of CNC particles clearly. Monitoring the growth of the spherulites in cooling profile of POM also suggested accelerated growth of the spherulites for all the nanocomposites. Although the nanocomposite with 4 wt.% of CNC showed slower rate of spherulites growth because of restricted free mobility of polymeric chains. Obtained results by AFM indicated that incorporating CNC modified the topography of the surface of the PHBV from nearly smooth to rough for nanocomposites. Roughness of the surface of the samples was intensified with increasing CNC concentration. Due to high importance of barrier properties for packaging materials, water vapor and oxygen transmission rate of PHBV and its nanocomposites were studied. Obtained results exhibited notable promotion in barrier properties of nanocomposites in comparison with neat polymer. This was explained by modified crystallinity of nanocomposites and more tortuosity in their morphology. Increased barrier properties were obtained for all nanocomposites in comparison with neat polymer. The

explanation of thermal properties, crystallization and barrier properties agree well with all morphological study.

3.5. References

[1] L. Pilon, C. Kelly, Modification of poly (3-hydroxybutyrate-co-3-hydroxyvalerate) properties by reactive blending with a monoterpene derivative, Journal of Applied Polymer Science, 133: DOI: 10.1002/APP.42588 (2016)

[2] D. Moorkoth, K. M. Nampoothiri, Production and characterization of poly (3-hydroxybutyrate-co-3 hydroxyvalerate) (PHBV) by a novel halotolerant mangrove isolate, Bioresource Technology, 201: 253 (2016)

[3] S. C. Napathorn, Biocompatibilities and biodegradation of poly (3-hydroxybutyrate-co-3-hydroxyvalerate)s produced by a model metabolic reaction-based system, BMC Microbiology, 14: 285 (2014)

[4] S. H. El-Taweel, M. Khater, Mechanical and Thermal Behavior of Blends of Poly (hydroxybutyrate-co-hydroxyvalerate) with Ethylene Vinyl Acetate Copolymer, Journal of Macromolar Science Part B: Physics, 54: 1225 (2015)

[5] N. Jiang, H. Abe, Miscibility and morphology study on crystalline/crystalline partially miscible polymer blends of 6-arm poly (l-lactide) and poly (3-hydroxybutyrate-co-3-hydroxyvalerate), Polymer, 60: 260 (2015)

[6] A. M. Diez-Pascual, A. L. Diez-Vicente, ZnO-reinforced poly (3-hydroxybutyrate-co-3-hydroxyvalerate) bionanocomposites with antimicrobial function for food packaging, Applied Materials and Interfaces, 6: 9822 (2014)

[7] L. Jiang, E. Moreluis, J. Zhang, M. Wolcott, J. Holbery, Study of the poly (3-hydroxybutyrate-co-3-hydroxyvalerate)/cellulose nanowhisker composites prepared by solution casting and melt processing, Journal of Composite Materials, 42: 2629 (2008)

[8] V. Sridhar, I. Lee, H. H. Chun, H. Park, Graphene reinforced biodegradable poly (3-hydroxybutyrate-co-3-hydroxyvalerate) nanocomposites, Polymer Letters, 7: 320 (2013)

[9] H. Y. Yu, Z. Y. Qin, B. Sun, X. G. Yang, J. M. Yao, Reinforcement of transparent poly (3-hydroxybutyrate-co-3-hydroxyvalerate) by incorporation of functionalized carbon nanotubes as a novel bionanocomposite for food packaging, Composite Science & Technology, 94: 96 (2014)

[10] R. Hema, P.N. Ng, A.A. Amirul, Green nanobiocomposites: reinforcement effect of montmorillonite clays on physical and biological advancement of various polyhydroxyalkanoates, Polymer Bulletin, 70(3): 755 (2013)

[11] B. Wang, J. Li, J. Zhang, H. Li, P. Chen, Q. Gu, Z. Wang, Thermo-mechanical properties of the composite made of poly (3-hydroxybutyrate-co-3-hydroxyvalerate) and acetylated chitin nanocrystals, Carbohydrate Polymers, 95: 100 (2013)

[12] H. Y. Yu, Z. Y. Qin, L. Liu, X. G. Yang, Y. Zhou, J. M. Yao, Comparison of the reinforcing effects for cellulose nanocrystals obtained by sulfuric and hydrochloric acid hydrolysis on the mechanical and thermal properties of bacterial polyester, Composite Science and Technology, 87: 22 (2013)

[13] H. Y. Yu, Z. Y. Qin, Y. N. Liu, L. Chen, N. Liu, Z. Zhou, Simultaneous improvement of mechanical properties and thermal stability of bacterial polyester by cellulose nanocrystals, Carbohydrate Polymers, 89: 971 (2012)

[14] E. Ten, J. Turtle, D. Bahr, L. Jiang, M. Wolcott, Thermal and mechanical properties of poly (3-hydroxybutyrate-co-3-hydroxyvaletare)/cellulose nanowhiskers composites, Polymer, 54: 2653 (2010)

[15] Y. Houyong, S. Bin, Z. Dongzi, C. Guoyin, Y. Xingyuan, Y. Juming, Reinforcement of biodegradable poly (3-hydroxybutyrate-co-3-hydroxyvaletare) with cellulose nanocrystal/silver nanohybrids as bifunctional nanifillers, Journal of Material Chemistry B, 2: 8479 (2014)

[16] N. Lin, H. Jin, P. R. Chang, J. Feng, J. Yu, Surface acetylation of cellulose nanocrystal and its reinforcing function in poly (lactic acid), Carbohydrate Polymers, 83(4): 1834 (2011)

[17] A. J. Owen, J. Heinzel, Z. Skrbic, V. Divjakovic, Crystallization and melting behaviour of PHB and PHB/HV copolymer, Polymer, 33(7):1563 (1992)

[18] T. L. Bluhm, G. K. Hamer, R. H. Marchessault, C. A. Fyfe, R. P. Veregin, Isodimorphism in bacterial poly (β-hydroxybutyrate-co-β-hydroxyvalerate), Macromolecules, 19(11): 2871 (1986)

[19] W. Qiu, T. Endo, T. Hirotsu, A novel technique for preparing of maleic anhydride grafted polyolefins, European Polymer Journal, 41(9): 1979 (2005)

[20] J. A. Martin, G. Gorrasi, López-Rubio, M. J. Fabra, L. C. Mas, M. A. López-Manchado, J. M. Lagaron, On the use of ball milling to develop PHBV–graphene nanocomposites (I)—Morphology, thermal properties, and thermal stability, Journal of Applied Polymer Science, 132: DOI:10.1002/APP.42101 (2015)

[21] I. H. Kim, Y. G. Jeong, Polylactide/exfoliated graphite nanocomposites with enhanced thermal stability, mechanical modulus, and electrical conductivity, Journal of Polymer Science Part B, 48(8): 850 (2010)

CHAPTER 4: Characterization and properties of extruded nanocomposites of PHBV/CNC

4.1. Introduction

Based on the effective role of CNC in PHBV matrix, it was concluded that CNC can improve the properties of PHBV matrix. In the previous chapter, incorporation of CNC particles in a PHBV matrix by solvent cast film method led to considerable improvements in crystallinity and thermal and barrier properties with respect to the PHBV. Thus, in order to further study the PHBV/CNC nanocomposites, a different method of sample preparation was selected in the present chapter. Also it was aimed to do some different complementary analysis.

In the present chapter, the crystallization behavior of PHBV and PHBV/CNC nanocomposites as well as morphological, mechanical and barrier properties against water vapor, oxygen and carbon dioxide were studied in detail. Structural changes of the nanocomposites were analyzed by SAXS/WAXS during dynamic crystallization. The impact of incorporation of cellulose nanocrystals in the matrix of PHBV was investigated in order to progress in the knowledge about application of these nanocomposites in food packaging. The goal of this study was to achieve well-dispersed nanocomposites with improved mechanical and barrier properties.

4.2. Experimental

4.2.1. Materials and processing

Used materials were PHBV and CNC.

Nanocomposites of PHBV/CNC with different content of CNC (2 wt.%, 4 wt.% and 6 wt.%) were prepared via extrusion. PHBV was dried in an oven at 70°C for 24 h before using. PHBV and CNC were melt mixed in a twin-screw mini-extruder (Haake Force Feeder Minilab II, Germany) with a rate of 60 rpm for

10 min at a temperature of 165 °C. Then, PHBV/CNC nanocomposites were cooled to room temperature. The samples for barrier tests were prepared by compression molding (IQAP LAB PL – 15, Spain) at 165 °C and 150 bar of pressure with thickness of 100 μm.

4.2.2. Characterization techniques

Used characterization techniques were dynamic DSC, time - resolved synchrotron X – ray scattering (rate of 2 °C min^{-1} was selected for cooling scan), TEM, SEM, tensile, WVTR (relative humidity of 10% and 100% in both sides), OTR and CDTR.

For further evaluation of the differences in the mechanical properties of the samples by filler loading, one-way analysis of variance (ANOVA) was done. In this regard, Young modulus, strength at yield point and strain at yield point were selected to analyze.

4.3. Results and discussion

4.3.1. Dynamic crystallization behavior

The crystallization behavior of PHBV and PHBV/CNC nanocomposites was studied under dynamic condition as a function of the cooling rate and the amount of CNC. As was indicated in the experimental part, the PHBV and its nanocomposites with CNC were tested under four dynamic conditions from 200 °C to 30 °C at different rates between 2 and 20 °C min^{-1}. From the thermograms, the parameters of the crystallization temperature (T_c) and crystallinity (χ_c) calculated by Eq. 1 in the previous chapter. Table 4.1 lists the results. Fig. 4.1 shows the cooling curves and the conversion curves as

function of temperature obtained while the PHBV and PHBV/CNC nanocomposites with 2 wt.%, 4 wt.% and 6 wt.% of CNC were cooled at different rates. For all samples studied, higher crystallization temperatures (T_c) and narrower crystallization exotherms at slower cooling rates were obtained. At faster cooling rates, the chain mobility was impeded due to this fact that the time is no sufficient for organize the polymer chains.

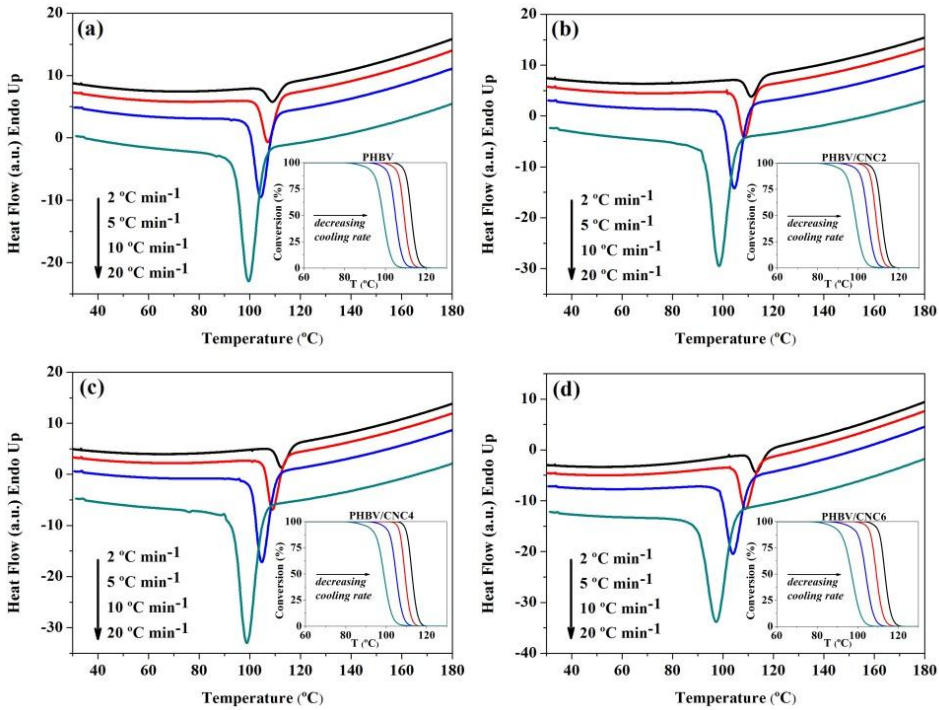

Figure 4.1: DSC thermograms for dynamic crystallization of PHBV (a), PHBV/CNC2 (b), PHBV/CNC4 (c), PHBV/CNC6 (d) at indicated cooling rates.

It can be observed that the incorporation of little amounts of CNC into the PHBV led to the temperatures of crystallization shift to higher temperatures

for all cooling rates, this being more evident at slower cooling rates. Although, only at the slowest cooling rate (2 °C min^{-1}), the crystallization temperature was noticeably affected by the addition of CNC. These results suggest that CNC, at very low percentages, behaves as an effective nucleating agent in PHBV matrix. The variation described in the crystallization temperatures of the PHBV/CNC nanocomposites is accompanied by changes in the crystallinity. The higher values of crystallinity were obtained at slower crystallization rates because the polymer chains have more time to be organized.

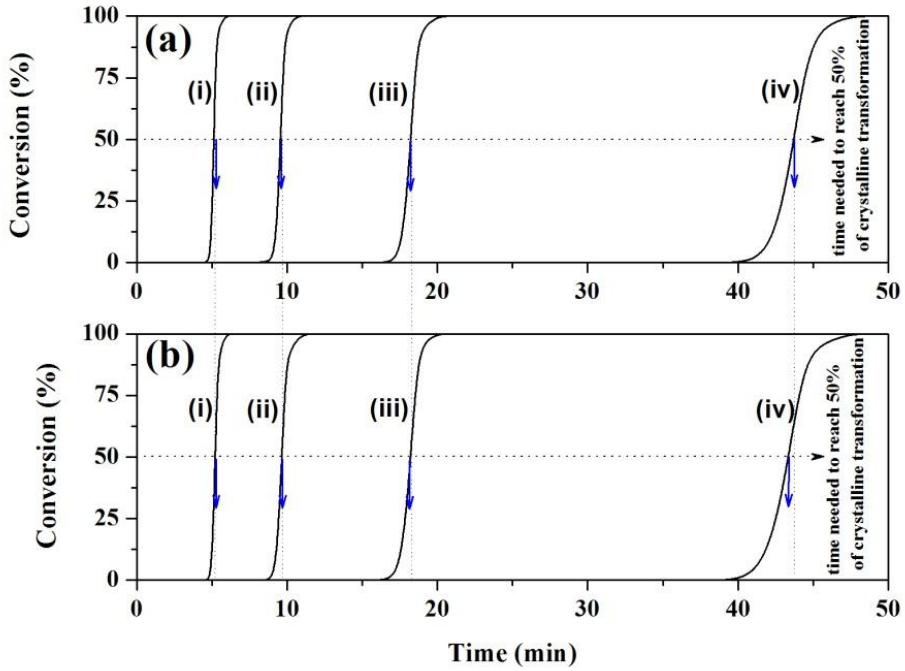

Figure 4.2: Conversion versus time curves for PHBV (a) and PHBV/CNC6 (b) at 20 °C min^{-1} (i), 10 °C min^{-1} (ii), 5 °C min^{-1} (iii) and 2 °C min^{-1} (iv) cooling rates.

The evolution of the crystallization process from the melt state was followed by conversion curves as a function of temperature for the various cooling rates analyzed.

Table 4.1: Dynamic crystallization parameters for PHBV and PHBV/CNC nanocomposites.

CNC (wt.%)	Cooling rate (°C min^{-1})	T_c (°C)	$\chi_{c\ (DSC)}$
0	20	99.6	47.7
	10	104.3	52.0
	5	107.1	54.0
	2	109.0	55.1
2	20	98.6	49.3
	10	104.5	53.7
	5	108.6	56.7
	2	111.2	58.4
4	20	98.9	51.9
	10	104.8	56.1
	5	109.0	56.7
	2	112.6	57.7
6	20	97.2	55.5
	10	104.0	57.0
	5	108.9	60.2
	2	113.1	68.4

The trend of the conversion curves shows a greatly accelerated primary crystallization even at the lowest cooling rate, Fig. 4.1. The transformation of

plots of conversion versus temperature to time was performed using a constant cooling rate [1] to verify the nucleating effect as is shown in Fig. 4.2. The lower is the cooling rate; the greater is the time (or temperature range) at which crystallization takes place. These plots indicate that the transformation is controlled by heterogeneous nucleation; similar results have been obtained for other nanocomposite systems [1, 2].

4.3.2. SAXS and WAXS analysis

Experiments of real – time variable temperature by using synchrotron radiation were used to obtain an improved understanding of the structural changes that occur during the crystallization of PHBV. Such experiments have been carried out on PHBV and PHBV/CNC6 samples. Fig. 4.3 gives WAXS evolution with temperature meanwhile the samples were subjected to cooling scan. WAXS pattern for CNC was presented in the previous chapter. As Fig. 4.3 shows, WAXS diffractograms of both PHBV and PHBV/CNC6 samples at room temperature contain the main characteristics diffraction peaks of orthorhombic α – type crystalline structure [3]. On increasing temperature until 200 °C, amorphous peaks centered nearly at $2\theta=14°$ for both samples were detected. According to this, the distance between PHBV macromolecules (d_{halo}) was calculated [4]. Results showed that d_{halo} was similar for both samples, nearly 0.5 nm. Both PHBV and PHBV/CNC6 samples behaved similar but crystallization process occurred at higher temperature for PHBV/CNC6 nanocomposite. Crystallization process begins at 126.5 °C and 132.5 °C for PHBV and PHBV/CNC6 nanocomposite, respectively. This suggested further evidence of nucleating agent effect of CNC particles in the PHBV matrix. Comparison of WAXS patterns in heating scan (results are not

shown here) showed that melting process began nearly at 142.8 °C and 145.4 °C for PHBV and PHBV/CNC6 nanocomposite, respectively, that supposed to be due to existence of more perfect crystalline structures in the latter one. Elsewhere, it was reported that melting process began with melting of less stable and thinner lamellae [5]. Accordingly, it can be concluded that earlier start of melting process in PHBV sample was due to presence of thinner and less stable crystalline lamellae.

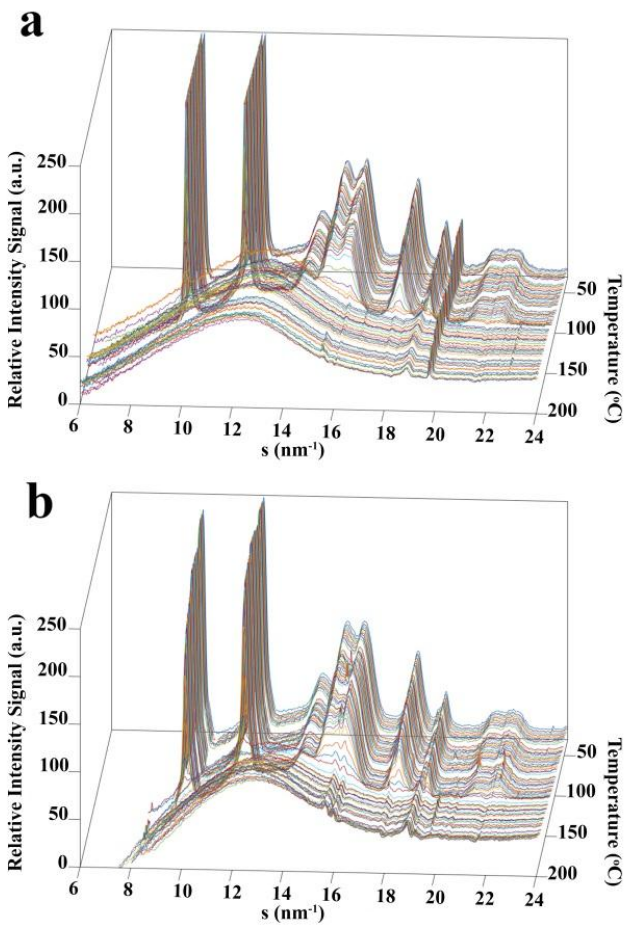

Figure 4.3: WAXS profiles of PHBV (a) and PHBV/CNC6 (b) samples.

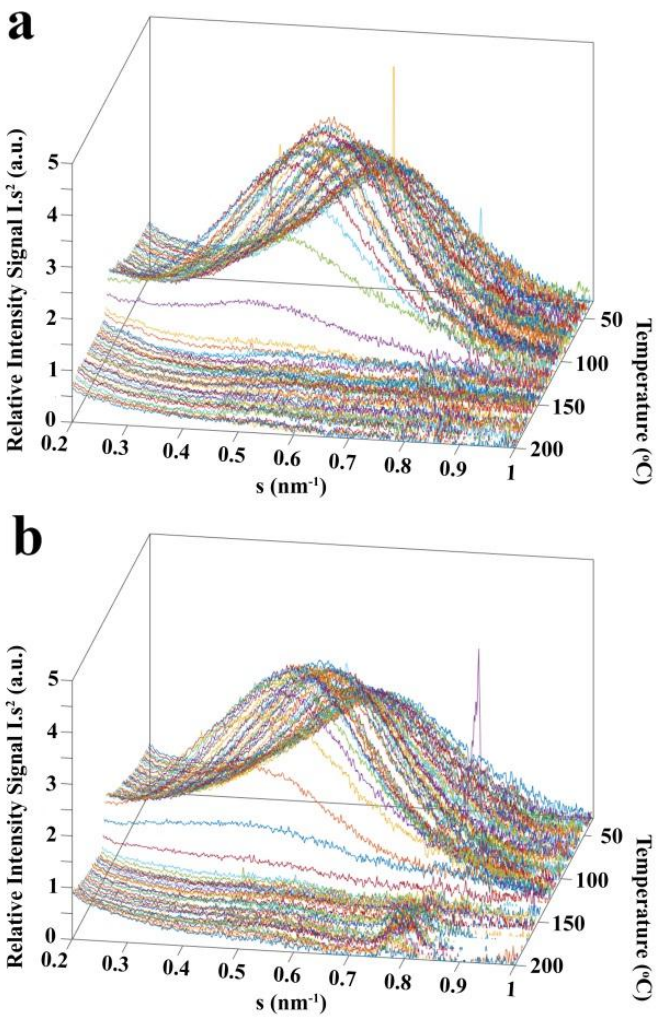

Figure 4.4: SAXS profiles of PHBV (a) and PHBV/CNC6 (b) samples.

Fig. 4.4 shows the SAXS patterns during the crystallization for both PHBV and PHBV/CNC6 samples. The overall behavior of each sample was similar. SAXS maxima position (s_{max}) shifted to higher values as temperature decreased. Using the position of mentioned parameter, summation of thickness of

repeating crystalline (L_c) and amorphous (L_a) regions which is called long spacing (L) can be calculated since $s_{max}=L^{-1}$ and $L=L_a+L_c$. The variation in long spacing with the temperature was calculated from the positions of the maxima in the SAXS plots, Fig. 4.5. Therefore, alteration in L value could be related with the change in the thickness of crystalline arrangements and/or intermolecular amorphous zones. Hence, several factors would contribute in the amount of each parameter. Luo et al. used one dimensional correlation function and Porod's law in order to calculate L, L_a and L_c parameters and study their relationship with molecular weight for PHBV with 9% hydroxyvalerate content and showed that all increased when molecular weight of PHBV increased [6]. Naffakh et al. reported greater crystalline size and nearly similar long spacing for poly (3-hydroxybutyrate) after incorporation of nanofiller with respect to the pure matrix [7]. Elsewhere, rising in long spacing was reported due to the thickening of average lamellar spacing [4].

Lorentz-corrected SAXS diffractograms ($I.s^2$ versus s), where I is intensity, at room temperature were employed to calculate the long spacing values for both samples and to study the effect of CNC filler in PHBV matrix. For both samples, a notable reduction of long spacing was seen at 140 °C. In the temperature range before this, long spacing decreased with slightly slower rate for the nanocomposite sample in comparison with PHBV, which supposed to be in relation with the presence of CNC particles that would serve as connection points and restrict the free chain mobility. Accordingly, long spacing reduction was also slower above 140 °C for the filled sample. Furthermore, it was measurable from around 164 °C for PHBV/CNC6, which was higher than that for PHBV (around 158 °C).

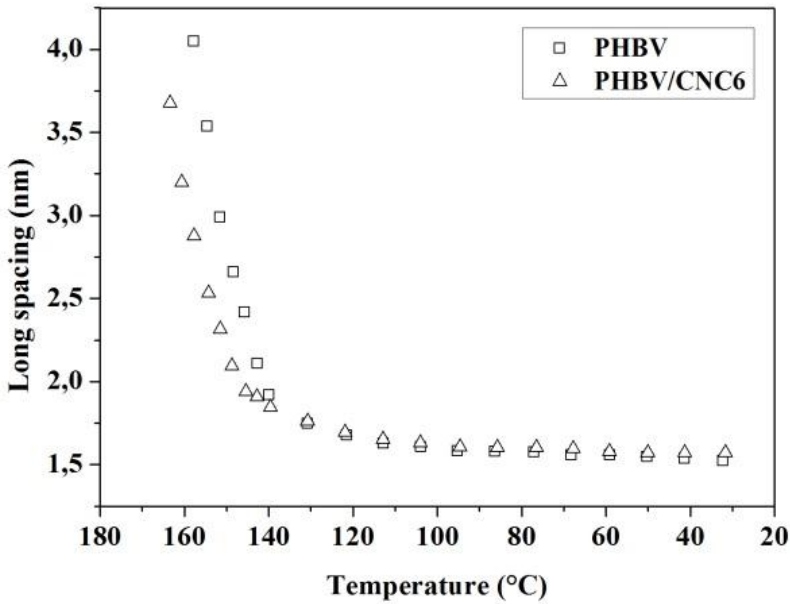

Figure 4.5: Variation in long spacing as a function of temperature of PHBV and PHBV/CNC6 samples.

4.3.3. Morphology

Dispersion state of nanoparticles in a polymeric matrix is a key issue in the final properties of the nanocomposites and it is affected by several parameters like method of preparation of the nanocomposites, filler-filler and filler-matrix interactions and filler concentration. In order to study the morphology of the nanocomposites, scanning electron microscopy (SEM) was carried out on cryo-fractured surfaces of the samples. Fig. 4.6 shows SEM images of PHBV and PHBV/CNC nanocomposites. Nearly smooth surface of PHBV indicated its well-known brittle behavior [8]. In the nanocomposite with 2 wt.% of CNC, more roughness and irregularity of the surface combined with no appearance of

agglomerations showed that CNC nanoparticles were dispersed well in the matrix. This could be explained by the hydrogen bonds formed in the nanocomposite. These bonds were created between CNC hydroxyl groups and PHBV carbonyl groups and had a compatibilizing effect [9]. As a result, cohesive interactions between molecules increased and more roughness at the surface was obtained.

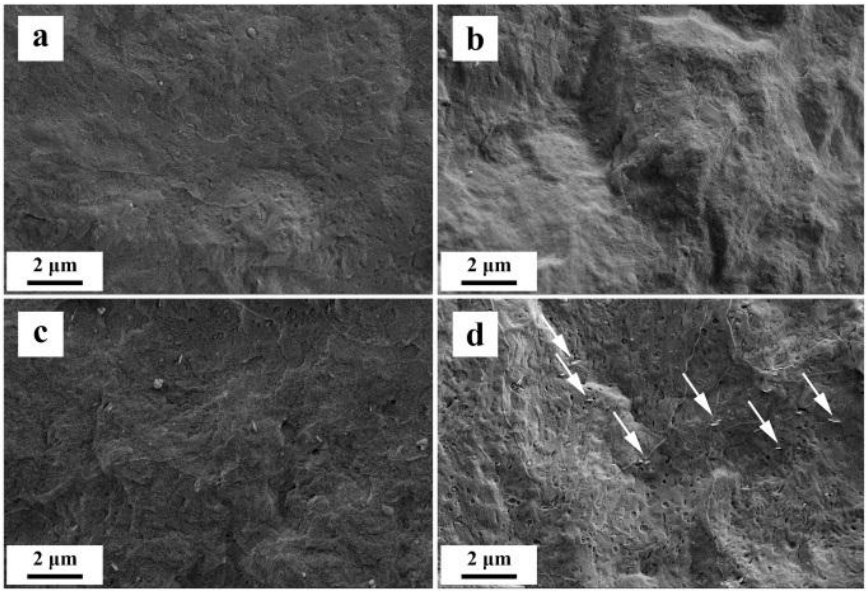

Figure 4.6: SEM images of PHBV (a), PHBV/CNC2 (b), PHBV/CNC4 (c) and PHBV/CNC6 (d).

Moreover, Díez-Pascual et al. [10] reported that a change in the roughness of the surface could be attributed to a change in the crystallinity. As Fig. 4.6c shows the nanocomposite with 4 wt.% of CNC had more roughness of the surface in comparison with nanocomposite with 2 wt.% of CNC. This could be due to higher amounts of hydrogen bonds. In the nanocomposite with 6 wt.%

of CNC, slightly agglomerations (marked with arrows in Fig. 4.6d) combined with some debonding zones and notable roughness were observable. It could be concluded that in one hand, roughness and irregularities in this sample showed high interaction between filler and matrix while in other hand, pull out zones and agglomerations implied poorer dispersion and weaker interaction in the interphase of CNC nanocrystals in PHBV matrix. Therefore, final properties of this nanocomposite would be result of these two opposite effects.

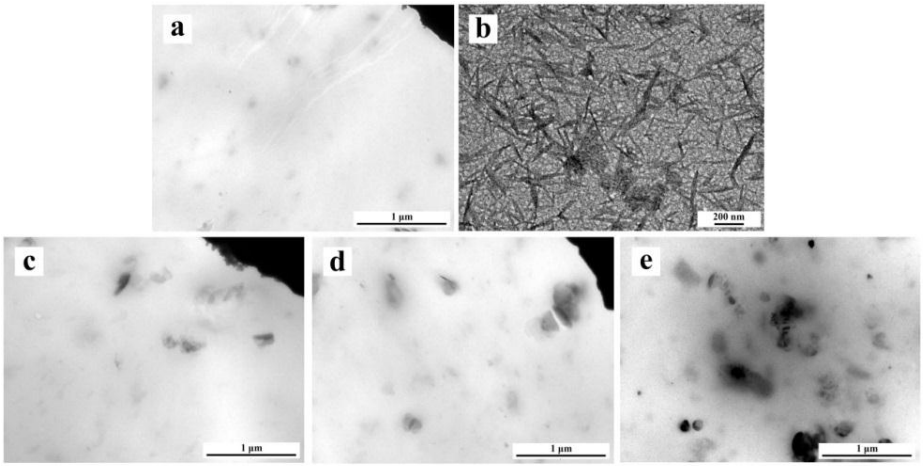

Figure 4.7: TEM image of PHBV (a), CNC (b), PHBV/CNC2 (c), PHBV/CNC4 (d) and PHBV/CNC6 (e).

For a further study of the morphology of the nanocomposites, TEM was done for the CNC and the samples and the results are presented in Fig. 4.7. While CNC particles seem to be dispersed well in the nanocomposites with 2 wt.% and 4 wt.%; formation of different level of agglomerations was obvious in the sample with 6 wt.% of CNC. Also, this confirmed the obtained results from

SEM images, which showed that occurring agglomerations started at a concentration of 6 wt.% of the CNC. Similar results were reported previously [9, 11].

4.3.4. Mechanical properties

Well-dispersed filler is a result of polymer-filler interactions, method of preparation of the composite and amount of filler. In the case of melt mixing, more parameters have contribution in the final state of dispersion like viscosity of the matrix or time and temperature of mixing process. In this regard, the impact of incorporation of CNC nanofiller to PHBV matrix was studied with tensile tests. Obtained results were plotted versus CNC content in Fig. 4.8. As Fig. 4.8 shows, Young modulus (E) of the nanocomposites improved with increasing CNC concentration. Also, it was confirmed that CNC was able to reinforce PHBV matrix and there was strong filler – matrix interfacial adhesion. This comes from creation of hydrogen bonds between hydroxyl groups in the CNC and carbonyl groups in the PHBV chemical structure. When there is interaction between matrix and filler, transfer of stress from matrix to filler particles during mixing process occurs effectively and as a result, filler will be dispersed well. Besides, it is reasonable to conclude that the amount of clusters in PHBV/CNC6 was too low to affect its Young modulus negatively. In addition, it is of great importance to mention that the improved Young modulus was attributed to enhanced crystallinity of the matrix.

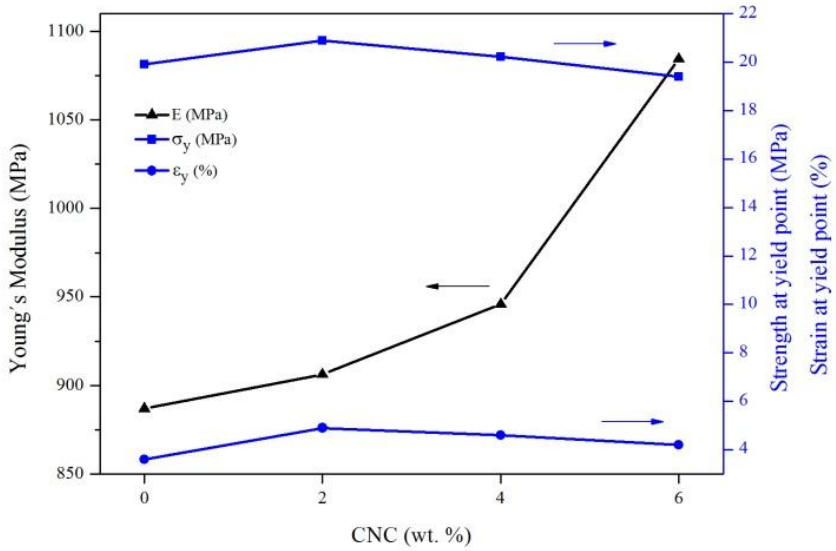

Figure 4.8: Mechanical properties of PHBV and PHBV/CNC nanocomposites.

Fig. 4.8 also gives results of strain and strength at the yield point for all samples. As can be seen with loading CNC nanoparticles to the PHBV matrix, strain at yield point slightly increased, reaching a maximum value for the nanocomposite with 2 wt.% of CNC and then decreased when increasing CNC loading but still was higher for nanocomposites than for the PHBV. It means that ductility of PHBV was not modified significantly with loading CNC nanoparticles. Simultaneously slight enhancement occurred for strength at yield point for the nanocomposite with 2 wt.% of CNC. As it was explained before in the SEM section, well dispersed morphology was obtained for the nanocomposite with 2 wt.% of CNC. It could be due to the low concentration of CNC, which reduce the probability of forming agglomerations. By increasing CNC content to 4 wt.% and 6 wt.%, strength at the yield point slightly

decreased. It was explained by the fact that in higher loading of CNC, possibility of forming agglomerations was bigger than in low concentrations. This is due to higher possibility of formation of hydrogen bonds between cellulose molecules as they are more accessible to each other. SEM studies also confirmed this result. It was concluded that the increment of nanofiller concentration was in favor of improving the Young modulus without significant changes in the ductility.

4.3.5. Barrier properties

The improvement of the barrier properties in order to control the gas diffusion into the packaging films is considered as an effective solution for preventing continuous spoilage, increasing chemical stability, storing time, safety and shelf life of packaged food. However, it should be noted that depending on the packaged food, the amount of permitted humidity and gas inside the packaging films would vary. In this context, the effect of introducing filler on the barrier properties of a polymeric matrix is of great importance. Therefore, the barrier properties of PHBV and its nanocomposites against water vapor, oxygen and carbon dioxide were examined and the results obtained are shown in Fig. 4.9.

As Fig. 4.9 shows, the incorporation of CNC nanoparticles led to a notable improvement in the barrier properties of PHBV. Water vapor transmission rate for the PHBV was 51 g $(m^2\ day)^{-1}$. In the nanocomposite with 2 wt.%, this value decreased to 29 g $(m^2\ day)^{-1}$. While CNC content was 4 wt.%, the water vapor transmission rate decreased to 16 g $(m^2\ day)^{-1}$. In the nanocomposite with 6 wt.% of CNC, the transmission rate values of water vapor molecules decreased to 14 g $(m^2\ day)^{-1}$.

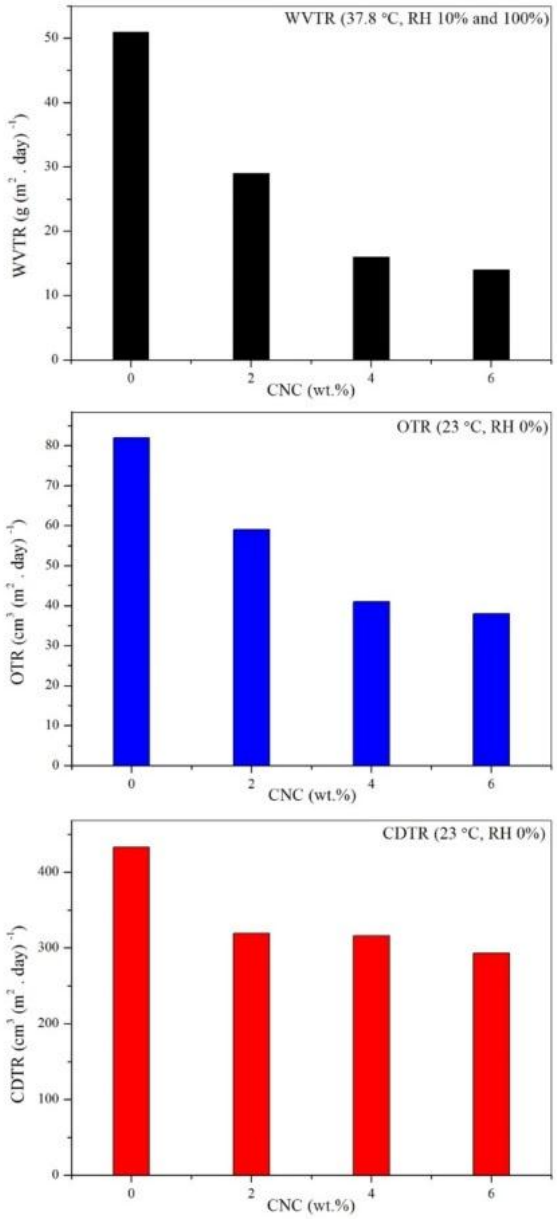

Figure 4.9: Water vapor, oxygen and carbon dioxide transmission rate against CNC content for PHBV and PHBV/CNC nanocomposites.

Oxygen transmission rate values for the PHBV and the nanocomposites with 2 wt.%, 4 wt.% and 6 wt.% were 82, 59, 41 and 38 cm^3 (m^2 day) $^{-1}$, respectively. Carbon dioxide transmission rate values for the PHBV and the nanocomposites with 2 wt.%, 4 wt.% and 6 wt.% were 433, 319, 316 and 293 cm^3 (m^2 day)$^{-1}$, respectively which are comparable with reported data for biopolymer films [12].

As can be seen, an improvement of the barrier properties against water vapor, oxygen and carbon dioxide occur upon addition of the filler content in PHBV nanocomposites. According to the nucleation effect of CNC in PHBV matrix, this could be explained by more crystalline zones, which were formed in the nanocomposites and acted as barriers for diffusion and passing of gas molecules. Furthermore, free mobility of PHBV chains, as a helpful factor for movement of gas molecules inside the matrix, would be restricted in the presence of CNC. Therefore, transmission rate values decreased in the nanocomposites in comparison with the values for the polymer. It should be noted that the formation of hydrogen bonds inside the matrix, led to chain bridging and consequently higher entanglements. These entanglements also could act as physical barriers in the pathways of gas molecules due to their compact structure and caused less transmission rate values [13]. In the previous chapter, which was dedicated to the preparation of PHBV/CNC nanocomposites by solvent cast film method, similar results were seen. So, this might be concluded that independent of the method of preparation, CNC would improve barrier properties mainly due to the increment of crystalline zones. However it is accepted that the order of improvement may differ.

Besides, higher barrier properties were attributed to high interaction at interphase of filler-matrix; hydrogen bonds interactions and more tortuosity resulted from incorporation of CNC in the PHBV matrix [14-16]. Díez - Pascual

et al. [10] mentioned that final barrier properties are result of crystallinity, dispersion state and concentration of the filler.

4.3.6. Statistical analysis

The effect of filler concentration on mechanical properties of PHBV was statistically analyzed by one-way analysis of variance (ANOVA) with significance level (α) of 0.05. Table 4.2 lists the results of P-value, F and F critic of the impact of filler concentration on Young modulus, strength and strain at yield point. It can be concluded from the results that filler loading did not have any significant effect on the strength and strain at yield point while it had a significant effect on the Young modulus.

Table 4.2: Description of P and F values.

	Young modulus			Strength at yield point			Strain at yield point		
	P-value	F	F critic	P-value	F	F critic	P-value	F	F critic
CNC wt.%	0.008	16.88	4.06	0.207	1.91	4.06	0.479	0.91	4.06

4.4. Conclusion

Extrusion was applied to produce nanocomposites of poly (3-hydroxybutyrate-co-3-hydroxyvalerate) with cellulose nanocrystals with 2 wt.%, 4 wt.% and 6 wt.%. The analysis of the influence of CNC on the dynamic crystallization kinetics of PHBV showed that the crystallization temperatures increase with CNC content for a given cooling rate. Therefore, CNC acted as a nucleating agent in the PHBV matrix. The incorporation of CNC implies an increase in the crystallinity. Results of synchrotron light showed that WAXS diffractograms of

both PHBV and PHBV/CNC6 samples at room temperature contain the main characteristics diffraction peaks of orthorhombic α – type crystalline structure. Crystallization process started at higher temperature for the PHBV/CNC6 sample, which confirmed nucleating agent effect of CNC particles in the PHBV matrix. The variation in long spacing with the temperature was slower in the PHBV/CNC6 sample when compared to the PHBV sample due to the presence of CNC particles that would serve as connection points and restrict the free chain mobility. Morphological studies indicated that the nanocomposites exhibited more roughness than the PHBV, which was due to creation of hydrogen bonds between filler and matrix. CNC content of 6 wt.% was considered as the concentration of the beginning of the appearance of slight clusters. Mechanical test revealed higher Young modulus for the nanocomposites. Also it was found that with increasing filler concentration Young modulus increased without decreasing ductility. One-way analysis of variance showed a statistically significant difference in the Young modulus of the samples upon filler loading while there was no significant effect of filler loading on both strength and strain at yield point. Permeation tests against water vapor, oxygen and carbon dioxide molecules showed improvement in the barrier properties of the nanocomposites due to compatibilization effect of CNC, more entanglements, higher crystallinity and more tortuosity in their morphology. These results seem to confirm that these nanocomposites processed by extrusion could be a good alternative for synthetic plastic packaging materials.

4.5. References

[1] M. Naffakh, M. Remskar, C. Marco, M. A. Gómez-Fatou, Dynamic Crystallization Kinetics and Nucleation Parameters of a New Generation of Nanocomposites Based on Isotactic Polypropylene and MoS_2 Inorganic Nanotubes, Journal of Physical Chemistry B, 115(12): 2850 (2011)

[2] R. Bouza, L. Barral, F. J. Díez, J. López, B. Montero, M. Rico, C. Ramírez, Study of thermal and morphological properties of a hybrid system, iPP/POSS. Effect of flame retardance, Composites: Part B, 58: 566 (2014)

[3] H. Sato, N. Suttiwijitpukdee, T. Hashimoto, Y. Ozaki, Simultaneous Synchrotron SAXS/WAXD Study of Composition Fluctuations, Cold-Crystallization, and Melting in Biodegradable Polymer Blends of Cellulose Acetate Butyrate and Poly (3-hydroxybutyrate), Macromolecules, 45: 2783 (2012)

[4] A. Muñoz-Bonilla, M. L. Cerrada, M. Fernández-García, A. Kubaka, M. Ferrer, M. Fernández-García, Biodegradable Polycaprolactone-Titania Nanocomposites: Preparation, Characterization and Antimicrobial Properties, International Journal of Molecular Science, 14: 9249 (2013)

[5] R. J. Rule, J. J. Liggat, Time-resolved synchrotron small angle X-ray scattering studies of poly (3-hydroxybutyrate) and poly (3-hydroxybutyrate-co-3-hydroxyvalerate) polymers, Polymer, 36: 3831 (1995)

[6] S. Luo, D. T. Grubb, A. N. Netravali, The effect of molecular weight on the lamellar structure, thermal and mechanical properties of poly (hydroxybutyrate-co-hydroxyvalerates), Polymer, 43: 4159 (2002)

[7] M. Naffakh, C. Marco, G. Ellis, Inorganic WS_2 nanotubes that improve the crystallization behavior of poly (3-hydroxybutyrate), CrystEngComm, 16: 1126 (2014)

[8] X. Wang, Z. Chen, X. Chen, J. Pan, K. Xu, Crystallization kinetics and mechanical properties of Poly (3-hydroxybutyrate-co-3-hydroxyvalerate) (PHBV) / Poly (3-hydroxybutyrate-co-4-hydroxybutyrate) (P3/4HB) blends, Journal of Applied Polymer Science, 117: 838 (2010)

[9] S. Malmir, B. Montero, M. Rico, L. Barral, R. Bouza, Morphology, thermal and barrier properties of biodegradable films of poly (3-hydroxybutyrate-co-3-hydroxyvalerate) containing cellulose nanocrystals, Composites Part A, 93: 41 (2017)

[10] A. M. Diez-Pascual, A. L. Diez-Vicente, ZnO-reinforced poly (3-hydroxybutyrate-co-3-hydroxyvalerate) bionanocomposites with antimicrobial function for food packaging, Applied Materials and Interfaces, 6: 9822 (2014)

[11] E. Ten, L. Jiang, M. P. Wolcott, Crystallization kinetics of poly (3-hydroxybutyrate-co-3-hydroxyvalerate)/cellulose nanowhiskers composites, Carbohydrate Polymers, 90: 541 (2012)

[12] K. S. Tumwesigye, J. C. Oliveira, M. J. Sousa-Gallagher, New sustainable approach to reduce cassava borne environmental waste and develop biodegradable materials for food packaging applications, Food Packaging and Shelf Life, 7: 8 (2016)

[13] M. Shahbazi, G. Rajabzadeh, A. Rafe, R. Ettelaie, S. J. Ahmadi, The physico-mechanical and structural characteristics of blend film of poly (vinyl alcohol) with biodegradable polymers as affected by disorder-to-order conformational transition, Food Hydrocolloids, 60: 393 (2016)

[14] H. Yu, B. Sun, D. Zhang, G. Chen, X. Yang, J. Yao, Reinforcement of biodegradable poly (3-hydroxybutyrate-co-3-hydroxyvalerate) with cellulose nanocrystal/silver nanohybrids as bifunctional nanofillers, Journal of Material Chemistry B, 2 (48): 8479 (2014)

[15] H. Yu, C. Yan, J. Yao, Fully biodegradable food packaging materials based on functionalized cellulose nanocrystals/poly (3-hydroxybutyrate-co-3-hydroxyvalerate) nanocomposites, RSC Advance, 4: 59792 (2014)
[16] G. Siqueira, J. Bras, A. Dufresne, Cellulose Whiskers versus Microfibrils: Influence of the Nature of the Nanoparticle and its Surface Functionalization on the Thermal and Mechanical Properties of Nanocomposites, Biomacromolecules, 10 (2): 425 (2009)

CHAPTER 5: PHBV/CNC nanocomposites: environmental effects, antimicrobial activity and biocompatibility

5.1. Introduction

It is generally accepted that contact with humidity, exposure to sunshine and diffusion of oxygen molecules into the material structure, might lead to photo-oxidation, degradation, changes in molecular weight, surface morphology, thermal behavior and/or material composition in polymeric materials. Hence, these could affect properties such as morphology, crystalline structure, thermal properties, mechanical resistance, ductility and color. In this sense, evaluation of variation of properties of polymeric materials and their degradation process and failure behavior with weathering exposure is of considerable importance. This would provide helpful pointers for calculation of shelf life and stability time of the packaging film as valuable crucial factors for tailoring film composition and estimation of its efficiency when food packaging applications are aimed.

To this end, the present chapter is concerned with the effect of introducing CNC on thermal properties and crystalline structure of PHBV as well as its morphological characteristics before and after different radiation doses of artificial weathering. Also, the influence of the incorporation of CNC as hydrophilic filler on the humidity absorption and water vapor transmission rate of PHBV matrix was evaluated. Moreover, antimicrobial and biocompatibility behavior of PHBV and its nanocomposites were studied.

5.2. Experimental

5.2.1. Materials and processing

Used materials were PHBV and CNC. In order to perform the humidity absorption tests, three types of salts with analytical grade were used to provide test mediums with different relative humidity of 95% (potassium

nitrate, KNO_3), 75% (sodium chloride, NaCl) and 54% (magnesium nitrate hexahydrate, $Mg(NO_3).6H_2O$). Also, for the antimicrobial studies, chitosan, zinc oxide and silver particles were used as antimicrobial agents.

According to different requirements of each test, the samples were prepared with different methods including melt mixing by internal mixer, extrusion, hot press and cast film. In all methods, PHBV was dried in an oven at 70 °C for 24 h before using. Also, three different CNC concentrations were selected i.e. 2 wt.%, 4 wt.% and 6 wt.%. All samples were kept in desiccator with silica gel for one week prior to do any experiments.

In the case of melt mixing by internal mixer, PHBV was melt mixed with CNC nanoparticles in an internal mixer (Brabender W50E, 3 zones, PL-type 2000-3, Germany) at 165 °C and with rotor speed of 60 rpm. CNC nanoparticles were added to the mixer after 5 min of the start of the process and mixing was continued up to 15 min. After cooling at room temperature, the samples were hot pressed (IQAP LAB PL – 15, Spain) at 165 °C and 150 bar of pressure to obtain films with thickness of 80 μm for artificial weathering and water vapor transmission rate studies.

Some samples with different antimicrobial agents were prepared by extrusion method for antimicrobial studies. PHBV was melt mixed with CNC nanoparticles/antimicrobial agent in a twin screw mini-extruder (Haake Force Feeder Minilab II, Germany) at 165 °C and with rotor speed of 60 rpm. PHBV was fed to the extruder firstly. Then, dry mixed CNC nanoparticles/antimicrobial agent were added to the mixer after 5 min of the start of the process and mixing was continued up to 15 min. Subsequently, resulting rod shape products were cooled at room temperature and then hot pressed with the same condition as explained above to obtain films for artificial weathering and water vapor transmission rate studies. For the

humidity absorption tests, rod shapes obtained with the mini-extruder were used. For the biocompatibility studies, samples were prepared by cast film method as it was described in the third chapter.

5.2.2. Characterization techniques

Used characterization techniques were artificial weathering, DSC, time - resolved synchrotron X – ray scattering, SEM, humidity absorption, WVTR (relative humidity of 10% and 100% in both sides), antimicrobial and biocompatibility studies. Table 5.1 shows the sample codes and total received radiation doses.

Table 5.1: Sample codes and total received radiation doses.

Code	CNC (wt.%)	Radiation doses (kJ m^{-2})
PHBV	0	0
PHBV2	2	0
PHBV4	4	0
PHBV6	6	0
PHBV-X	0	16500
PHBV2-X	2	16500
PHBV4-X	4	16500
PHBV6-X	6	16500
PHBV-4X	0	66000
PHBV2-4X	2	66000
PHBV4-4X	4	66000
PHBV6-4X	6	66000

5.3. Results and discussions

5.3.1. Artificial weathering process

5.3.1.1. Thermal properties

In order to study the CNC effect on thermal characteristics of PHBV, DSC experiments were carried out. Fig. 5.1 shows the thermograms of PHBV and PHBV/CNC nanocomposites before (fresh samples) and after two steps of artificial weathering. Table 5.2 lists the related thermal parameters.

Considering fresh samples, it can be observed from Fig. 5.1 (cooling) that crystallization peak moved to higher temperatures for nanocomposites when compared to PHBV. This confirmed the nucleating agent effect of CNC in the PHBV matrix. From Fig. 5.1 (heating) it can be observed a slightly higher melting temperature in nanocomposites when compared to PHBV. This fact can be explained because of the formation of more perfect and thicker spherulites in composite samples [1]. Besides, it should be noted that bimodal endothermic melting peaks are related to two types of crystalline microstructures. The lower peak was attributed to less perfect crystals with thinner lamellae while the higher peak was related to more perfect thicker lamellae [2]. Elsewhere, it was discussed that lower melting peak is referred to original crystals whereas the higher one is referred to recrystallized ones [3]. Higher crystalline temperatures for PHBV/CNC nanocomposites confirmed the nucleating agent effect of CNC inside the matrix, but reduction in the crystallinity percent in PHBV6 nanocomposite showed that concentration of 6 wt.% of CNC could be considered the start of restriction of PHBV chain mobility. This might be due to the fact that CNC nanoparticles acted as physical barriers inside the PHBV matrix. In this case, diffusion and folding of polymeric chains to crystalline zones might be hindered. Consequently, the crystallinity would be smaller.

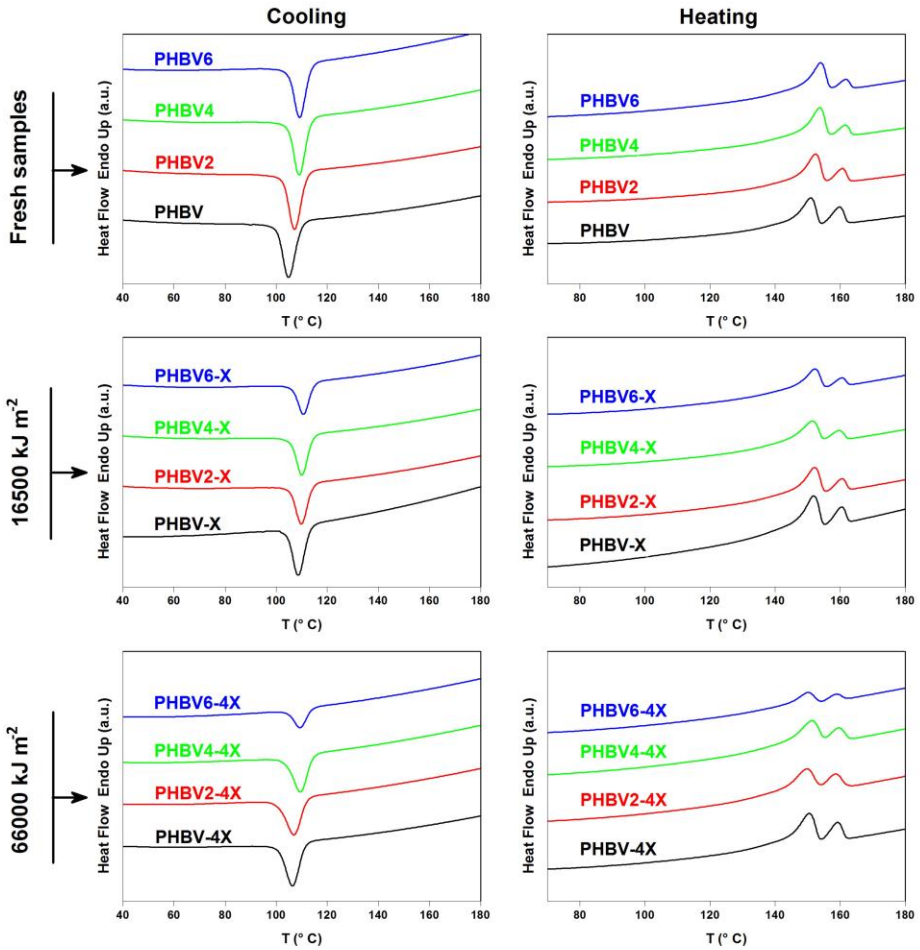

Figure 5.1: DSC thermograms during cooling from the melt and posterior heating of PHBV and PHBV/CNC nanocomposites.

The analysis of the artificial weathering on crystallization behavior from DSC cooling scans (Fig. 5.1 (cooling) and Table 5.2) reflected that after the first step of artificial weathering, all the samples have less crystallinity percent

compared to fresh samples. After the second step of artificial weathering, different results were obtained for the samples. While PHBV-4X, PHBV2-4X and PHBV4-4X showed an increase in crystallinity percent, PHBV6-4X showed a reduction of crystalline zones. These observations showed that artificial weathering might lead to competition of different approaches in the samples.

Table 5.2: Thermal parameters of non-isothermal crystallization and melting process of PHBV and PHBV/CNC nanocomposites.

Sample	**T_c (°C)**	**T_{m1} (°C)**	**T_{m2} (°C)**	**ΔH_c (J g^{-1})**	**X_c (%)**
PHBV	104.8	151.0	159.8	58.5	53.7
PHBV2	107.2	152.3	160.6	57.4	53.7
PHBV4	109.0	153.8	161.5	56.2	53.7
PHBV6	109.2	154.0	161.8	53.4	52.1
PHBV-X	107.7	151.8	160.3	55.5	50.9
PHBV2-X	108.8	152.1	160.5	53.2	49.8
PHBV4-X	109.0	151.3	159.8	52.7	50.4
PHBV6-X	109.7	152.1	160.5	50.1	48.9
PHBV-4X	106.3	150.4	159.2	56.9	52.2
PHBV2-4X	107.0	149.6	158.6	55.9	52.3
PHBV4-4X	109.5	151.2	159.6	53.5	51.1
PHBV6-4X	109.3	150.1	158.8	48.8	47.6

It is well accepted that weathering might led to photo-oxidation in both crystalline and amorphous phases, preferentially in amorphous phase. Not all but some possible consequences of photo-oxidation that are in favor of increasing degree of crystallinity can be explained as follows. Firstly, photo-oxidation in amorphous phase might cause a kind of secondary crystallization called chemi-crystallization related to the reduction of molecular weight through chain scission [4-7]. Secondly, during artificial weathering, side products could be produced which might leave the samples via volatilization. This would be in the favor of increment the crystallinity degree [8]. Conversely, some consequences that are in the favor of decreasing degree of crystallinity could be summarized as follows. Firstly, photo-oxidation in crystalline phase might lead to destruction of crystalline structure [9]. Secondly, chain scission could be in such level that produced chains were too short to be able to fold and form crystalline parts. Also, they might create agglomerations of joined short chains with CNC or other unknown arrangements that could restrict other chains free mobility and reduce their crystallization capacity. Thirdly, impurities that might be produced are able to disturb or even suppress rearrangements of polymeric chains and consequently reduction of crystallinity. Finally, photo-degradation could create molecular defects, which might not fit into crystalline arrangements and might be rejected from crystalline structures.

It is clear that contribution percent of these facts would tailor the final crystallinity percent. For all the samples after first step of artificial weathering, predominant mechanisms were against the growth of crystalline phase. After second step of artificial weathering, PHBV-4X, PHBV2-4X and PHBV4-4X increased the crystallinity again. Rabello et al. [4] considered an incubation time in initial steps of artificial weathering, which is considered as a delay

before rearrangement of the scission chains and occurrence of secondary crystallinity. This could be considered as the reason of increment in crystallinity percent in these samples. PHBV6-4X did not show increased crystallinity. One possible explanation could be high physical barrier due to high concentration of CNC, which restricted the rearrangement of PHBV chains.

5.3.1.2. Crystal structure

Simultaneous synchrotron SAXS/WAXS study as a powerful complementary technique provides fairly reliable understanding of crystalline evolution of materials and filler dispersion state in composite samples. Dynamic crystalline development was studied by simultaneous SAXS/WAXS technique to evaluate the possible influence of CNC on crystalline structure of PHBV. Fig. 5.2 gives WAXS patterns of the PHBV, PHBV6, PHBV-4X and PHBV6-4X samples. At room temperature, all main characteristic diffraction peaks of PHBV can be detected, including those located at $2\theta \approx 8.8$ ° and $2\theta \approx 11$ ° which correspond to the (020) and (110) planes of orthorhombic α – type crystalline structure of HB units, in respective order [10]. WAXS diffractograms of PHBV and its nanocomposites were similar, new peaks were not appeared and they do not shift to higher or lower angles in the nanocomposites.

The crystallization process started at higher temperatures for nanocomposites with respect to the PHBV, which confirmed the nucleating agent effect of CNC in the PHBV matrix as DSC results showed. Crystallization process started at 117.9 °C and 121.9 °C for PHBV and PHBV6, respectively. After artificial weathering, both crystalline temperatures shifted slightly to higher temperatures.

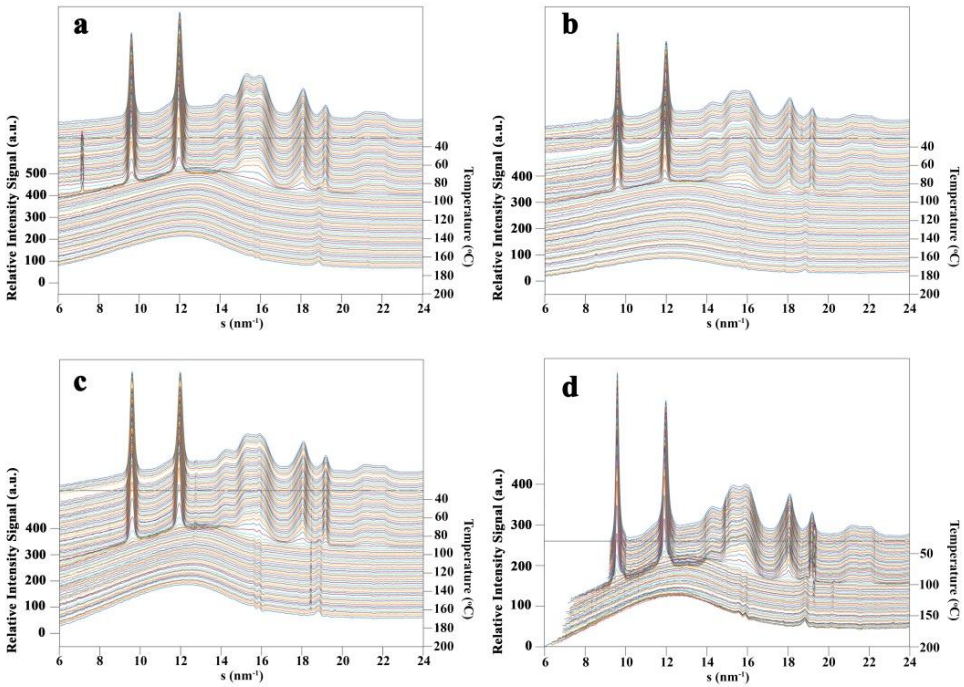

Figure 5.2: WAXS patterns of PHBV (a), PHBV6 (b), PHBV-4X (c) and PHBV6-4X (d) nanocomposites.

Evolution of SAXS intensity as a function of temperature during crystallization for PHBV, PHBV6, PHBV-4X and PHBV6-4X nanocomposites is illustrated in Fig. 5.3. For all samples, the position of SAXS maxima (s_{max}) moved to higher values as temperature decreased. Based on s_{max} value, long spacing parameter (L) can be calculated since $s_{max} = 1/L$.

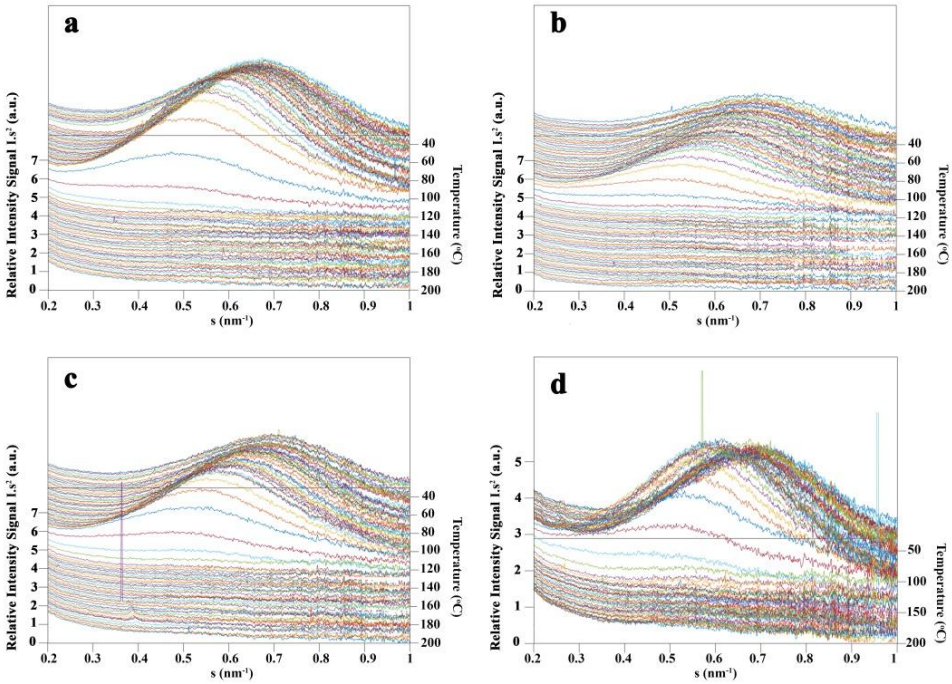

Figure 5.3: SAXS patterns of PHBV (a), PHBV6 (b), PHBV-4X (c) and PHBV6-4X (d) nanocomposites.

Fig. 5.4 exhibits the alteration in long spacing parameter with the temperature. For all samples, a remarkable reduction occurred at a border near of 140 °C. PHBV and PHBV6 behaved similar before and after the mentioned border while there was a small difference between each sample in its fresh condition and after artificial weathering. PHBV-4X and PHBBV6-4X were slower in decreasing long spacing parameter with respect to fresh samples. Also their long spacing parameters were measurable from higher temperatures (nearly 158 °C) when compared to PHBV and PHBV6 (nearly 152

°C). This indicated restricted chain mobility in PHBV-4X and PHBV6-4X as it was expected from their smaller crystalline degree in DSC results.

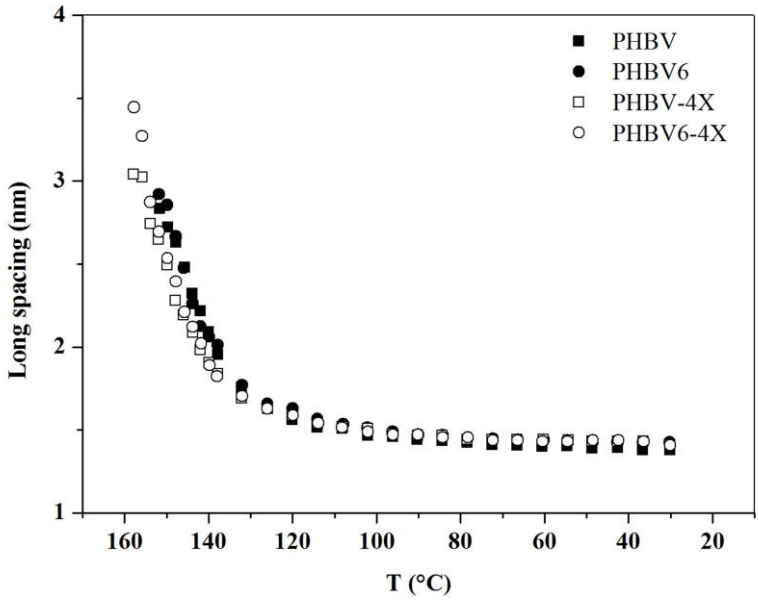

Figure 5.4: Long spacing against temperature for PHBV and PHBV/CNC nanocomposites.

5.3.1.3. Morphological studies

Filler dispersion state contributes a significant role in the final properties of nanocomposites. This could be affected by several factors such as preparation method, filler-matrix interaction, filler concentration or polarity of each phase. In this sense, surface morphology of all samples before and after subjecting to artificial weathering was studied by SEM. Achieved results are given in Fig. 5.5.

This figure suggests that before artificial weathering, there was good filler dispersion in all nanocomposites. It is due to effective filler-matrix interaction and strong adhesive forces in their interphase driven from formation of hydrogen bonds which acted as compatibilizer [3]. SEM micrographs after artificial weathering revealed appearing of white blister-like points in all samples as a combined effect of photo-oxidation and water absorption.

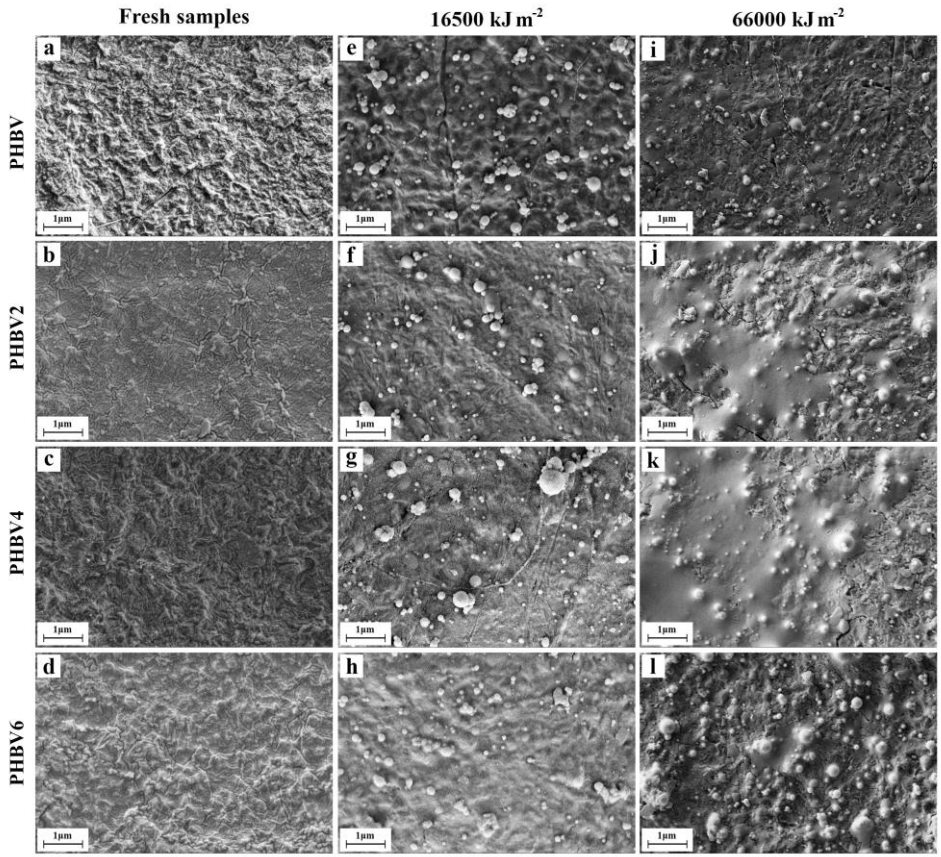

Figure 5.5: SEM images of PHBV and PHBV/CNC nanocomposites before and after two steps of artificial weathering.

5.3.2. Humidity absorption

As it is known, humidity has detrimental effects on quality, chemical resistance and mechanical properties of packaged materials. Therefore, materials with hydrophobic characteristic like PHBV could be considered as desirable candidates for packaging applications. By the other side, CNC possess hydrophilic nature. So, enhancement of hydrophilicity of PHBV upon compounding with CNC was a concern that should be evaluated.

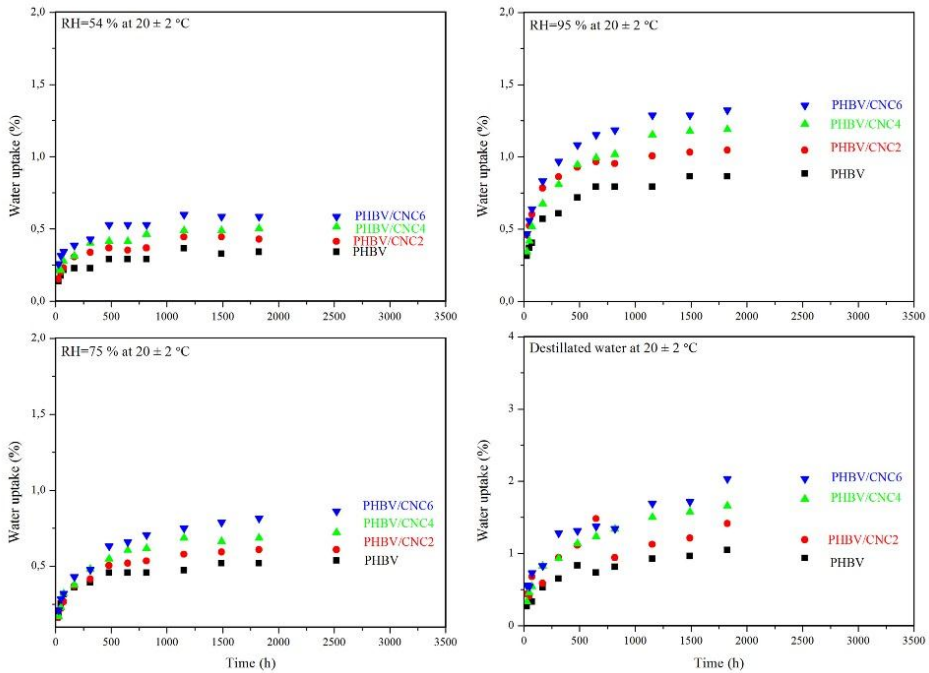

Figure 5.6: Humidity absorption of PHBV and PHBV/CNC nanocomposites as a function of time in different humidity mediums: 54% RH, 75% RH, 95% RH and distilled water.

Fig. 5.6 presents humidity absorption percent versus time in four different relative humidity mediums i.e. immerged in distilled water and relative humidity of 95%, 75% and 54%. Table 5.3 shows the final humidity absorption percent (after 2520 h of being in contact with test medium) for all samples in different test mediums. As it was expected, humidity absorption was dependent on the humidity of the test medium and more absorption was achieved for samples that were put in more humid test cells. Results showed that although all nanocomposites exhibited slightly more hydrophilic properties compared to the PHBV but the difference was such low that all nanocomposites could be considered as hydrophobic material quietly well. Comparison the rates of humidity absorption at the beginning of the test showed that the rate of absorption was higher for nanocomposites with higher CNC concentration as hydrophilic filler. This rate was increased with the increment of relative humidity percent of the test mediums.

Table 5.3: Final humidity absorption percent and WVTR of PHBV and PHBV/CNC nanocomposites.

Sample	Medium of humidity absorption test				**WVTR g $(m^2\ day)^{-1}$**
	Distilled Water	**RH 95%**	**RH 75%**	**RH 54%**	
PHBV	0.9	0.9	0.5	0.3	71
PHBV2	1.2	1.0	0.6	0.4	51
PHBV4	1.7	1.2	0.7	0.5	38
PHBV6	2.0	1.4	0.9	0.6	28

5.3.3. Water vapor transmission rate

Developing of packaging materials with suitable barrier properties could be regarded as an effective strategy to reserve the food in healthy and safe condition, expand shelf time, prevent chemical reactions, protect the chemical composition of the packaged food and reduce the costs. In this sense, water vapor transmission rate of PHBV and its nanocomposites was measured and the results are presented in Table 5.3. Results showed that WVTR reduced by 28%, 46% and 61% for PHBV2, PHBV4 and PHBV6 with reference to PHBV, respectively. This can be explained by the presence of CNC as physical barriers in the matrix that create more tortuosity in the pathways of water vapor molecules. Further, hydrophilic nature of CNC might lead to absorb and keep water vapor molecules and cease their movement in the matrix [11].

5.3.4. Antimicrobial activity

Antimicrobial activity of the samples was examined against *L. monocytogenes, S. enterica, S. aureus* and *E. coli* and the results after 24 h exposure are shown in Fig. 5.7. PHBV and PHBV6 and those supplemented with *Zn* or *Ag* showed a clear inhibition of growth for all assayed strains; however, polymers supplemented with chitosan have not shown this inhibition.

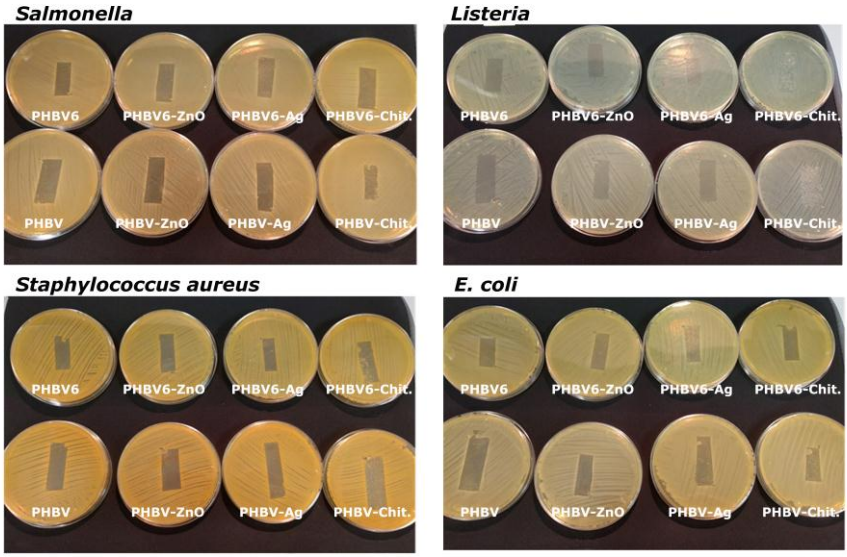

Figure 5.7: Antimicrobial activities of PHBV and PHBV6 with different antimicrobial agents.

5.3.5. Biocompatibility studies

5.3.5.1. Effect of PHBV and its nanocomposites on cell viability

To address the effect of the different samples on J774A.1 macrophages viability was used the MTT assay, adding polymyxin B (10 µg/mL) to eliminate the effect of possible LPS contamination in the samples. As shown in Fig. 5.8, samples treatment for 24 h has little or no effect on cell viability at doses of 1-100 µg/mL, while the dose of 1000 µg/mL induced an increase in cell viability in all the treatments but PHBV4, which exhibits the more innocuous profile.

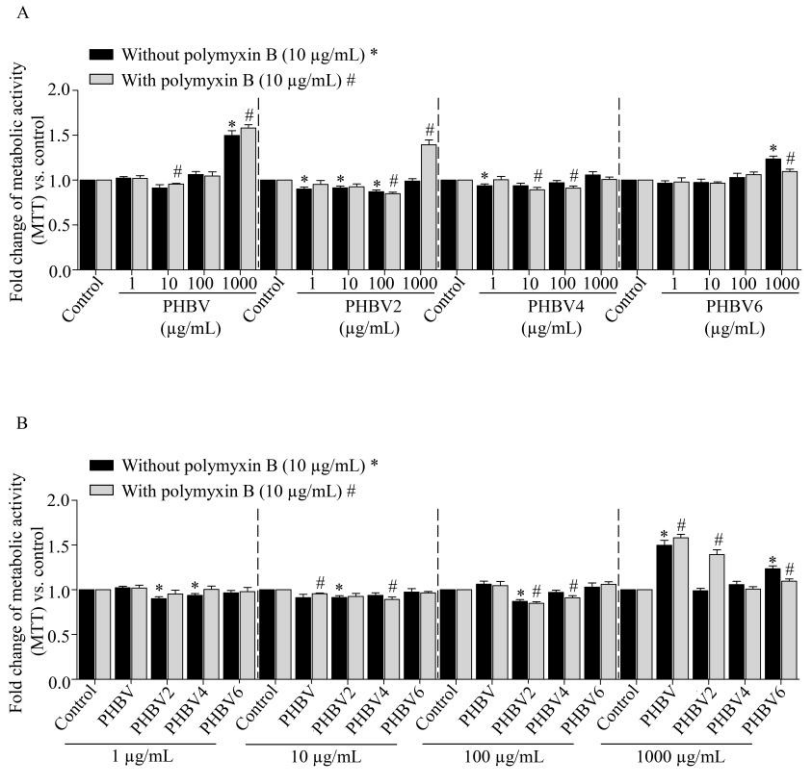

Figure 5.8: Effect of PHBV and PHBV/CNC nanocomposites on J774.A1 macrophages mitochondrial metabolic activity. Statistical analysis of the effect of the treatment with the samples for 24 h on J774.A1 macrophages mitochondrial metabolic activity, represented according to the different doses of treatment for each sample (A) or to each dose of treatment for the different samples (B). #,*$p<0.05$. n=6.

5.3.5.2. Effect of PHBV and its nanocomposites on inflammation

It was used the nitrite assay to study the effect of the samples on J774A.1 macrophages inflammatory response [12]. 250 ng/mL LPS was used as a positive control and 10 µg/mL polymyxin B was added to eliminate the effect of possible LPS contamination in the samples. As shown in Fig. 5.9, samples

treatment for 24 h has no effect on nitrite production in J774A.1 macrophages.

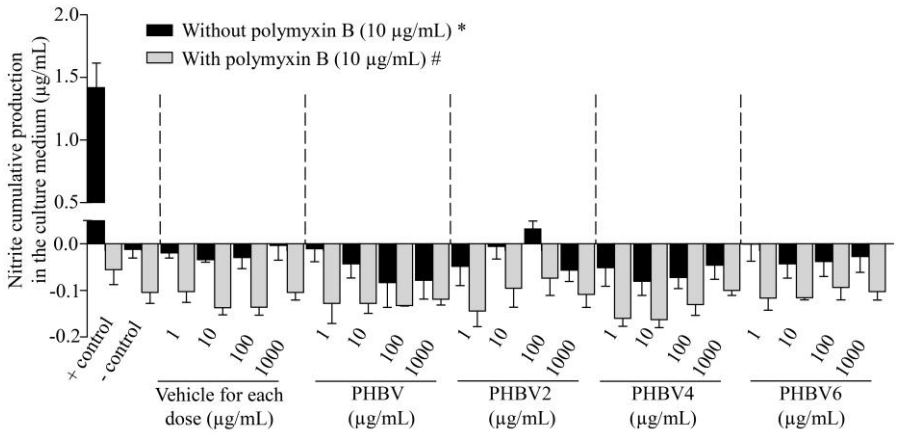

Figure 5.9: Effect of PHBV and PHBV/CNC nanocomposites on J774.A1 macrophages nitrite production. 250 ng/mL LPS was used as a positive control, and culture medium from untreated cells as a negative control. n=6.

5.4. Conclusions

Nanocomposites of poly (3-hydroxybutyrate-co-3-hydroxyvalerate)/cellulose nanocrystals with 2 wt.%, 4 wt.% and 6 wt.% of CNC were prepared. Samples were exposed to two steps of artificial weathering (16500 and 66000 kJ m^{-2}) and their thermal, structural and morphological properties were investigated by DSC, simultaneous SAXS/WAXS and SEM techniques, respectively. DSC and simultaneous SAXS/WAXS experiments results exhibited that crystallization process of nanocomposites began in higher temperatures when compared to PHBV, which verified the nucleating agent role of CNC. The analysis of thermal behavior in weathering samples revealed a decrease of crystallinity, although there was a secondary crystallization in the sample more exposed to radiation. Simultaneous SAXS/WAXS results showed that incorporation of CNC did not

lead to creation of new crystalline structures. SEM images showed well-dispersed morphology of all nanocomposites. Changes of the morphology of PHBV and its nanocomposites meanwhile artificial weathering were noted by appearance of blister-like points. Hydrophobicity of nanocomposites was found to be slightly lower than PHBV in humidity absorption tests. Results of water vapor transmission rate tests showed smaller values in nanocomposites, it was explained by less chain mobility, higher tortuosity and presence of CNC as physical barrier. Antimicrobial studies showed that samples containing zinc oxide and silver showed antimicrobial inhibition behavior against *L. monocytogenes, S. enterica, S. aureus* and *E. coli* strains. Also, it was confirmed that the PHBV and its nanocomposites are biocompatible. These nanocomposites could be a good alternative for packaging or other applications.

5.5. References

[1] E. Ten, J. Turtle, D. Bahr, L. Jiang, M. Wolcott, Thermal and mechanical properties of poly (3-hydroxybutyrate-co-3-hydroxyvalerate)/cellulose nanowhiskers composites, Polymer, 51: 2652 (2010)

[2] N. Lin, H. Jin, P. R. Chang, J. Feng, J. Yu, Surface acetylation of cellulose nanocrystal and its reinforcing function in poly (lactic acid), Carbohydrate Polymers, 83(4): 1834 (2011)

[3] S. Malmir, B. Montero, M. Rico, L. Barral, R. Bouza, Morphology, thermal and barrier properties of biodegradable films of poly (3-hydroxybutyrate-co-3-hydroxyvalerate) containing cellulose nanocrystals, Composites Part A, 93: 41 (2017)

[4] M. S. Rabello, J. R. White, Crystallization and melting behaviour of photodegraded polypropylene-I. Chemi-crystallization, Polymer, 38: 6379 (1997)

[5] Y. W. Leong, M. B. Abu Bakar, Z. A. Mohd Ishak, A. Ariffin, Characterization of talc/calcium carbonate filled polypropylene hybrid composites weathered in a natural environment, Polymer Degradation and Stability, 83(3): 411 (2004)

[6] B. Terseluis, U. W. Gedde, J. F. Jansson, Structure and morphology of thermally oxidized high density polyethylene pipes, Polymer Engineering Science, 22: 422 (1982)

[7] J. Scheirs, S. W. Bigger, O. Delatycki, Characterizing the solid-state thermal oxidation of poly (ethylene oxide) powder, Polymer, 32: 2014 (1991)

[8] A. K. Kulshreshta, Hand book of polymer degradation, Marcel Dekker, New York (1992)

[9] I. H. Craig, J. R. White, P. C. Kin, Crystallization and chemi - crystallization of recycled photo - degraded polypropylene, Polymer, 46: 505 (2005)

[10] H. Sato, N. Suttiwijitpukdee, T. Hashimoto, Y. Ozaki, Simultaneous Synchrotron SAXS/WAXD Study of Composition Fluctuations, Cold-Crystallization, and Melting in Biodegradable Polymer Blends of Cellulose Acetate Butyrate and Poly (3-hydroxybutyrate), Macromolecules, 45: 2783 (2012)

[11] U. A. Sezer, V. Sanko, Z. N. Yuksekdag, D. Uzundag, S. Sezer, Use of oxidized regenerated cellulose as bacterial filler for food packaging applictions, Cellulose, 23(5):3209 (2016)

[12] C. A. Davies, S. A. Rocks, M. C. O'Shaughnessy, D. Perrett, P. G. Winyard, Inflammation protocols, New Jersey: Humana Press, pages 305–320 (2003)

CHAPTER 6: Biocomposites of starch/PHBV microparticles: solvent cast film method

6.1. Introduction

Another biodegradable polymer which was studied in the present thesis was starch. As it was mentioned in the first chapter, starch possesses several desirable and some undesirable properties. Similar to other biodegradable polymers, introducing filler is considered as an effective solution to improve its properties.

Since one of the main challenges is preserving of biocompatibility of generated product, bio-based fillers are preferentially considered and selected. PHBV is a natural bacterial derivative polyester with marked biodegradability and biocompatibility activities. It had been used in several scientific reports as a natural-based matrix in polymeric composites and/or blends whereas its application as reinforcing agent for polymeric matrices has been barely tested [1-4].

To this end, starch/PHBV composites would be fitted in the classification of fully biodegradable materials. Thus, the principle objectives of present chapter consisted on firstly, analyze the role of PHBV microparticles as filler on the final properties of potato starch plasticized by glycerol and secondly, investigate the influence of glycerol concentration on the impact of PHBV microparticles in the starch. Obtained biocomposites were examined and discussed in the terms of crystalline structure, dynamic mechanical behavior, morphology and thermal stability as well as their humidity absorption and water vapor transmission rate. Obtained biocomposites could be considered for food packaging applications.

6.2. Experimental

6.2.1. Materials and processing

Used materials were potato starch, microparticles of PHBV and glycerol.

Biocomposites of potato starch/PHBV microparticles with two different concentrations (3 wt.% and 6 wt.% based on total dry mass) were prepared via solvent cast film method. Starch was kept in a desiccator at room temperature for one week before using. Then 2.1 g of starch were mixed with two different amounts of glycerol (0.90 g and 0.45 g) as plasticizer. Table 6.1 lists the sample codes and composition.

Table 6.1: Sample codes and compositions.

Sample	Starch (g)	Glycerol (g)	PHBV microparticles (wt.%)
PoS/Gly0.90	2.1	0.90	0
PoS/Gly0.90/PHBV3	2.1	0.90	3
PoS/Gly0.90/PHBV6	2.1	0.90	6
PoS/Gly0.45	2.1	0.45	0
PoS/Gly0.45/PHBV3	2.1	0.45	3
PoS/Gly0.45/PHBV6	2.1	0.45	6

In the case of biocomposites, PHBV microparticles were dry mixed with starch with specific concentration as indicated above. Meanwhile stirring with a glass bar, distilled water was introduced to the solution until reach the completely homogenous dispersion with the final volume of 60 mL. Then the mixture was heated in a microwave oven with manual stirring in order to complete the plasticizing process. Then it was poured onto a Teflon® sheet lined petri dish and was left for drying in an oven for 24 h at 30 °C. For the equilibration of the water content, all films were kept in a humidity chamber with 40% RH at room

temperature for 72 h prior to do any experiments. Films thicknesses were 0.10 - 0.12 mm after complete drying.

6.2.2. Characterization techniques

Used characterization techniques were WASX, SEM, DMA, TGA, humidity absorption and WVTR (relative humidity of 5% and 40% in both sides).

6.3. Results and discussions

6.3.1. X-ray diffraction analysis

WAXS patterns can be considered as a fairly reliable indicator of crystalline features of polymeric materials and composites. Formation and growth of the crystalline structures depend on several factors including chain mobility, thermal history, purity of the sample, concentration of different phases and crystal surface energy. In the case of starch, botanical origin also plays a vital role in crystalline structure. Fig 6.1 shows WAXS patterns for potato starch with different glycerol contents and its corresponding biocomposites. Fig 6.1a, also includes the WAXS patterns for PHBV microparticles. Potato starch granules presented B - type structure, characterized by two diffraction peaks located at $2\theta = 5.8°$ and $2\theta = 17.3°$. WAXS profile of potato starch granules was reported elsewhere [5]. As inferred from Fig. 6.1a, plasticizing process successfully occurred, concluding from appearance of a broad hump centered at $2\theta \approx 19°$ indicating amorphous state of the material [6]. However, peak intensities increased slightly in PoS/Gly0.90/PHBV3 and PoS/Gly0.90/PHBV6 biocomposites that might be resulted from residual crystalline structures that remained after plasticizing process or even process-induced crystalline arrangements. It was reported that during the process of starch with

plasticizer, amylose chains might form a single helix complex with plasticizer molecules or other lipids [7, 8]. Elsewhere, substituting of strong interactions between hydroxyl groups of starch molecules with hydrogen bonds between starch and plasticizer molecules was mentioned as a reason of process - induced crystallinity [9].

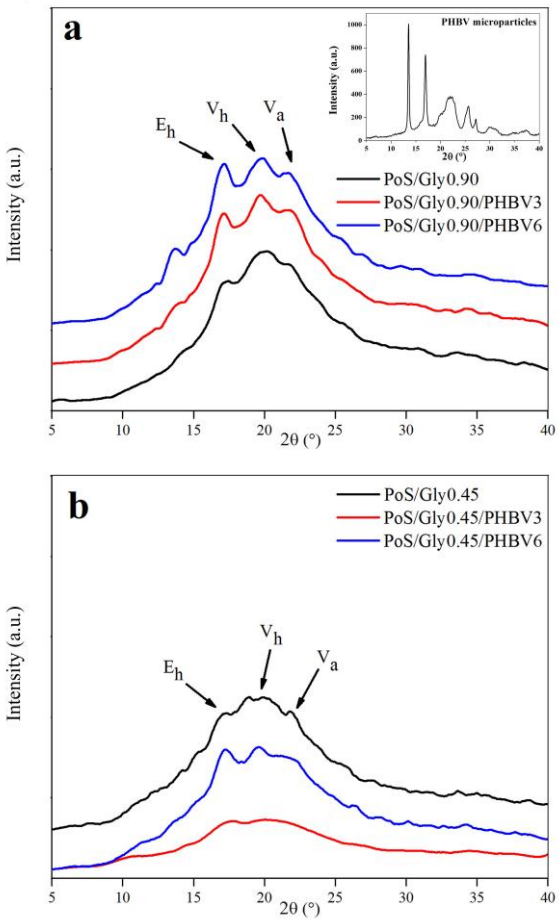

Figure 6.1: WAXS patterns of samples with higher glycerol content (a) and PHBV microparticles and samples with less glycerol content (b).

Depending on the botanical origin of the starch, three process-induced crystal arrangements, namely E_h ($2\theta = 18.0°$), V_h ($2\theta = 19.6°$) and V_a-type ($2\theta = 21.6°$) could be considered [5]. V_h-type and E_h-type structure consist of six-fold and seven-fold single helices of amylose-glycerol complex, in respective order. V_h-type structure is convertible to V_a-type structure under dehydration conditions. Results showed that PoS/Gly0.90, PoS/Gly0.90/PHBV3 and PoS/Gly0.90/PHBV6 contain all mentioned crystalline structures. V_h-type and V_a-type structures were nearly similar, confirming that these crystalline structures of the starch remained unchanged upon PHBV microparticles incorporation. At the same time, peak ascribed to E_h-type structures was intensified. As a matter of fact, E_h-type structures are more stable in low humidity environments [8]. So, it might be concluded that in PoS/Gly0.90/PHBV3 and PoS/Gly0.90/PHBV6 biocomposites, less hydrophilic nature of the PHBV microparticles would be favorable to E_h-type orientation. Fig. 6.1b shows WAXS patterns of PoS/Gly0.45, PoS/Gly0.45/PHBV3 and PoS/Gly0.45/PHBV6. The amorphous halo was more pronounced in these samples when compared to Fig. 6.1a. Besides, peak intensity was less for PoS/Gly0.45/PHBV3 and PoS/Gly0.45/PHBV6 biocomposites with respect to the PoS/Gly0.45. Although, it would be fairly complicated to rule out the accurate relative contributing parameters in limiting the crystallization capacity of PoS/Gly0.45/PHBV3 and PoS/Gly0.45/PHBV6 biocomposites, lower chain movement ability due to simultaneous presence of PHBV microparticles and less glycerol content is thought to be an effective factor. Higher peak intensity in the PoS/Gly0.45/PHBV6 biocomposite was supposed to be due to as a result of higher PHBV microparticles concentration that would favor the chain orientation. Teixeira et al. reported that less glycerol content in cassava starch nanocomposites would lead to reduction of the quantity of glycerol-

amylose complexes that resulted in lesser V_h-type crystalline arrangements [10]. Róz et al. observed higher crystallinity in plasticized corn starch when concentration of plasticizer was higher and justified it with higher starch chain mobility [11].

6.3.2. Morphological aspects

Dispersion state of the reinforcement agent into the matrix is remarkably involved in determination of the ultimate efficiency and performance of composite materials. Activity of matrix/filler interphase, adhesion forces and interactions, sample preparation techniques, filler characteristics such as shape, size, functionality or concentration would alter the morphological properties. In this regard, morphology of starch and starch/PHBV microparticles biocomposites were compared by SEM and the corresponding images are shown in Fig. 6.2. PoS/Gly0.90 (Fig. 6.2a) exhibited uniform surface. The incorporation of the PHBV microparticles did not cause any significant change in the biocomposite with 3 wt.% of the PHBV microparticles (Fig. 6.2b) indicating good dispersion state of the PHBV microparticles in the starch. Increasing PHBV microparticles content to 6 wt.% led to formation of few visible agglomerations (Fig. 6.2c).

SEM micrographs for PoS/Gly0.45/PHBV3 and PoS/Gly0.45/PHBV6 showed well dispersion state in the film surface that also was preserved with increment of the PHBV microparticles content. There were not observable agglomerations in these biocomposites even at high level of PHBV microparticles concentration (6 wt.%) (Fig. 6.2f). This might be in relation with confined segmental mobility and consequently higher viscosity of the starch in the presence of less glycerol, which would induce more effective forces to be transferred from starch to the PHBV microparticles meanwhile stirring. This

would be helpful for PHBV microparticles to be distributed individually and with more homogeneity in the starch.

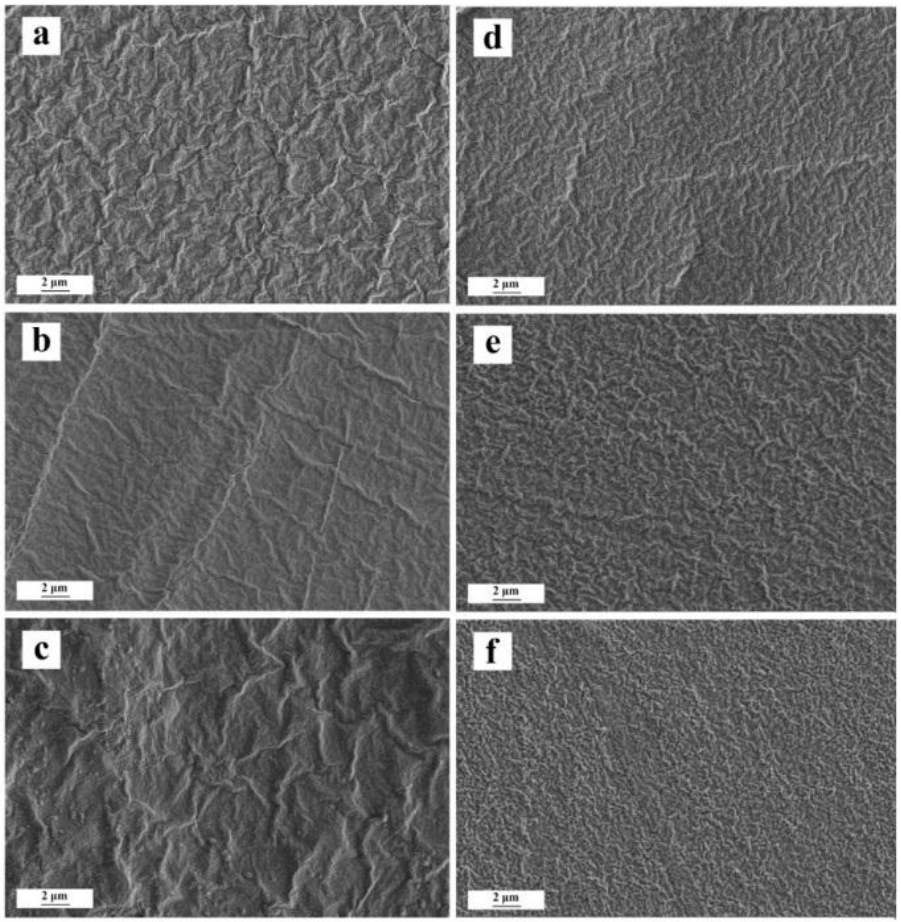

Figure 6.2: SEM images of PoS/Gly0.90 (a), PoS/Gly0.90/PHBV3 (b), PoS/Gly0.90/PHBV6 (c), PoS/Gly0.45 (d), PoS/Gly0.45/PHBV3 (e) and PoS/Gly0.45/PHBV6 (f).

6.3.3. Dynamic mechanical analysis

Stiffness and damping properties are two important characteristics of the polymeric materials which are reflected in storage modulus (E') and tan δ, respectively. Both parameters were measured as a function of temperature and the obtained values are presented in Fig. 6.3 and Table 6.2. When packaging applications are aimed, 20 °C (room temperature) would be the temperature of interest. As can be seen, all developed biocomposites show higher E' in whole range of temperature than starch and the increment of PHBV microparticles content provided stiffer biocomposites. This confirmed the reinforcing effect of the PHBV microparticles in the starch similar to other systems [12]. It could be explained by formation of inter molecular hydrogen bonds between –OH groups of starch and –C=O groups of PHBV microparticles and also intra molecular hydrogen bonds between –C–H and O=C– groups of different PHBV microparticles chains which served as physical cross-links inside the biocomposite [13]. However, decreasing trend of the E' with increasing the temperature was linked with dissociation of mentioned interactions which would further progress as test temperature increased.

Results of tan δ showed two peaks associated with two relaxations for the starch and its biocomposites, Table 6.2. As reported in the literature, starch and glycerol are partially immiscible and heterogeneous. This is why in a glycerol plasticized starch system, two separate phases titled as glycerol-rich and starch-rich are formed. In a tan δ curve, molecular motions in glycerol-rich phase are corresponded to the lower tan δ maximum (T_1) and molecular motions in starch-rich are ascribed to the higher tan δ maximum (T_2) [14-16]. Table 6.2 summarizes T_1 and T_2 temperatures for starch and the biocomposites. As Fig. 6.3b shows, by addition of PHBV microparticles, T_1 position was approximately remained almost constant and the second

relaxation peak shifted to higher temperatures and broadened, even it was difficult to assess its exact temperature. It is well accepted that higher glass transition is arisen from chain mobility reduction. Hence, this suggested the higher interaction and compatibility of the PHBV microparticles with starch-rich phase which led to the major part of PHBV microparticles to be located in this phase and disturb free motion of starch chains. This might concern with formation of hydrogen bonds between hydroxyl groups in the starch structure and carbonyl groups in the PHBV microparticles. Yu et al. proposed that the filler might serve as junction points for polymeric chains, which would reduce the free volume and chain mobility [17].

Results of dynamic mechanical analysis showed that reduction in glycerol content would promote the stiffness in the whole temperature range. If recall here SEM results, it could be explained by the fact that, higher viscosity of the starch matrix with diminished glycerol content would favor better PHBV microparticles dispersion and consequently more increment in the storage modulus. This confirmed the reinforcing effect of PHBV microparticles inside the starch, effective stress transfer from starch to PHBV microparticles and simultaneously showed strong adhesion forces and hydrogen bonds interactions at starch/PHBV microparticles interface [18].

As Fig. 6.3d shows, the position of both relaxation temperatures associated with glycerol-rich and starch-rich phases were altered and moved to higher temperature after incorporation of PHBV microparticles.

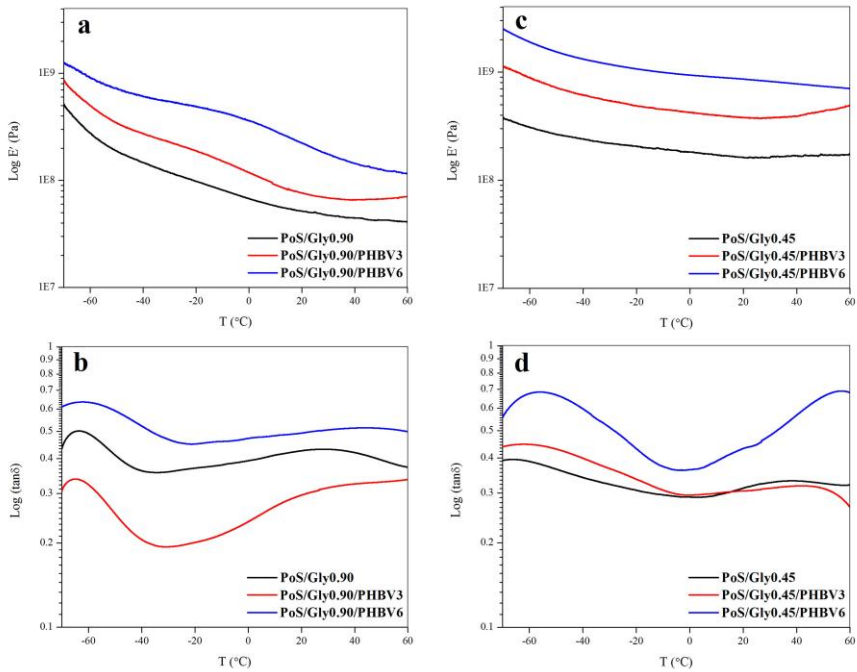

Figure 6.3: Storage modulus (a) and tan δ (b) curves versus temperature for samples with higher glycerol content and storage modulus (c) and tan δ (d) curves versus temperature for samples with less glycerol content.

Table 6.2: Storage modulus at 20 °C and temperatures of relaxation of glycerol-rich (T_1) and starch-rich (T_2) phases.

Sample	E´ (Pa)	T_1 (°C)	T_2 (°C)
PoS/Gly0.90	5.2E+07	-63.3	33.2
PoS/Gly0.90/PHBV3	7.6E+07	-63.6	-
PoS/Gly0.90/PHBV6	2.2E+08	-57.4	50.0
PoS/Gly0.45	1.6E+08	-63.6	40.6
PoS/Gly0.45/PHBV3	3.8E+08	-57.1	42.9
PoS/Gly0.45/PHBV6	8.7E+08	-55.4	53.1

However, T_1 and T_2 shifts were higher for the biocomposites with less glycerol content. In particular, PoS/Gly0.45/PHBV6 displayed a drop after the first relaxation. Montero et al. related the intensity of the mentioned drop to the degree of free glycerol molecules mobility [5]. It could be concluded that some glycerol molecules interacted with PHBV microparticles as it was reflected by the shift of T_1 to higher temperatures, but the majority of the PHBV microparticles are located in the starch – rich phase.

6.3.4. Thermal stability

Thermal stability of starch, biocomposites and glycerol was evaluated by means of TGA and the related curves are displayed in Fig. 6.4.

Starch and biocomposites behaved similar in the temperature range of the test and showed three main temperature ranges of weight loss in agreement with previous studies [5, 15, 19]. First, in the range of 50 °C to 120 °C related to water loss, second in the range of 120 °C to 300 °C corresponds to the glycerol-rich phase thermal degradation and the last one in the range of 300 °C to 450 °C corresponds to the starch-rich phase thermal degradation.

Results showed that thermal stability for the biocomposites was higher than for starch for both glycerol contents. In the case of loss water, lower weigh loss of biocomposites was due to lower hydrophilicity of PHBV microparticles. In the case of glycerol-rich phase degradation, this might be due to the fact that in the biocomposites, some glycerol molecules were interacted with the PHBV microparticles and less glycerol molecules were free. For the last degradation step, PHBV microparticles/starch hydrogen bonds interactions should be taken into account as a reason.

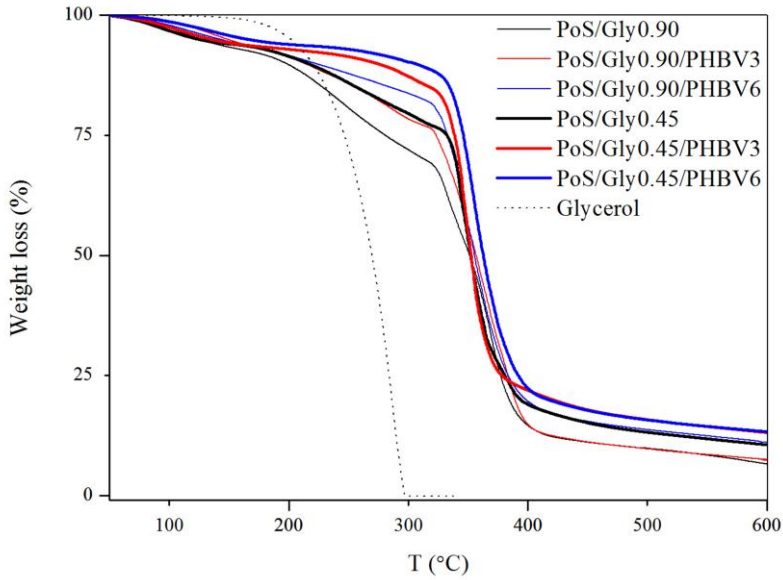

Figure 6.4: TGA curves of potato starch, its biocomposites and glycerol.

Further, it was obvious that all the samples with less glycerol content exhibited higher thermal stability with respect to their corresponding samples with higher glycerol content in all over range. This might be raised from lower free glycerol molecules and more restricted mobility of starch chains in the presence of less glycerol and PHBV microparticles. Also in overall, the amount of remained char percent increased as PHBV microparticles concentration increased.

6.3.5. Humidity absorption

Hydrophilic nature of starch makes it vulnerable in dimensional stability, mechanical, thermal and barrier properties since it leads to weakening molecular interactions. Incorporation of PHBV microparticles supposed to be effective in reduction of hydrophilicity and humidity sensitivity of starch and

make it more efficient in food packaging applications .The evolution of humidity absorption with the time in three different relative humidity chambers (95%, 75% and 54 %) is plotted in Fig. 6.5. Results showed that independent of the composition of each sample, they behaved nearly similar in three steps. Humidity absorption started with the initial absorption, followed by reach to a maximum range and then finalized by an equilibrium plateau zone. However, dropping of the humidity absorption after maximum point was more pronounced for the highest relative humidity chamber (95%). This reflected the retrogradation phenomena when the absorbed humidity leaves the starch.

Comparison between the results of three humidity chambers showed that the higher the relative humidity, the greater the percentage of humidity absorption would be. Also, as it was expected, the amount of humidity absorption was smaller for the biocomposites when compared with the starch due to lower hydrophilicity of biocomposites.

Comparison of the humidity absorption behavior of all samples revealed that samples with less glycerol content absorbed less humidity. This can be explained by less chain mobility in them that hinder free molecules movement.

The study of humidity absorption provides a qualitative understanding about the hydrophilicity feature of the material, but still there are uncertainties about the diffusion of external gases and their movement inside the material to deal with. Accordingly, as a solution, humidity absorption experiment could be completed with the measurements of water vapor transmission rate as discussed below.

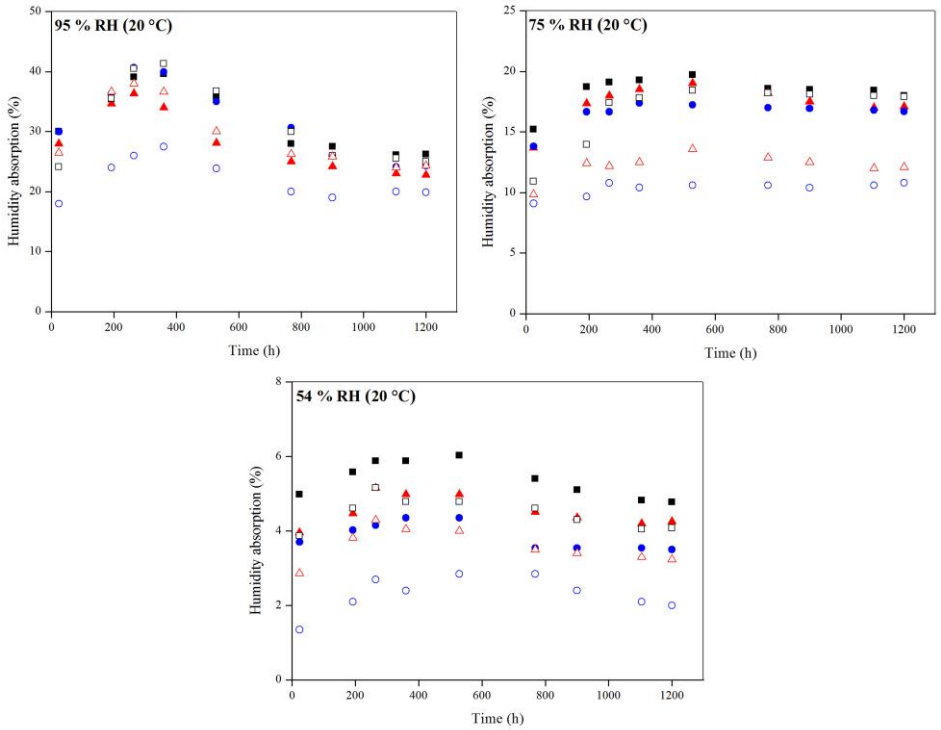

Figure 6.5: Humidity absorption versus time curves for potato starch and its biocomposites in different relative humidity environments: 95%, 75% and 54%. PoS/Gly0.90 (■),PoS/Gly0.90/PHBV3 (▲), PoS/Gly0.90/PHBV6 (●), PoS/Gly0.45 (□), PoS/Gly0.45/PHBV3 (△) and PoS/Gly0.45/PHBV6 (○).

6.3.6. Water vapor transmission rate

It is widely recognized that water vapor diffusion inside the packaging space is one of the main factors for the deterioration the composition and quality of the food and consequently reduces shelf life and storage time. For this reason, production of food packaging articles with low water vapor transmission rate, which are favorable in both economic and health aspects is of great importance. Water vapor transmission rates for all samples were measured

and displayed in Fig. 6.6. Results showed that water vapor transmission rate was reduced after the incorporation of PHBV microparticles.

Water vapor transmission through films would be disturbed upon enlarging of migration gas pathways and increasing tortuosity after addition of PHBV microparticles, which act as physical barriers in the starch. Increasing PHBV microparticles concentration was beneficial to reduction of water vapor transmission rate.

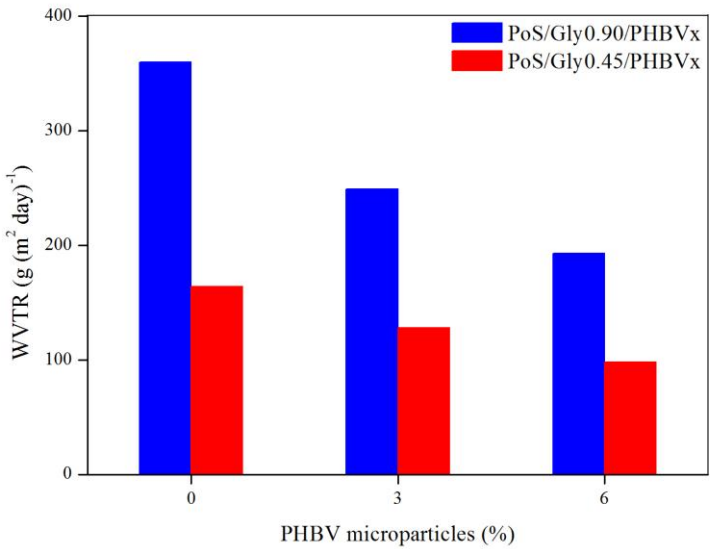

Figure 6.6: Water vapor transmission rate against PHBV microparticles content for potato starch and its biocomposites. The x symbol refers to the PHBV microparticles content.

However, samples with less glycerol content exhibited smaller water vapor transmission rate when compared to samples with higher glycerol content.

Similar to the given interpretation in the humidity absorption section, this is linked with the less movement ability of the polymeric chains in the samples with less glycerol content. Chain mobility can facilitate the passing gas molecules to move inside the film. Samples with less glycerol content have less chain mobility and also contain less free volume to host water vapor molecules.

6.4. Conclusions

Development of potato starch/PHBV microparticles biocomposite films for food packaging applications was aimed in the present chapter. Starch was plasticized with glycerol. Both influences of PHBV microparticles and glycerol concentration on crystallinity, mechanical and thermal properties as well as humidity absorption and water vapor transmission rate were analyzed. Wide angle X-ray scattering (WAXS) results confirmed the occurrence of plasticizing process and showed that process-induced crystallinity degree was reduced when starch chain mobility was low. Morphological studies showed well dispersed state in biocomposites. However, less glycerol concentration allowed incorporation of more PHBV microparticles in biocomposites associated with good dispersion state. Results of dynamic mechanical analysis showed that introducing of PHBV microparticles led to notable improvement in mechanical properties of potato starch. Higher storage modulus was obtained upon introducing the PHBV microparticles. Effective interaction between the PHBV microparticles and starch-rich phase was confirmed from alteration of second relaxation peak in tan δ curves to higher temperatures. TGA results strengthened the given explanation about DMA and SEM analysis and showed that reduced glycerol content favored more thermal stability. All biocomposites absorbed less humidity when compared to potato starch.

However, biocomposites with less glycerol were more humidity resistant. They possessed lower water vapor transmission rate due to less chain mobility and higher tortuosity. To summarize, it was found that introducing PHBV microparticles was in the favor of potato starch properties improvement and at the same time, glycerol concentration has an extensive contribution in the biocomposites characteristics.

6.5. References

[1] B. Wang, J. Li, J. Zhang, H. Li, P. Chen, Q. Gu, Z. Wang, Thermo-mechanical properties of the composite made of poly (3-hydroxybutyrate-co-3-hydroxyvalerate) and acetylated chitin nanocrystals, Carbohydrate Polymers, 95: 100 (2013)

[2] H. Y. Yu, Z. Y. Qin, Z. Zhou, Cellulose nanocrystals as green fillers to improve crystallization and hydrophilic property of poly (3-hydroxybutyrate-co-3-hydroxyvalerate, Progress in Natural Science: Materials International, 21: 478 (2011)

[3] H. Y. Yu, Z. Y. Qin, L. Liu, X. G. Yang, Y. Zhou, J. M. Yao, Comparison of the reinforcing effects for cellulose nanocrystals obtained by sulfuric and hydrochloric acid hydrolysis on the mechanical and thermal properties of bacterial polyester, Composite Science and Technology, 87: 22 (2013)

[4] H. Y. Yu, Z. Y. Qin, Y. N. Liu, L. Chen, N. Liu, Z. Zhou, Simultaneous improvement of mechanical properties and thermal stability of bacterial polyester by cellulose nanocrystals, Carbohydrate Polymers, 89: 971 (2012)

[5] B. Montero, M. Rico, S. Rodriguez-Llamazares, L. Barral, R. Bouza, Effect of nanocellulose as a filler on biodegradable thermoplastic starch films from tuber, cereal and legume, Carbohydrate Polymers, 157: 1094 (2017)

[6] H. Angellier, S. Molina-Boisseau, P. Dole, A. Dufresne, Thermoplastic starch-waxy maize starch nanocrystals nanocomposites, Biomacromolecules, 7: 531 (2006)

[7] Y. Nishiyama, K. Mazeau, M. Morin, M. B. Cardoso, H. Chanzy, J. L. Puteaux, Molecular and Crystal Structure of 7-Fold V-Amylose Complexed with 2-Propanol, Macromolecules, 43: 8628 (2010)

[8] M. Rico, S. Rodriguez-Llamazares, L. Barral, R. Bouza, B. Montero, Processing and characterization of polyols plasticized-starch reinforced with microcrystalline cellulose, Carbohydrate Polymers, 149: 83 (2016)

[9] J. Yang, J. Yu, X. Ma, Study on the properties of ethylenebisformamide and sorbitol plasticized corn starch (ESPTPS), Carbohydrate Polymers, 66: 110 (2006)

[10] E. M. Teixeira, D. Pasquini, A. A. S. Curvelo, E. Corradini, M. N. Belgacem, A. Dufresne, Cassava bagasse cellulose nanofibrils reinforced thermoplastic cassava starch, Carbohydrate Polymers, 78: 422 (2009)

[11] A. L. D. Roz, A. J. F. Carvalho, A. Gandini, A. A. S. Curvelo, The effect of plasticizers on thermoplastic starch compositions obtained by melt processing, Carbohydrate Polymers, 63: 417 (2006)

[12] J. I. Moran, A. Vazquez, V. P. Cyras, Bio-nanocomposites based on derivatized potato starch and cellulose, preparation and characterization, Jornal of Material Science, 48: 7196 (2013)

[13] H. Sato, N. Suttiwijitpukdee, T. Hashimoto, Y. Ozaki, Simultaneous Synchrotron SAXS/WAXD Study of Composition Fluctuations, Cold-Crystallization, and Melting in Biodegradable Polymer Blends of Cellulose Acetate Butyrate and Poly (3-hydroxybutyrate), Macromolecules, 45: 2783 (2012)

[14] H. M. Wilhelm, M. R. Sierakowski, G. P. Souza, F. Wypych, Starch films reinforced with mineral clay, Carbohydrate Polymers, 52: 101 (2003)

[15] N. L. Garcia, L. Ribba, A. Dufresne, M. I. Aranguren, S. Goyanes, Physico-Mechanical Properties of Biodegradable Starch Nanocomposites, Macromolecular Materials and Engineering, 294: 169 (2009)

[16] L. Castillo, O. Lopez, C. Lopez, N. Zaritzky, M. A. Garcia, S. Barbosa, M. Villar, Thermoplastic starch films reinforced with talc nanoparticles, Carbohydrate Polymers, 95: 664 (2013)

[17] J. G. Yu, N. Wang, X. F. Ma, Fabrication and characterization of Poly (lactic acid)/Acetyl Tributyl Citrate/Carbon Black as Conductive Polymer Composites, Biomacromolecules, 9: 1050 (2008)

[18] K. Gonzalez, A. Retegi, A. Gonzales, A. Eceiza, N. Gabilondo, Starch and cellulose nanocrystals together into thermoplastic starch bionanocomposites, Carbohydrate Polymers, 117: 83 (2015)

[19] J. W. Lawton, Effect of starch type on the properties of starch containing films, Carbohydrate Polymers, 29: 203 (1996)

CHAPTER 7: Self-reinforced biocomposites of PHBV/PHBV microparticles: solvent cast film method

7.1. Introduction

As discussed before, the introduction of fillers is a common solution to improve different properties of polymeric matrix. However, it should be noted that applying mentioned solution could be favorable but due to differences in the material nature of phases and fillers, they might be associated with some drawbacks such as low compatibility, deboning zones or appearance of cracks. In this sense, another strategy in order to overcome mentioned problems might be self - reinforcement, which means production of composites with the same matrix and filler material. The purpose of the present chapter focuses for the first time on the use of microparticles of PHBV as a novel reinforcement for improving and modification the properties of PHBV. Microparticles of PHBV were incorporated into a PHBV matrix through solvent cast film method. The influence of the microparticles of PHBV concentration on thermal, morphological and barrier properties (against water vapor, oxygen and carbon dioxide) of the self-reinforced films (srPHBV) as well as their crystal structure were discussed in detail. In particular, these studies were undertaken in order to design films that could be used in food packaging industry.

7.2. Experimental

7.2.1. Materials and processing

Used materials were PHBV, microparticles of PHBV and dichloromethane.

Self – reinforced films of PHBV with different concentration of PHBV microparticles (2 wt.%, 4 wt.% and 6 wt.% corresponded to srPHBV-2, srPHBV-4 and srPHBV-6 samples) were prepared via solvent cast film method. PHBV was dried in an oven at 70 °C for 24 h before using and then it was dissolved in dichloromethane at 80 °C for 2 h. After, it was left for cooling at room

temperature. A suspension of PHBV microparticles/dichloromethane was prepared and kept in an ice bath to reach the temperature of 0 °C. After that, it was added to PHBV solution and ultra-sonicated in an ice bath for 1 h. Then, the mixture was placed in a petri dish and was left overnight for the evaporation of the solvent at room temperature. Thickness of the obtained films was 90±5 μm. All films were kept in desiccator with silica gel for one week prior to do any analysis.

7.2.2. Characterization techniques

Used characterization techniques were DSC, SAXS/WAXS, TEM, SEM, POM, AFM, WVTR (relative humidity of 10% and 100% in both sides), OTR and CDTR.

7.3. Results and discussions

7.3.1. Thermal properties and crystallization

DSC tests were done to investigate the effect of incorporation of PHBV microparticles on thermal properties and crystallinity of PHBV films. Obtained cooling and heating thermograms and thermal parameters are shown in Fig. 7.1 and Table 7.1, respectively. Fig. 7.1a exhibits DSC crystallization exotherms of PHBV microparticles, PHBV and srPHBV films during cooling scan from 200 °C to 30 °C at 10 °C min^{-1}. It can be observed that the incorporation of PHBV microparticles in the PHBV led to a shift of the crystallization temperature to higher temperatures. On the other hand, the crystallization peak of srPHBV films sharpened, showing that microparticles of PHBV acted as a nucleating agent and increase the overall crystallization rate. The influence of microparticles of PHBV on the crystallinity of PHBV films is shown in Table 7.1. The presence of PHBV microparticles induces an increase in the X_c values.

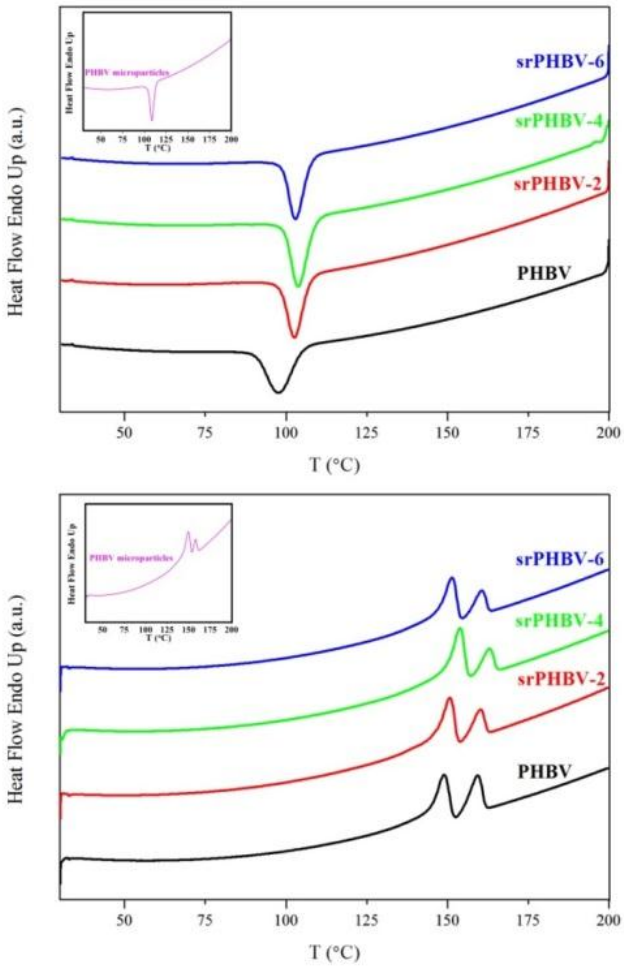

Figure 7.1: DSC thermograms during cooling from the melt (a) and posterior heating (b) of PHBV and srPHBV films.

Fig. 7.1b shows the heating thermograms obtained after cooling process. Thermograms of PHBV microparticles, PHBV and srPHBV films show bimodal endothermic peaks. According to the literature, the lower melting peak is

assigned to the less perfect crystals while the upper one is related to more perfect recrystallized crystals [1-3].

Both melting peaks shift to higher temperatures with increasing the PHBV microparticles content. The most relevant result was the reduction of the enthalpy corresponding to the second melting peak, due to the nucleation effect of the PHBV microparticles that accelerates the crystallization of PHBV in the srPHBV films. Therefore, the crystals formed are smaller than those in PHBV film.

Table 7.1: Thermal parameters of non-isothermal crystallization and melting process of PHBV microparticles, and PHBV and srPHBV films.

Sample	**T_c (°C)**	**T_{m1} (°C)**	**T_{m2} (°C)**	**ΔH_c (J g^{-1})**	**X_c (%)**
PHBV microparticles	108.7	149.6	158.1	54.7	50.2
PHBV	97.6	148.9	159.3	50.3	46.1
srPHBV-2	102.6	150.8	160.1	53.4	49.0
srPHBV-4	103.8	153.9	162.9	54.1	49.6
srPHBV-6	103.0	151.4	160.6	51.4	47.2

7.3.2. SAXS and WAXS analysis

Combination of SAXS and WAXS techniques can provide reliable estimation about the thickness of crystalline lamellae, dispersion state of the filler and crystalline structure of polymeric materials [4-6]. In this sense, simultaneous SAXS/WAXS experiments were performed for PHBV and srPHBV-6 films in

order to determine the possible influence of the filler on crystalline structure of the PHBV.

WAXS diffractograms during thermal scans for PHBV and srPHBV-6 films are given in Fig. 7.2. As can be seen at room temperature, all main characteristic diffraction peaks of orthorhombic α – type crystalline structure of PHBV can be observed [7, 8]. Unchanged peaks positions also confirmed the orthorhombic crystalline structure of srPHBV-6 sample.

The crystallinity ($\chi_{c\,(WAXS)}$) of all samples was calculated using WAXS patterns at 30 °C with the following equation, Eq. 1:

$$\chi_{c(WAXS)} = \frac{Ac}{A_a + A_c} \cdot 100 \qquad (1)$$

Where A_a and A_c are the areas of amorphous and crystalline peaks in WAXS patterns, respectively. Obtained data are listed in Table 7.2. As it was expected from DSC results in the previous section, the incorporation of the filler led to an increase in the crystallinity degree.

Furthermore, from WAXS patterns at 200 °C, amorphous peak was detected which was centered nearly at 2θ=14° for both samples. According to this, the distance between PHBV macromolecules (d_{halo}) was calculated [9] and reported in Table 7.2. Results showed that d_{halo} was slightly higher for srPHBV-6 film with respect to PHBV film that might be explained by the filler-PHBV interactions. The microparticles were located between PHBV macromolecules. Because of this fact, the intermolecular distance increases.

As Fig. 7.2 shows, both PHBV and srPHBV films behaved similar but some differences are visible in the crystallization and melting temperatures. The

crystallization of PHBV started at 112 °C while for srPHBV-6 the crystallization started at 114 °C.

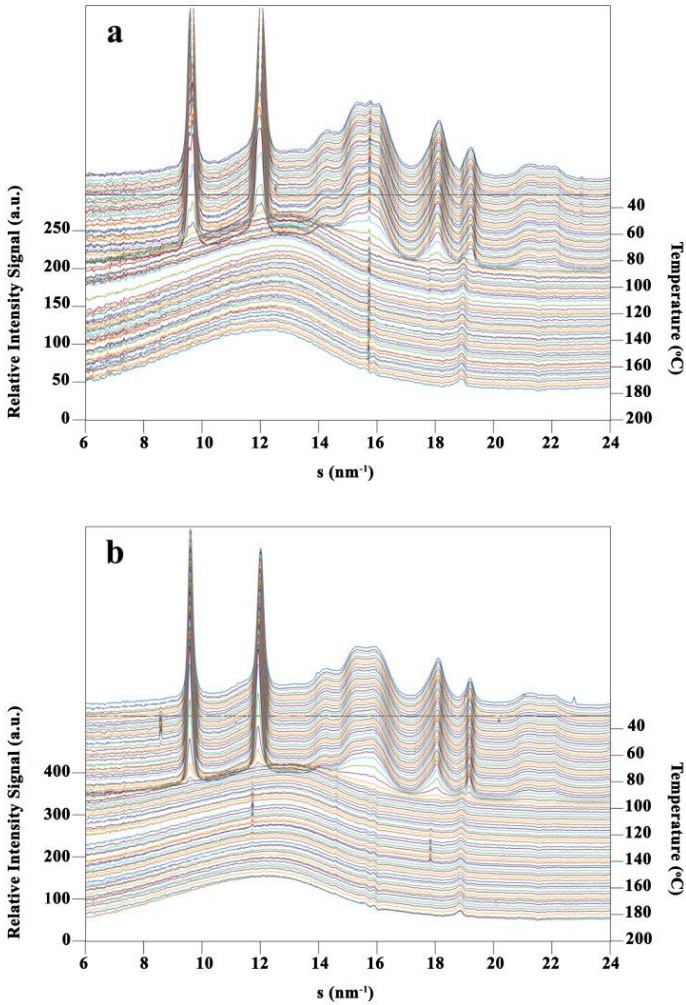

Figure 7.2: WAXS profiles of PHBV (a) and srPHBV-6 (b) films**.**

Considering WAXS evolution in heating scan showed that the melting process of crystallites started at 130 °C for PHBV and at 146 °C for srPHBV-6. In this case, decreasing peak intensity showed the melting of the thinner, smaller and less stable crystalline structure at early stages of the melting which then follows by thicker and more stable ones. Rule et al. used Guinier approximation for calculating the thickness of crystalline lamellae in the PHBV copolymer and observed that thicker lamellae preserved their structure until higher temperatures and were the last to be melted [10]. Furthermore, as it is evidenced, peak location remained unchanged meanwhile heating process.

Representative SAXS difractograms obtaining during crystallization for PHBV and srPHBV-6 films are shown in Fig. 7.3. As it was explained before, the parameter s_{max} is defined as the inverse of the long spacing *(L)*, where *L* is the sum of thickness of repeating crystalline (L_c) and amorphous (L_a) sections. Therefore an increment in *L* value happened which might be raised from growth in lamellar arrangements thickness and/or amorphous spacing. This can affect the electron density fluctuations between amorphous and crystalline layers, which it is considered in vertical direction to the lamellae planes [9, 10]. In a similar study for poly (3-hydroxybutyrate) (PHB), it was reported that decrement of s_{max} was due to the growth of crystalline lamellar and thickening of the average lamellar spacing [7].

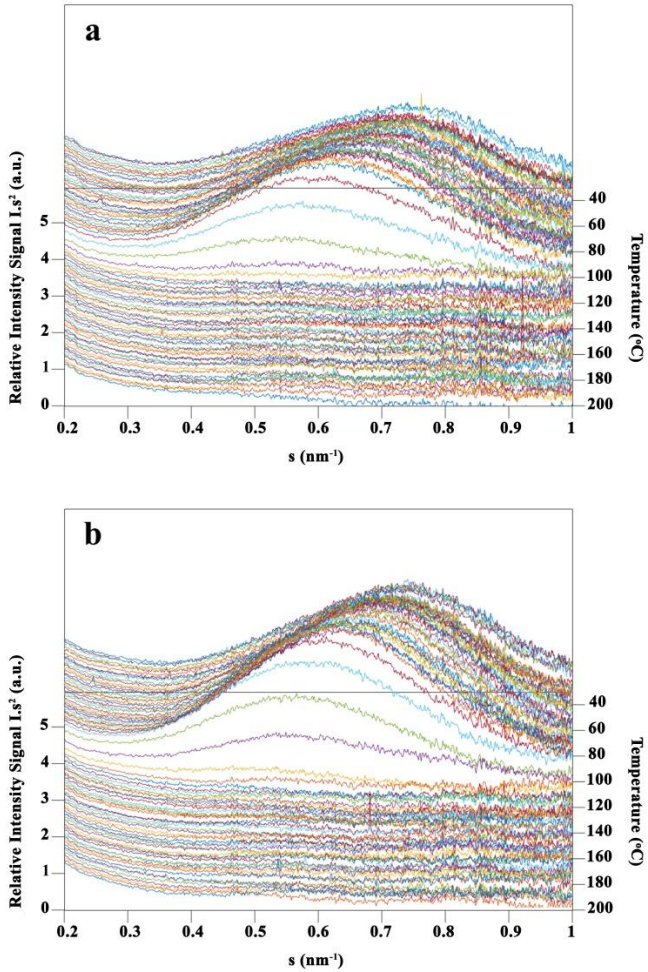

Figure 7.3: SAXS profiles of PHBV (a) and srPHBV-6 (b) films**.**

In order to study the effect of filler loading on crystalline features of PHBV more accurately, Lorentz-corrected SAXS diffractograms (Is^2 versus s) at room temperature were used to calculate long spacing parameter and the results are shown in Table 7.2. Results showed nearly same long spacing for both samples.

The DSC results proved both higher crystallinity degree and higher melting temperature in srPHBV-6 film with respect to PHBV film as discussed in WAXS section too. Thus, it can be concluded that slightly thicker crystalline lamellae were formed in srPHBV-6 film. In order to elucidate more of this, semicrystalline samples were considered as a binary system consist of two phases and then thickness of crystalline sections (L_c) calculated simply using Eq. 2:

$$L_c = L \times \chi_{c\,(WAXS)} \qquad (2)$$

Obtained results are summarized in Table 7.2 and confirmed that L_c was higher in the srPHBV-6 film.

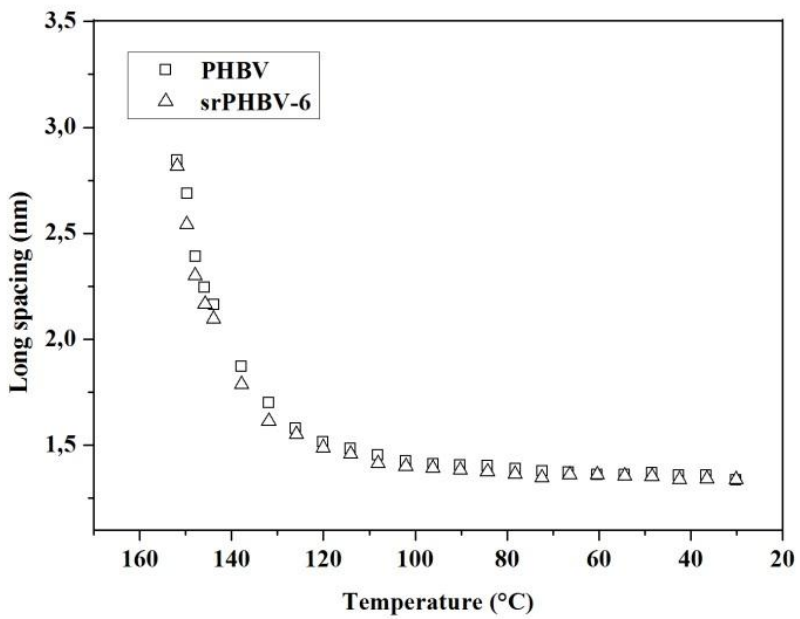

Figure 7.4: Variation of long spacing as a function of temperature of PHBV and srPHBV-6 films.

Fig. 7.4 shows the variation of long spacing parameter with temperature for PHBV and srPHBV-6 films. Both samples exhibited similar behavior with a significant increment at around 140 °C. However, for self - reinforced films the long spacing parameter was measurable from slightly higher temperatures (154 °C) when compared to the PHBV (152 °C).

Table 7.2: SAXS/WAXS data of PHBV and srPHBV-6 films.

Sample	**$\chi_{c\,(WAXS)}$ (%)**	**d_{halo} (nm)**	**L (nm)**	**L_c (nm)**
PHBV	58.9	0.511	1.3	0.77
srPHBV-6	64.2	0.517	1.4	0.90

7.3.3. Morphology

The filler dispersion state plays an important role on the final properties of the composites. This is connected with several factors such as filler-matrix interactions, method and conditions of the filler incorporation, filler particle size and filler content. In this regard, the study of the morphologies of the films was done via TEM and SEM. Also, to complete the morphological study, AFM and POM were used.

TEM results (Fig. 7.5) show individual and uniform dispersion of microparticles in the srPHBV-2 film (Fig. 7.5b). By increasing the filler loading to 4 wt.% and 6 wt.%, homogenous and individual distribution of PHBV microparticles can be seen in Figs 7.5c and 7.5d, respectively. Therefore, there was good dispersion of PHBV microparticles in all srPHBV films studied.

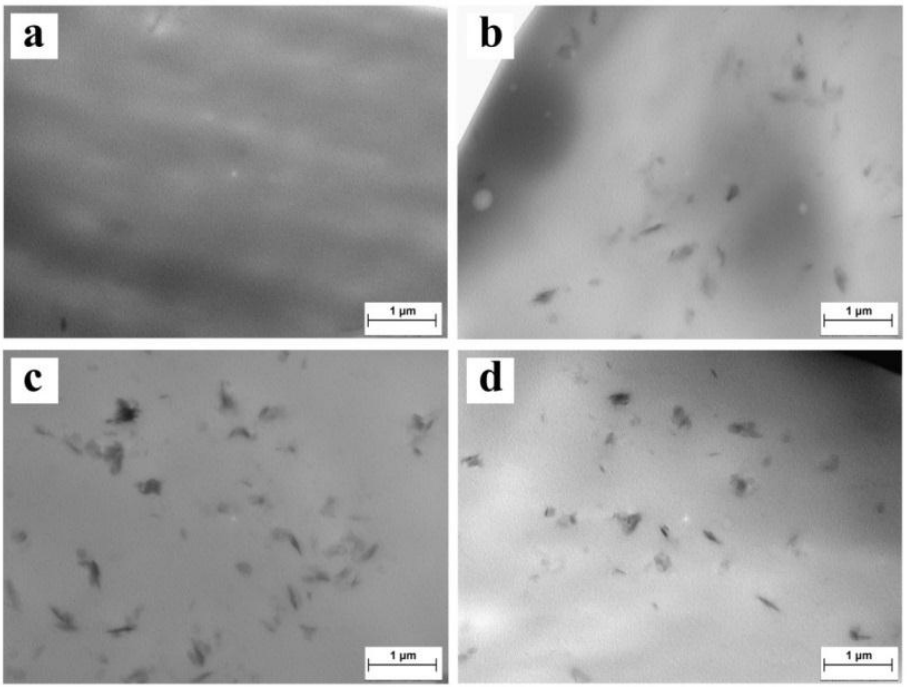

Figure 7.5: TEM images of PHBV (a), srPHBV-2 (b), srPHBV-4 (c) and srPHBV-6 (d) films.

Figure 7.6 exhibits SEM images of PHBV and srPHBV films. PHBV, srPHBV-2 and srPHBV-4 films had porous morphology with numerous holes, which were distributed uniformly in the whole samples (Figs. 7.6a, 7.6b and 7.6c). However, there is a difference in the size of the pores, which are significantly smaller in the srPHBV-4 film. By contrast, SEM image of the srPHBV-6 film showed dense morphology without any open holes (Fig. 7.6d). These facts can be related with the interactions between PHBV microparticles and PHBV which reducing free volumes and finally covering the pores. The uniform morphology of all srPHBV films showed that the interactions are extended in all directions in the matrix that also confirmed the good dispersion state of PHBV

microparticles. For a more precise analysis, the mean pore diameters in all samples were measured via *ImageJ* software [11]. Mean pore diameters for PHBV, srPHBV-2 and srPHBV-4 films were 2.6 µm, 1.2 µm and 0.9 µm, respectively. There is no pore in the srPHBV-6 film.

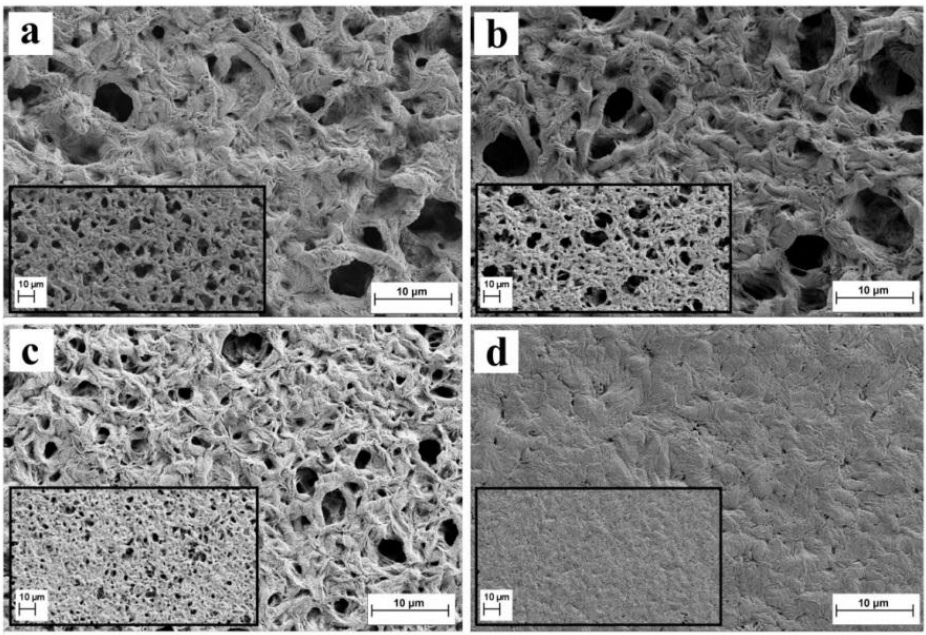

Figure 7.6: SEM images of PHBV (a), srPHBV-2 (b), srPHBV-4 (c) and srPHBV-6 (d) films.

Spherulitic morphology and the nucleating agent effect of PHBV microparticles in the PHBV were analyzed by POM direct observation. Images were taken during cooling step and some of them are shown in Fig. 7.7. Remarkable differences can be observed between the growing rate, quantity and size of spherulites in PHBV and srPHBV films. PHBV film had less quantity of spherulites with bigger size and more perfection. In this sample, due to

absence of PHBV microparticles, the quantity of spherulites was small, so, they had more space to grow uniformly in radial direction until contact with each other.

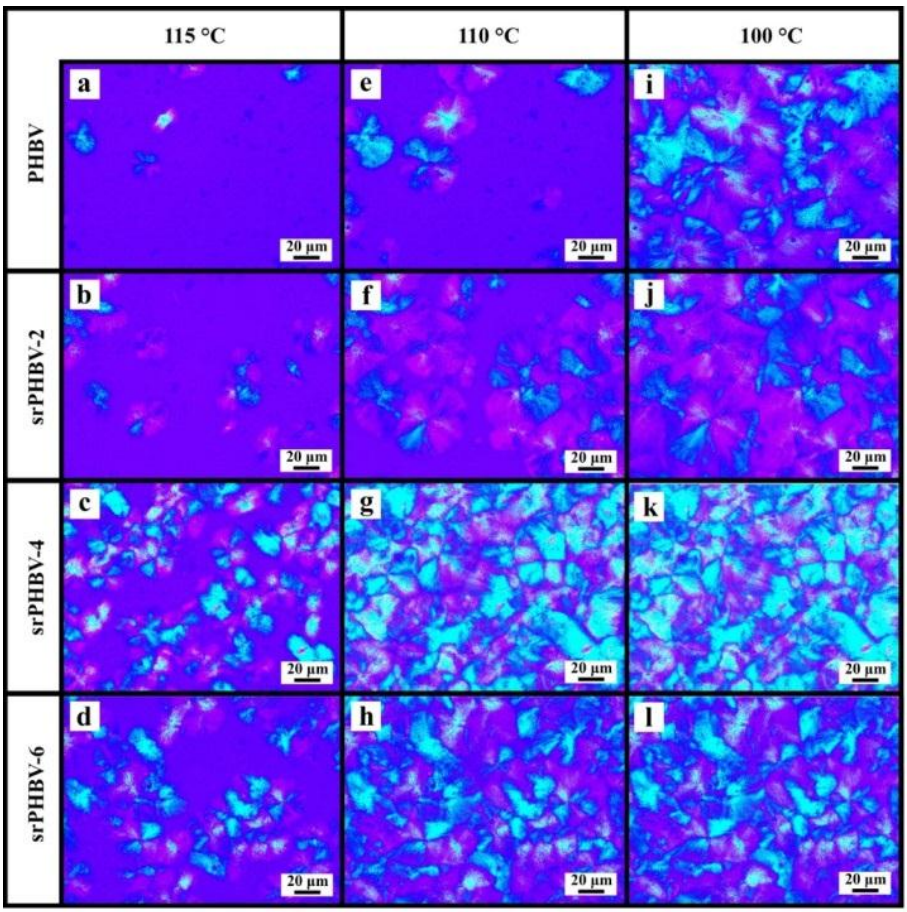

Figure 7.7: POM images of PHBV, srPHBV-2, srPHBV-4 and srPHBV-6 films at 115 °C (a-d), 110 °C (e-h) and 100 °C (i-l).

In srPHBV films, the appearance of more spherulites started at higher temperature and their growth continued with higher rate. Due to the higher

rate of crystallization in the srPHBV films and the existence of numerous spherulites, which act as physical barriers and disturb freely growing of neighbor developing fronts, these spherulites were smaller and less perfect. Comparing the crystal morphologies and considering SEM images and DSC results of srPHBV films, it was revealed that poreless morphology of the srPHBV-6 film provided less space for polymeric chains to move and form spherulites while available free volumes in the srPHBV-2 and srPHBV-4 film samples led to accelerated mobility, form and completion of numerous spherulites.

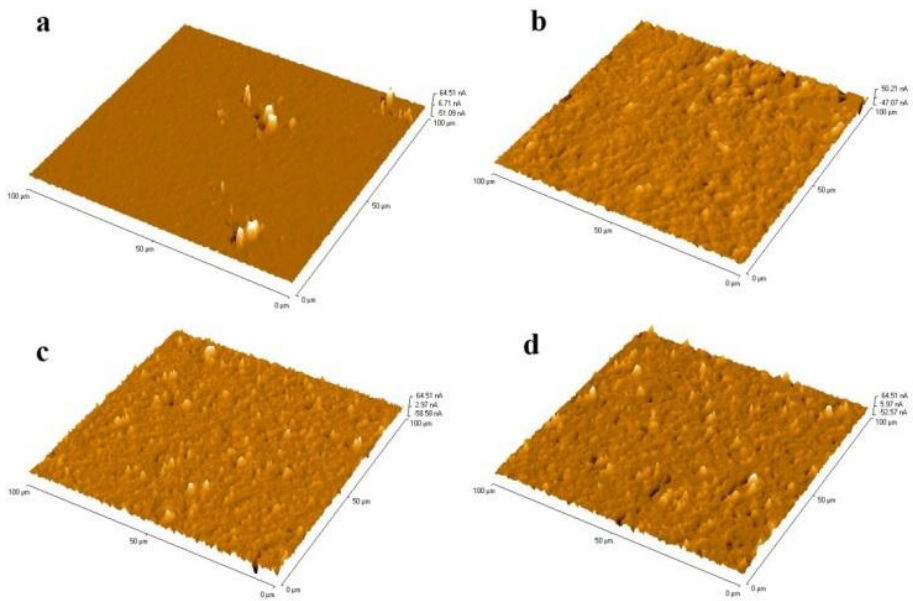

Figure 7.8: AFM images of PHBV (a), srPHBV-2 (b), srPHBV-4 (c) and srPHBV-6 (d).

AFM was done in order to deepen more in the morphological aspects of the incorporation of PHBV microparticles in a PHBV film. Fig. 7.8 gives surface

topography of the films studied. Variation of the surface roughness of PHBV film when is compared with the surface roughness of srPHBV films could be observed clearly. Smooth and plain surface of PHBV film changed to rough surface in srPHBV films. Roughness was intensified uniformly in all surface areas with PHBV microparticles content. This was consistent with TEM, SEM and POM observations.

7.3.4. Water vapor, oxygen and carbon dioxide transmission rate

Preservation, safety and quality of packaged food, extending the shelf and storage period are aims which are seriously pursued by packaging material designers and are related strongly on barrier properties of the packaging materials. High barrier films prevent the diffusion of humidity, contaminants and gases inside the packaged volume. In this sense, the effect of PHBV microparticles on barrier properties of srPHBV films against water vapor, oxygen and carbon dioxide were examined. The results of water vapor, oxygen and carbon dioxide transmission rate are shown in Fig. 7.9.

Results show that the transmission rate of PHBV film against water vapor, oxygen and carbon dioxide was reduced in all srPHBV films. Reviewing SEM results, it is reasonable to conclude that the modified morphologies of srPHBV films had remarkable influence in this improvement.

Higher barrier properties for all srPHBV films were due to their less open holes in the case of srPHBV-2 and srPHBV-4 films and poreless morphology in the case of srPHBV-6 film. Also, it could be explained by the higher crystallinity of srPHBV films and by the presence of more crystal zones with less free volumes in srPHBV films, which provide more tortuosity in the running pathway of gas molecules. Crystal zones perform like physical barriers in molecules pathways that limit free mobility and diffusion of gas molecules.

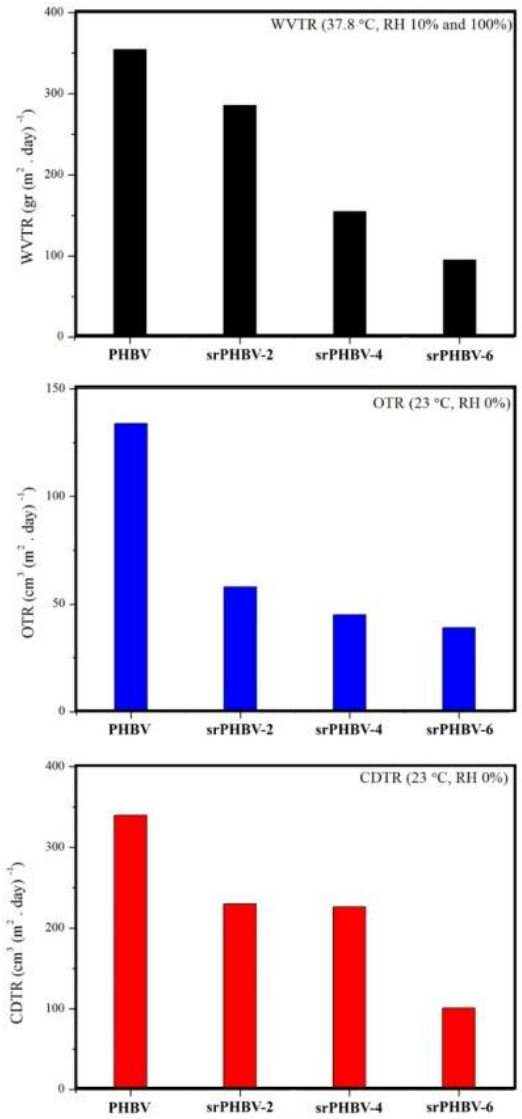

Figure 7.9: Water vapor, oxygen and carbon dioxide transmission rate for PHBV and srPHBV films.

7.4. Conclusions

Biodegradable self-reinforced films of PHBV and PHBV microparticles were prepared by solvent cast film method (srPHBV). Thermal, morphological and barrier properties as well as their crystalline structure were investigated. DSC, WAXS and POM findings revealed that due to nucleating agent effect of the PHBV microparticles in the PHBV film crystallization process began at higher temperatures for srPHBV films compared to PHBV film. Results of WAXS showed also that diffractograms of both PHBV and srPHBV-6 samples at room temperature contain the main characteristics diffraction peaks of orthorhombic α – type crystalline structure. SAXS data revealed that the variation in long spacing with the temperature was similar in PHBV film and srPHBV-6 film. SAXS/WAXS data exhibited higher lamellae thickness for srPHBV-6 film sample. Uniform dispersion of microparticles of PHBV was obvious from TEM images in all srPHBV films. Considerable change in the morphologies of the srPHBV films was obvious from SEM images. Porous morphology with numerous open holes in the PHBV film changed to less porous morphology with smaller holes for srPHBV-2 and srPHBV-4 films. However, srPHBV-6 film showed completely poreless compact morphology. In addition, significantly higher quantities of spherulites with smaller size were formed in all srPHBV films. AFM results showed that PHBV microparticles affected the surface topography of the srPHBV films. Nearly smooth and plain surface of PHBV film was turned to rough surface for srPHBV films and the scale of roughness was intensified with the content of PHBV microparticles. Barrier properties against water vapor, oxygen and carbon dioxide were improved significantly due to incorporation of PHBV microparticles in the PHBV film.

7.5. References

[1] E. Ten, J. Turtle, D. Bahr, L. Jiang, M. Wolcott, Thermal and mechanical properties of poly (3-hydroxybutyrate-co-3-hydroxyvaletare)/cellulose nanowhiskers composites, Polymer, 54: 2653 (2010)

[2] S. Malmir, B. Montero, M. Rico, L. Barral, R. Bouza, Morphology, thermal and barrier properties of biodegradable films of poly (3-hydroxybutyrate-co-3-hydroxyvalerate) containing cellulose nanocrystals, Composites Part A, 93: 41 (2017)

[3] J. Qian, L. Zhu, J. Zhang, R. S.Whitehouse, Comparison of different nucleating agents on crystallization of poly (3-hydroxybutyrate-*co*-3-hydroxyvalerates), Journal of Polymer Science Part B: Polymer Physics, 45: 1564 (2007)

[4] L. N. Carli, O. Bianchi, G. Machado, J. S. Crespo, R. S. Mauler, Morphological and structural characterization of PHBV/organoclay nanocomposites by small angle X-ray scattering, Materials Science and Engineering: C, 33: 932 (2013)

[5] E. M. Benetti, V. Causin, C. Marega, A. Marigo, G. Ferrara, A. Ferraro, M. Consalvi, F. Fantinel, Morphological and structural characterization of polypropylene based nanocomposites, Polymer, 46: 8275 (2005)

[6] R. Wilson, T. S. Plivelic, A. S. Aprem, C. Ranganathaiagh, S. A. Kumar, S. Thomas, Preparation and characterization of EVA/clay Nanocomposites with improved barrier performance, Journal of Applied Polymer Science, 123: 3806 (2012)

[7] H. Sato, N. Suttiwijitpukdee, T. Hashimoto, Y. Ozaki, Simultaneous Synchrotron SAXS/WAXD Study of Composition Fluctuations, Cold-Crystallization, and Melting in Biodegradable Polymer Blends of Cellulose Acetate Butyrate and Poly (3-hydroxybutyrate), Macromolecules, 45: 2783 (2012)

[8] M. Naffakh, C. Marco, G. Ellis, Inorganic WS_2 nanotubes that improve the crystallization behavior of poly (3-hydroxybutyrate), CrystEngComm, 16: 1126 (2014)

[9] A. Muñoz-Bonilla, M. L. Cerrada, M. Fernández-García, A. Kubaka, M. Ferrer, M. Fernández-García, Biodegradable Polycaprolactone-Titania Nanocomposites: Preparation, Characterization and Antimicrobial Properties, International Journal of Molecular Science, 14: 9249 (2013)

[10] R. J. Rule, J. J. Liggat, Time-resolved synchrotron small angle X-ray scattering studies of poly (3-hydroxybutyrate) and poly (3-hydroxybutyrate-co-3-hydroxyvalerate) polymers, Polymer, 36: 3831 (1995)

[11] C. A. Schneider, W. S. Rasband, K. W. Eliceiri, NIH Image to ImageJ: 25 years of image analysis, Nature Methods, 9(7): 671 (2012)

CHAPTER 8: Conclusion

In the present thesis, biodegradable composites and nanocomposites obtained from natural resources were prepared and studied for application in food packaging industry. In this regard, two types of polymeric matrices, namely PHBV and potato starch, and two types of filler, CNC and PHBV microparticles, were selected. Fillers were incorporated in the matrices via different methods, solvent cast film, internal mixing and extrusion. It was tried to follow two different approaches in the sample preparation: reinforcement and self-reinforcement. PHBV/CNC bionanocomposites and potato starch/PHBV microparticles biocomposites were prepared and classified as reinforced materials. PHBV/PHBV microparticles biocomposites were prepared and classified as self-reinforced materials. Samples were studied in different aspects such as thermal, morphological, mechanical and barrier properties as well as their crystallinity, humidity absorption, antimicrobial activity and biocompatibility. To summarize, it was concluded that both PHBV and potato starch matrices were modified by incorporation of fillers by all preparation methods. This strongly confirmed the nucleating agent effect of the fillers in the polymeric matrices due to formation of hydrogen bonds. After filler incorporation, thermal, mechanical and barrier properties of the polymeric matrices were improved as well as their crystallinity behavior.

All the biocomposites developed, PHBV/CNC, potato starch/PHBV microparticles and PHBV/PHBV microparticles could be good candidates for food packaging applications.

Funding

Financial support was provided from:

- Ministerio de Economía y Competitividad (MAT2013-41892-R, Project NanoCompBioPol).
- Xunta de Galicia Government (Autonomous Community Government)/FEDER: Program of Consolidation and Structuring Competitive Research Units (GRC 2014/036).
- CELLS – ALBA synchrotron Ref. 2016091826.

Annexes

Anexo I: Resumen

Introducción

Hoy en día, está bien aceptado que los plásticos sintéticos a base de petróleo producen contaminaciones que se consideran amenazas graves con efectos notablemente perjudiciales para el medio ambiente. Además, sus productos y residuos secundarios tóxicos, los altos costes de separación y reciclaje y la no renovabilidad de los recursos petroleros, dan lugar a la necesidad de desarrollar materiales biodegradables y compostables. En este sentido, se ha realizado un notable esfuerzo para introducir productos respetuosos con el medio ambiente en las diferentes industrias y mercados, tales como medicamentos, revestimientos, cosméticos o envases de alimentos, que actualmente están dominados por materiales procedentes del petróleo [1, 2]. Las proteínas, polisacáridos (tales como diferentes tipos de almidón, glucógeno y celulosa) y biopoliésteres tales como polihidroxialcanoatos (PHA), polihidroxibutirato (PHB) y ácido poliláctico (PLA) son algunos ejemplos bien conocidos de polímeros biodegradables que actualmente se usan y se estudian ampliamente [3-7]. Los biopolímeros exhiben varias ventajas, como la sostenibilidad, la neutralidad del carbono, la renovabilidad, la no toxicidad, la biocompatibilidad y la biodegradabilidad. Aunque las preocupaciones medioambientales se satisfacen mediante el uso de materiales poliméricos biodegradables, su aplicación podría estar limitada debido a algunas desventajas, como el alto precio y la debilidad en las propiedades mecánicas, térmicas y de barrera, una vez comparadas con los polímeros tradicionales basados en petróleo. Para superar los inconvenientes mencionados de estos polímeros y obtener productos más eficientes, la copolimerización, la mezcla o el uso de diferentes tipos de rellenos y aditivos son estrategias comunes. Existen numerosas investigaciones publicadas sobre estas modificaciones [8, 9].

El grupo de los biopoliésteres es uno de los grupos más importantes de biopolímeros. Los biopoliésteres de polihidroxialcanoato (PHA) son una familia de termoplásticos renovables y biodegradables. El poli (3-hidroxibutirato-co-3-hidroxivalerato) (PHBV) es un poliéster orgánico natural del grupo de polihidroxialcanoatos (Fig. 1.3). Es biosintetizado por microorganismos como muchos tipos de bacterias y algunos tipos de plantas [10]. El PHBV se puede usar para aplicaciones industriales, liberación controlada de medicamentos, implantes médicos y dispositivos ortopédicos. Gracias a sus propiedades combinadas, como la excelente biocompatibilidad, la renovabilidad y los residuos de degradación inofensivos, ha atraído un interés considerable como material biodegradable ecológico para su uso en la industria del envase y del embalaje [11-13]. Sin embargo, la aplicación de films de PHBV está restringida debido a algunas desventajas, tales como el estrecho rango de procesado debido a la baja estabilidad térmica, alta fragilidad, baja velocidad de cristalización, propiedades mecánicas y barrera bajas y alto precio [14, 15]. Wang et al. publicaron que los inconvenientes mencionados podrían atribuirse a la baja densidad de nucleación y la velocidad de cristalización de PHBV [16]. Varias publicaciones se han dedicado a la mezcla, la mezcla reactiva, el refuerzo y la modificación de PHBV con diferentes biopolímeros y rellenos tales como PHBV/óxido de zinc [17], PHBV/derivado de monoterpeno [18], PHBV/grafeno [9], PHBV/acetato de etileno y vinilo [19], PHBV/poli (l-láctico) [20], PHBV/nanowhiskers de celulosa [21], PHBV/nanotubos de carbono [22], PHBV/poli (3-hidroxibutirato) [23].

Existen muchos tipos de rellenos para la producción de nanocompuestos biopoliméricos. Como relleno bien conocido, los nanocristales de celulosa (CNC) (Fig. 1.4) se usan en matrices biodegradables debido a sus propiedades, tales como buenas propiedades mecánicas, baja densidad, alta abundancia y

alta actividad superficial. Con este fin y según la literatura, está confirmado que el CNC afecta y modifica las propiedades del PHBV. Yu et al. [24-26] mostraron que la presencia de nanocristales de celulosa en la matriz de PHBV dio resultados mejores en propiedades térmicas, mecánicas, cristalización y biodegradación. Se acepta que la razón principal de estos efectos eficientes del CNC en la matriz de PHBV es que el CNC podría servir como un agente de nucleación para aumentar la velocidad de cristalización del PHBV.

Otro grupo importante de materiales poliméricos biodegradables son los diferentes tipos de almidón (Fig. 1.5). El almidón se puede encontrar en plantas como el trigo, la patata, el maíz y la tapioca. El almidón como candidato potencial ha sido ampliamente probado en la producción de films comestibles, láminas agrícolas, bolsas compostables, bolsas de basura y envases de alimentos [27-30]. Esto es debido a su combinación única de propiedades beneficiosas, tales como biocompatibilidad,biodegradabilidad, renovabilidad, abundancia, no toxicidad, bajo coste, versatilidad, pureza y procesabilidad [31-33]. Los gránulos de almidón se convierten en almidón termoplástico introduciendo una cantidad adecuada de plastificante y en condiciones específicas de temperatura, presión y cizalla. El almidón termoplástico podría luego simplemente procesarse mediante las diferentes técnicas de procesado que se aplican a los polímeros sintéticos convencionales tales como extrusión, moldeo, termoformado y soplado [28, 34]. El tipo y la cantidad de plastificante usado, así como otras condiciones del proceso, incluyendo el tiempo, la temperatura, la cizalla, son profundamente determinantes para el rendimiento final del almidón plastificado. Glicerol, sorbitol, etilenglicol, xilitol, urea y maltitol se han propuesto como plastificantes para varios tipos de almidón [33].

El almidón presenta un grupo de propiedades favorables. Pero se debe subrayar que la sensibilidad a la humedad, la baja eficiencia mecánica y la pobre estabilidad dimensional se identifican como algunas de las propiedades indeseadas más importantes del mismo, que comúnmente se relacionan con su naturaleza hidrofílica. Además, los fenómenos de cristalización y retrogradación durante el envejecimiento provocan la pérdida de propiedades del almidón. Algunas soluciones para eliminar o mejorar estos inconvenientes críticos y hacer que el almidón proporcione más funcionalidad, estabilidad y eficiencia podrían ser modificaciones en la composición y en introducción de rellenos y agentes de refuerzo [31, 32, 35].

Rellenos con grupos polares tales como caolín, quitina, arcilla, nanotubos de carbono, óxido de zinc (ZnO), dióxido de titanio (TiO_2) y nanofibras de celulosa (CNF) se comportan como rellenos efectivos en diferentes matrices de almidón [35-37]. Obviamente, las interacciones de la interfase matriz/relleno y el estado de dispersión del relleno dentro de la matriz juegan un papel esencial para lograr las propiedades modificadas esperadas.

Objetivos y estructura de la tesis

La presente tesis se ha centrado en nanocompuestos y biocompuestos poliméricos obtenidos a partir de recursos naturales, reforzados y auto-reforzados para su aplicación en envase y embalaje de alimentos. Se estudiaron dos tipos de matriz diferentes: PHBV y almidón de patata. La aplicación de las matrices poliméricas mencionadas se restringe debido a algunas características indeseables tales como baja barrera y cristalinidad, débiles propiedades mecánicas y térmicas. Por lo tanto, esta tesis doctoral se ha enfocado en la modificación de estos inconvenientes y el desarrollo de envases y embalajes eficientes. A este respecto, se seleccionaron dos tipos de

relleno, CNC y las micropartículas de PHBV. Los rellenos se incorporaron a las matrices considerando dos enfoques diferentes: el refuerzo y el auto-refuerzo. Como resultado, se desarrollaron tres grupos diferentes de materiales que incluían biocompuestos de PHBV/CNC y almidón/micropartículas de PHBV como compuestos reforzados y biocompuestos de PHBV/micropartículas de PHBV como compuestos auto-reforzados. Las muestras se evaluaron y se caracterizaron en diferentes aspectos, tales como la cristalinidad, las propiedades térmicas, mecánicas y morfológicas, así como la absorción de humedad y propiedades barrera.

A continuación, se presentan los resultados brevemente.

Nanocompuestos de PHBV/CNC: método de cast film

En este capítulo se seleccionó el PHBV como matriz polimérica biodegradable. Además, como una de las soluciones más efectivas para superar las propiedades no deseadas de los biopolímeros, se seleccionó la introducción de relleno. El CNC se introdujo en la matriz de PHBV como relleno con eficacia probada en sistemas poliméricos biodegradables. Se aceptó que los grupos hidroxilo del CNC reaccionan mediante enlaces de hidrógeno con grupos carbonilo de PHBV y esto daría como resultado la modificación de las propiedades de la matriz. Se analizaron en detalle las muestras de nanocompuestos preparadas mediante el método de cast film y la influencia de la concentración de nanocristales de celulosa en las propiedades térmicas, los aspectos morfológicos y las propiedades de barrera (frente al oxígeno y al vapor de agua).

Las técnicas de caracterización utilizadas fueron DSC, WAXS, TEM, SEM, POM, AFM, WVTR y OTR. Los resultados de DSC mostraron que durante la etapa de enfriamiento, el proceso de cristalización comenzó antes y continuó con una

velocidad más alta en nanocompuestos en comparación con el polímero puro. Esto confirmó el efecto de agente de nucleación del CNC en la matriz de PHBV (Fig. 3.1). Además, el CNC no modificó la estructura cristalina del PHBV como se demostró por WAXS (Fig. 3.2). Las imágenes de TEM mostraron claramente la distribución homogénea de las partículas del CNC en la matriz en concentraciones del 2 wt.% y 4 wt.% del CNC, aunque en este último caso aparecieron pequeñas aglomeraciones de partículas. Mientras que en la concentración de 6 wt.% de CNC, la presencia de aglomeraciones era clara (Fig. 3.3). Los resultados de SEM revelaron un cambio considerable en la morfología de las muestras, desde la morfología porosa para PHBV puro hasta morfología muy compacta para el nanocompuesto con 4 wt.% de CNC. El efecto compatibilizante de nanopartículas de CNC se debe a que se forman enlaces de hidrógeno que actúan como puentes para conectar cadenas de PHBV y cubrir los poros. La obtención de morfología porosa sucedió una vez más en la concentración más alta (Fig. 3.4). Los resultados del POM demostraron una reducción en el tamaño y un incremento en la cantidad de esferulitas en los nanocompuestos en comparación con el PHBV puro. En consecuencia, se confirmó claramente el efecto del agente de nucleación de las partículas del CNC. Observar el crecimiento de las esferulitas en el perfil de enfriamiento de POM también sugiere un crecimiento acelerado de las esferulitas para todos los nanocompuestos. Aunque el nanocompuesto con 4 wt.% de CNC mostró un crecimiento más lento de las esferulitas debido a la movilidad restringida de las cadenas poliméricas (Fig. 3.5). Los resultados obtenidos por AFM indicaron que la incorporación de CNC modificó la topografía de la superficie de casi plana para el PHBV a rugosa para los nanocompuestos. La rugosidad de la superficie de las muestras se intensificó con el aumento de la concentración del CNC (figura 3.6). Debido a la alta

importancia de las propiedades de barrera para los materiales de embalaje, se estudiaron la velocidad de transmisión de vapor de agua y oxígeno del PHBV y sus nanocompuestos. Los resultados obtenidos mostraron una mejora notable en las propiedades de barrera de los nanocompuestos en comparación con el polímero puro (Fig. 3.7). Esto se explicó por la cristalinidad modificada de nanocompuestos y más tortuosidad en su morfología. Los resultados de las propiedades térmicas, la cristalización y las propiedades de barrera concuerdan bien con todo el estudio morfológico.

Caracterización y propiedades de nanocompuestos de PHBV/CNC: método de extrusión

En el capítulo anterior, se concluyó que el CNC puede mejorar las propiedades de la matriz de PHBV. Por lo tanto, para seguir estudiando los nanocompuestos de PHBV/CNC, se seleccionó un método diferente de preparación de muestra en el presente capítulo. También se buscó realizar unos análisis complementarios diferentes.

En el presente trabajo, nanocompuestos de PHBV/CNC que contienen 2 wt.%, 4 wt.% y 6 wt.% de CNC se prepararon con éxito mediante extrusión. El comportamiento de cristalización así como las propiedades morfológicas, mecánicas y de barrera contra el vapor de agua, el oxígeno y el dióxido de carbono fueron estudiadas en detalle. Los cambios estructurales de estos nanocompuestos fueron analizados por SAXS/WAXS durante la cristalización dinámica.

Las técnicas de caracterización utilizadas fueron DSC, SAXS/WAXS, TEM, SEM, ensayos mecánicos en tracción, WVTR, OTR y CDTR.

El análisis de la influencia del CNC en la cinética de cristalización dinámica de PHBV mostró que las temperaturas de cristalización aumentan con el

contenido del CNC para una velocidad de enfriamiento dada. Por lo tanto, se concluyó que CNC actuó como un agente de nucleación en la matriz de PHBV (Fig. 4.1 y Fig 4.2). Además, la incorporación de CNC implicó un aumento en la cristalinidad (Tabla 4.1). Los resultados de dispersión de rayos X de sincrotrón (SAXS/WAXS) mostraron que los difractogramas de WAXS de muestras de PHBV y PHBV/CNC6 a la temperatura ambiente contienen los picos de difracción con las características principales de la estructura cristalina de tipo α ortorrómbica. El proceso de cristalización comenzó a una temperatura más alta para la muestra PHBV/CNC6, lo que confirmó el efecto del agente de nucleación de nanopartículas de CNC en la matriz PHBV (Fig. 4.3). La variación en el espaciado largo (long spacing) con la temperatura fue más lenta en la muestra PHBV/CNC6 en comparación con la muestra PHBV debido a la presencia de nanopartículas de CNC que servirían como puntos de conexión y restringirían la movilidad libre de las cadenas de PHBV (Fig. 4.5). Los estudios de SEM indicaron que los nanocompuestos tuvieron más rugosidad que el PHBV, lo que se debió a la creación de enlaces de hidrógeno entre el relleno y la matriz. El contenido de CNC del 6 wt.% se consideró como la concentración del comienzo de la aparición de ligeras acumulaciones de nanopartículas del relleno (Fig. 4.6). Los estudios de TEM confirmaron que el CNC está bien distribuido en PHBV/CNC2 y PHBV/CNC4. Algunas aglomeraciones eran visibles en PHBV/CNC6 (Fig. 4.7). La prueba mecánica reveló que el módulo de Young para los nanocompuestos aumentó en comparación con el del PHBV puro. También se descubrió que con el aumento de la concentración de relleno, el módulo de Young aumentó sin disminuir la ductilidad (Fig. 4.8). El análisis unidireccional de la varianza (ANOVA) mostró una diferencia estadísticamente significativa en el módulo de Young de las muestras con la carga de relleno, mientras que no hubo un efecto significativo de la carga de relleno en la fuerza

y la deformación en el punto de cedencia (Yield) (Tabla 4.2). Las pruebas de barrera frente a las moléculas de vapor de agua, oxígeno y dióxido de carbono mostraron una modificación positiva en las propiedades de barrera de los nanocompuestos debido a mayor cristalinidad y más tortuosidad en su morfología (Fig. 4.9).

Nanocompuestos PHBV/CNC: efectos ambientales, actividad antimicrobiana y biocompatibilidad.

Generalmente se acepta que el contacto con la humedad, la exposición a la luz solar y la difusión de moléculas de oxígeno en la estructura del material, pueden conducir a fotooxidación, degradación, cambios en el peso molecular, morfología superficial, comportamiento térmico y/o composición en materiales poliméricos. Por lo tanto, estos pueden afectar a propiedades como la morfología, la estructura cristalina, las propiedades térmicas, la resistencia mecánica, la ductilidad y el color. En este sentido, la evaluación de las propiedades de los materiales poliméricos y su proceso de degradación con la exposición a la intemperie es de considerable importancia. Esto proporcionaría indicadores para el cálculo de la vida útil y el tiempo de estabilidad de los films como factores cruciales valiosos para adaptar la composición de los films y la estimación de su eficacia cuando se apunta a aplicaciones de envasado de alimentos.

Por lo tanto, el presente capítulo se refiere a los efectos simultáneos de la carga de relleno y de la intemperie artificial en las propiedades térmicas y morfológicas de los nanocompuestos PHBV/CNC, así como de su estructura cristalina. Se produjeron nanocompuestos de PHBV/CNC con 2 wt.%, 4 wt.% y 6 wt.% de CNC. Se investigó la influencia de la incorporación de CNC como relleno hidrófilo en la absorción de humedad y en la velocidad de transmisión

de vapor de agua en la matriz de PHBV. También se estudió el comportamiento antimicrobiano y la biocompatibilidad de las muestras.

Las técnicas de caracterización utilizadas fueron la intemperie artificial (Tabla 5.1), DSC, dispersión de rayos X de sincrotrón, SEM, DMA, absorción de humedad, WVTR, estudio antimicrobiano y biocompatibilidad.

Los resultados de DSC y dispersión de rayos X de sincrotrón (SAXS/WAXS) mostraron que el proceso de cristalización de los nanocompuestos comenzó a temperaturas más altas comparado con el PHBV, lo que verificó el efecto de agente nucleante del CNC. El análisis del comportamiento térmico en muestras expuestas a la intemperie artificial reveló una disminución de la cristalinidad, aunque hubo una cristalización secundaria en la muestra más expuesta a la radiación (Fig. 5.1, Tabla 5.2). Los resultados simultáneos de SAXS/WAXS mostraron que la incorporación de CNC no condujo a la creación de nuevas estructuras cristalinas (Fig. 5.2). Las imágenes de SEM mostraron una morfología bien dispersa de todos los nanocompuestos. El efecto del envejecimiento en cámara climática del PHBV y sus nanocompuestos produjo cambios en la morfología con la aparición de puntos similares a burbujas (Fig. 5.5). Se encontró que la hidrofobicidad de los nanocompuestos es ligeramente menor que la del PHBV en las pruebas de absorción de humedad (Fig. 5.6 y Tabla 5.3). Los resultados de las pruebas de velocidad de transmisión de vapor de agua mostraron valores más pequeños en los nanocompuestos, lo que se explica por mayor tortuosidad y presencia de CNC como barrera física que implica una menor movilidad de las cadenas de PHBV (Tabla 5.3). Los estudios antimicrobianos mostraron que las muestras que contienen óxido de zinc y plata presentaron un comportamiento de inhibición antimicrobiana contra cepas de *L. monocytogenes, S. enterica, S. aureus* y *E. coli* (Fig. 5.7). Además,

se confirmó que el PHBV y sus nanocompuestos son biocompatibles (Fig. 5.8 y Fig. 5.9).

Biocompuestos de almidón/micropartículas de PHBV: método de cast film

Otro polímero biodegradable que se estudió en la presente tesis fue el almidón. La introducción del relleno se considera una solución efectiva para mejorar las propiedades del almidón.

Los principales objetivos novedosos del presente capítulo consistieron en primer lugar en analizar el efecto de las micropartículas de PHBV en las propiedades finales de la matriz de almidón de patata plastificada por glicerol y, en segundo lugar en investigar la influencia de la concentración de glicerol en el impacto del refuerzo de las micropartículas de PHBV en el almidón. Se aplicó el método de cast film para preparar los biocompuestos. Las muestras obtenidas fueron ampliamente examinadas y discutidas en términos de estructura cristalina, comportamiento mecánico, morfología y estabilidad térmica, así como también su absorción de humedad y propiedades barrera.

Las técnicas de caracterización usadas fueron WASX, SEM, DMA, TGA, absorción de humedad y WVTR.

Los resultados de la dispersión de WAXS confirmaron buena plastificación y mostraron que el grado de cristalinidad inducido por el proceso se redujo cuando la movilidad de la cadena de la matriz era baja (figura 6.1). Los estudios morfológicos mostraron que menos cantidad de glicerol permitió más carga de relleno en biocompuestos asociados con buen estado de dispersión (Figura 6.2). La mejora en el módulo de Young se volvió más significativa al cargar más relleno y menos plastificante. Los biocompuestos mostraron propiedades mecánicas mejoradas especialmente a menor concentración de plastificante, lo que confirmó que el relleno conduciría a mejoras en las

propiedades mecánicas cuando actúa en una matriz menos plastificada (Figura 6.3). Los resultados de TGA reforzaron la explicación dada por el análisis DMA y SEM y mostraron que el contenido reducido de glicerol era ventajoso para la estabilidad térmica (figura 6.4). Los biocompuestos menos plastificados fueron más resistentes a la humedad (figura 6.5). Poseían menor velocidad de transmisión de vapor de agua debido a la menor movilidad de las cadenas y mayor tortuosidad (figura 6.6). En resumen, se descubrió que la introducción de micropartículas de PHBV favorecía la mejora de las propiedades de los films y, que al mismo tiempo, la concentración de plastificante tiene una contribución importante en las características de los biocompuestos.

Biocompuestos auto-reforzados de PHBV/micropartículas de PHBV: método de cast film

Como se discutió anteriormente, la introducción de relleno es una solución común para mejorar diferentes propiedades de la matriz polimérica. Sin embargo, debe tenerse en cuenta que la aplicación de la solución mencionada podría ser favorable, pero debido a las diferencias en la naturaleza del material de las fases y los rellenos, podrían estar asociados con algunas desventajas, como la baja compatibilidad o la aparición de grietas. En este sentido, otra estrategia para superar los problemas mencionados podría ser el auto-refuerzo, lo que significa la producción compuestos con la misma matriz y material de relleno. El propósito del presente capítulo se centra por primera vez en el uso de micropartículas de PHBV como refuerzo novedoso para mejorar el rendimiento del PHBV. Se incorporaron micropartículas de PHBV (2 wt.%, 4 wt.% y 6 wt.%) en una matriz de PHBV mediante el método de cast film. Se discutió en detalle la influencia de la concentración de las micropartículas PHBV en las propiedades térmicas, morfológicas y de barrera

(frente al vapor de agua, el oxígeno y el dióxido de carbono) de los films auto-reforzados, así como su estructura cristalina.

Las técnicas de caracterización utilizadas fueron DSC, SAXS/WAXS, TEM, SEM, POM, AFM, WVTR, OTR, CDTR.

Los resultados de DSC, WAXS y POM revelaron que debido al efecto del agente de nucleación de las micropartículas de PHBV en los films de PHBV, el proceso de cristalización comenzó a temperaturas más altas para los films de srPHBV en comparación con el film de PHBV (Figuras 7.1, 7.2 y 7.7). Los resultados de WAXS mostraron también que los difractogramas de muestras de PHBV y srPHBV-6 a temperatura ambiente contienen los picos de difracción con las características principales de la estructura cristalina de tipo α ortorrómbica (Figura 7.2). Los datos de SAXS revelaron que la variación en el largo espaciado con la temperatura era similar en el film de PHBV y en el film de srPHBV-6 (Fig. 7.4). La dispersión uniforme de micropartículas de PHBV fue evidente a partir de imágenes de TEM en todos los films de srPHBV (Fig. 7.5). Se evidenció un cambio considerable en las morfologías de los films de srPHBV en las imágenes de SEM. La morfología porosa con numerosos agujeros abiertos en el film de PHBV cambió a una morfología menos porosa con agujeros más pequeños para los films srPHBV-2 y srPHBV-4. Sin embargo, el film srPHBV-6 mostró una morfología completamente compacta (figura 7.6). Además, se formaron cantidades significativamente más altas de esferulitas de menor tamaño en todos los films de srPHBV (Figura 7.7). Los resultados de AFM mostraron que las micropartículas de PHBV afectaban la topografía de la superficie de los films srPHBV. La superficie lisa del film de PHBV se convirtió en una superficie rugosa para los films srPHBV y la escala de rugosidad se intensificó con el contenido de micropartículas de PHBV (figura 7.8). Las propiedades de barrera contra el vapor de agua, el oxígeno y el dióxido de carbono se mejoraron

significativamente debido a la incorporación de micropartículas de PHBV en los films de PHBV (figura 7.9).

Conclusión

Se desarrollaron compuestos y nanocompuestos reforzados y auto-reforzados poliméricos, obtenidos de recursos naturales, para la industria del envasado de alimentos. A este respecto, se utilizaron dos tipos de matrices de biopolímero, poli (3-hidroxibutirato-co-3-hidroxivalerato) (PHBV) y almidón de patata y dos tipos de relleno, nanocristales de celulosa (CNC) y micropartículas de PHBV. Los rellenos se introdujeron en las matrices con diferentes métodos, incluido el cast film, mezcla en estado fundido y extrusión. Se produjeron bionanocompuestos de PHBV/CNC y biocompuestos de almidón/micropartículas de PHBV en el enfoque de refuerzo y biocompuestos de PHBV/micropartículas de PHBV en el enfoque de auto-refuerzo. Se estudiaron diferentes propiedades, tales como propiedades térmicas, morfológicas, estructurales, mecánicas, absorción de humedad y de barrera. Además, se investigó el efecto del envejecimiento artificial, así como la actividad antimicrobiana y el comportamiento de biocompatibilidad.

Los resultados generalmente mostraron que, independientemente del método de preparación de las muestras, en todos los casos, el relleno actuó exitosamente como agente de nucleación dentro de la matriz. Esto se debió a la formación de enlaces de hidrógeno entre la matriz y las partículas de relleno. Así pues, las muestras con el relleno mostraron propiedades mejoradas en todos los aspectos estudiados. En consecuencia, se obtuvieron tres biocompuestos diferentes, PHBV/CNC, almidón de patata/PHBV micropartículas y PHBV/PHBV micropartículas, con propiedades mejoradas

que hacen a estos materiales ecológicos ser buenos candidatos para aplicaciones de envase y embalaje alimentario.

Referencias

[1] V. K. Thakur, Green Composites from Natural Resources, CRC Press, Florida (2013)

[2] S. Kalia, Biodegradable Green Composites, John Wiley & Sons, New Jersey (2016)

[3] L. Averous, E. Pollet, Biodegradable Polymers, Springer, New York (2012)

[4] L. Han, H. Xu, X. Sui, L. Zhang, Y. Zhong, Z. Mao, Preparation and properties of poly (ε-caprolactone) self-reinforced composites based on fibers/matrix structure, Journal of Applied Polymer Science, 134: DOI: 10.1002/APP.44673 (2017)

[5] L. T. Sin, A. R. Rahmat, W. A. W. A. Rahman, Polylactic Acid. PLA Biopolymer Technology and Applications, Elsevier, Oxford (2013)

[6] R. L. Whistler, J. N. BeMiller, Starch Chemistry and Technology, Elsevier, Oxford (2009)

[7] R. Ipsita, P. M. Visakh, Polyhydroxyalkanoate (PHA) based blends, composites and nanocomposites, Royal Society of Chemistry, Cambridge (2014)

[8] P. A. Pawar, A. H. Purwar, Biodegradable polymers in food packaging, American Journal of Engineering Research, 2: 151 (2013)

[9] V. Sridhar, I. Lee, H. H. Chun, H. Park, Graphene reinforced biodegradable poly (3-hydroxybutyrate-co-3-hydroxyvalerate) nanocomposites, Polymer Letters, 7: 320 (2013)

[10] A. Buzarovska, A. Grozdanov, M. Avella, G. Gentile, M. Errico, Poly (3-hydroxybutyrate-co-3-hydroxyvalerate)/titanium dioxide nanocomposites: a degradation study, Journal of Applied Polymer Science, 114: 3118 (2009)

[11] L. Martino, M. A. Berthet, H. Angellier-Coussy, N. Gontard, Understanding external plasticization of melt-extruded PHBV-wheat straw fibers biodegradable composites for food packaging, Journal of Applied Polymer Science, 132: DOI: 10.1002/APP.41611 (2015)

[12] V. Chea, H. Angellier-Coussy, S. Peyron, D. Kemmer, N. Gontard, Poly (3-hydroxybutyrate-co-3-hydroxyvalerate) films for food packaging: physical-chemical and structural stability under food contact conditions, Journal of Applied Polymer Science, 133: DOI: 10.1002/APP.41850 (2016)

[13] M. A. Berthet, H. Angellier-Coussy, V. Chea, V. Guillard, E. Gastaldi, N. Gontard, Sustainable food packaging: valorising wheat straw fibres for tuning PHBV based composites properties, Composites: Part A, 72: 139 (2015)

[14] D. G. Brunel, W. M. Pachekoski, C. Dalmolin, J. A. M. Agnelli, Natural additives for poly (hydroxybutyrate - co - hydroxyvalerate) - PHBV: effect on mechanical properties and biodegradation, Materials Research, 17(5): 1145 (2014)

[15] H. Y. Yu, Z. Y. Qin, Surface grafting of cellulose nanocrystals with poly (3-hydroxybutyrate-co-3-hydroxyvalerate), Carbohydrate Polymers, 101: 471 (2014)

[16] B. Wang, J. Li, J. Zhang, H. Li, P. Chen, Q. Gu, Z. Wang, Thermo-mechanical properties of the composite made of poly (3-hydroxybutyrate-co-3-hydroxyvalerate) and acetylated chitin nanocrystals, Carbohydrate Polymers, 95: 100 (2013)

[17] A. M. Diez-Pascual, A. L. Diez-Vicente, ZnO-reinforced poly (3-hydroxybutyrate-co-3-hydroxyvalerate) bionanocomposites with antimicrobial function for food packaging, Applied Materials and Interfaces, 6: 9822 (2014)
[18] L. Pilon, C. Kelly, Modification of poly (3-hydroxybutyrate-co-3-hydroxyvalerate) properties by reactive blending with a monoterpene derivative, Journal of Applied Polymer Science, 133: DOI: 10.1002/APP.42588 (2016)
[19] S. H. El-Taweel, M. Khater, Mechanical and Thermal Behavior of Blends of Poly (hydroxybutyrate-co-hydroxyvalerate) with Ethylene Vinyl Acetate Copolymer, Journal of Macromolar Science Part B: Physics, 54: 1225 (2015)
[20] N. Jiang, H. Abe, Miscibility and morphology study on crystalline/crystalline partially miscible polymer blends of 6-arm poly (l-lactide) and poly (3-hydroxybutyrate-co-3-hydroxyvalerate), Polymer, 60: 260 (2015)
[21] L. Jiang, E. Moreluis, J. Zhang, M. Wolcott, J. Holbery, Study of the poly (3-hydroxybutyrate-co-3-hydroxyvalerate)/cellulose nanowhisker composites prepared by solution casting and melt processing, Journal of Composite Materials, 42: 2629 (2008)
[22] H. Y. Yu, Z. Y. Qin, B. Sun, X. G. Yang, J. M. Yao, Reinforcement of transparent poly (3-hydroxybutyrate-co-3-hydroxyvalerate) by incorporation of functionalized carbon nanotubes as a novel bionanocomposite for food packaging, Composite Science and Technology, 94: 96 (2014)
[23] M. Scandola, M. L. Focarete, G. Adamus, W. Sikroska, I. Baranowska, S. Swierczek, M. Gnatowski, M. Kowalczuk, Z. Jedlinski, Polymer blends of natural poly (3-hydroxybutyrate-co-3-hydroxyvalerate) and a synthetic atactic poly (3-hydroxybutyrate). Characterization and biodegradation studies, Macromolecules, 30: 2568 (1997)

[24] H. Y. Yu, Z. Y. Qin, Z. Zhou, Cellulose nanocrystals as green fillers to improve crystallization and hydrophilic property of poly (3-hydroxybutyrate-co-3-hydroxyvalerate, Progress in Natural Science: Materials International, 21: 478 (2011)

[25] H. Y. Yu, Z. Y. Qin, L. Liu, X. G. Yang, Y. Zhou, J. M. Yao, Comparison of the reinforcing effects for cellulose nanocrystals obtained by sulfuric and hydrochloric acid hydrolysis on the mechanical and thermal properties of bacterial polyester, Composite Science and Technology, 87: 22 (2013)

[26] H. Y. Yu, Z. Y. Qin, Y. N. Liu, L. Chen, N. Liu, Z. Zhou, Simultaneous improvement of mechanical properties and thermal stability of bacterial polyester by cellulose nanocrystals, Carbohydrate Polymers, 89: 971 (2012)

[27] R. L. Whistler, J. N. BeMiller, Starch Chemistry and Technology, Elsevier, Oxford (2009)

[28] F. Xie, E. J. Pollet, P. Halley, L. Avérous, Starch-based nano-biocomposites, Progress in Polymer Science, 38: 1590 (2013)

[29] A. M. Shi, L. J. Wang, D. Li, B. Adhikari, Characterization of starch films containing starch nanoparticles: part 1: physical and mechanical properties, Carbohydrate Polymers, 96: 593 (2013)

[30] T. H. Yun, S. D. Yoon, Effect of amylose contents of starches on physical properties and biodegradability of starch/PVA-blended films, Polymer Bulletin, 64: 553 (2010)

[31] M. J. Fabra, A. Lopez-Rubio, J. Ambrosio-Martin, J. M. Lagaron, Improving the barrier properties of thermoplastic corn starch-based films containing bacterial cellulose nanowhiskers by means of PHA electrospun coatings of interest in food packaging, Food Hydrocolloids, 61: 261 (2016)

[32] H. Angellier, S. Molina-Boisseau, P. Dole, A. Dufresne, Thermoplastic starch-waxy maize starch nanocrystals nanocomposites, Biomacromolecules, 7: 531 (2006)

[33] K. Gonzalez, A. Retegi, A. Gonzales, A. Eceiza, N. Gabilondo, Starch and cellulose nanocrystals together into thermoplastic starch bionanocomposites, Carbohydrate Polymers, 117: 83 (2015)

[34] M. J. Fabra, R. Perez-Masia, P. Talens, A. Chiralt, Influence of the homogenization conditions and lipid self-association on properties of sodium caseinate based films containing oleic and stearic acids, Food Hydrocolloids, 25: 1112 (2011)

[35] D. Le Corre, J. Bras, A. Dufresne, Starch Nanoparticles: A Review, Biomacromolecules, 11: 1139 (2010)

[36] P. R. Chang, R. Jian, J. Yu, X. Ma, Starch-based composites reinforced with novel chitin nanoparticles, Carbohydrate Polymers, 80: 420 (2010)

[37] M. Wollerdorfer, H. Bader, Influence of natural fibres on the mechanical properties of biodegradable polymers, Industrial Crops and Products, 8: 105 (1998)